Photocatalytic Oxidation of Anesthetic Gases

by

Shruthi Srinivasan

A thesis

presented to the University of Waterloo

in fulfillment of the
thesis requirement for the degree of

Master of Applied Science

in

Chemical Engineering

Waterloo, Ontario, Canada, 2020

AUTHOR'S DECLARATION

I hereby declare that I am the sole author of this thesis. This is a true copy of the thesis, including any required final revisions, as accepted by my examiners.

I understand that my thesis may be made electronically available to the public.

ABSTRACT

Inhaled anesthetics used in surgeries are typically volatile halogenated hydrocarbons. In a typical situation only 5% of the administered anesthetic is metabolized by the human body, while the remaining 95% is exhaled through the ventilation systems eventually into the environment as it is. The anesthetics contribute to global warming and stratospheric ozone depletion. This research focuses on using advanced oxidation processes as a treatment system for the common anesthetic gases namely Halothane, Sevoflurane and Isoflurane.

The first step was to determine an appropriate reactor setup which could contain the light source and the catalyst medium with an accessible sampling port. The loss of anesthetic gas due to leaks and wall effects were measured and considered to be a baseline for further tests. In developing a treatment system, UV-photolysis, UV-ozonation, and UV-photocatalysis were tested in different batch experiments using Halothane, and UV-photocatalysis was found to be the most effective advanced oxidation process among the ones tested. Since UV-photocatalysis was efficient in degrading ~ 99.9 % of the anesthetic gas in 20 min, the influence of several parameters such as the type of catalyst, the type of catalyst support surface, the catalyst loading, the incident light wavelength, the power of the incident light, catalyst surface area illuminated, inlet reactant concentration and the moisture content on the degradation efficiency of UV-photocatalysis was tested. Based on the results obtained UV-photocatalysis with the appropriate conditions was used to test the degradation of Isoflurane and Sevoflurane.

The post oxidation contents of the reactor with Isoflurane and Sevoflurane were measured using Ion Chromatography for their anion concentration and a possible degradation mechanism was suggested for their Photocatalytic degradation in the presence of TiO_2.

ACKNOWLEDGEMENTS

This research could not have been done without funding from NSERC and the Ontario Centers of Excellence.

I would like to specially thank Dr.William A.Anderson for his supervision, guidance and suggesting improvements in my thesis.

I would like to thank Dr. Carol Moralejo for all her endless experimental and analytical advice and her wonderful revision of my thesis.

I would like to thank all the professors in the Department of Chemical Engineering whose extensive knowledge helped me during my time in masters.

I would like to thank my friends and colleagues for their motivation and support during this journey.

DEDICATION

This thesis is dedicated to my family who never stopped believing in me.

Table of Contents

List of Figures

List of Tables

1. Introduction and Literature Review

1.1.Anesthetic gases

New modern anesthetics are made of halogenated hydrocarbons or ethers that are often liquid at room temperature and are evaporated using a vaporizer before inhalation. Commonly used anesthetics are Halothane (2-bromo-2-chloro-1,1,1-trifluoroethane), Isoflurane (2,2,2-trifluoro-1-chloroethyl difluoro methyl ether), Desflurane (1,2,2,2-tetraflurorethyl difluoromethyl ether), Sevoflurane (1,1,1,3,3,3-hexafluoro-2-fluoromethoxy propane) and nitrous oxide. Halothane was the first fluorinated inhaled anesthetic to rapidly replace all the other potent inhaled anesthetics. Efforts to develop a rather ideal volatile anesthetic eventually led to the invention and use of Desflurane, Sevoflurane and Isoflurane. Halothane is currently being predominantly used only in developing nations. N_2O is the only non-volatile gas which is administered in the gaseous state at room temperature.[1]

An ideal inhaled anesthetic agent property include ample potency, resistance to physical and metabolic degradation, odorless to inhale, rapid in onset and offset, low solubility in blood and tissues and a protective effect by preventing lack of injury to vital tissues. Other characteristics include a lack of ability to cause seizures and respiratory irritation and low acquisition cost. An ideal anesthetic is difficult to obtain, while many have suitable characteristics. The currently used anesthetic gases undergo very little in-vivo metabolism during inhalation.

1.1.1.Halothane

Halothane (2-bromo-2-chloro-1,1,1-trifluoroethane) is a volatile anesthetic gas with a boiling point of 50.2^{o}C that has been replaced with the newer generation of anesthetic gases (Isoflurane, Sevoflurane

and Desflurane) because it is susceptible to inducing adverse effects, namely hepatic necrosis.[2] Due to its low cost and easy availability, Halothane was used for many initial experiments in this study. Since Halothane's physiochemical properties are similar to the other halogenated anesthetics the experiments often gave similar results when repeated with the other anesthetics.

1.1.2. Sevoflurane

Sevoflurane (fluoromethyl 2,2,2-trifluoro-l(trifluoromethyl) ethyl ether) is a non-flammable and non-explosive liquid administered by vaporization. Sevoflurane is a colorless liquid containing no additives. It is a non-pungent liquid miscible with organic solvents and is slightly soluble in water. Sevoflurane with a boiling point of 58.6ºC is often bottled in amber glass bottles with water to prevent degradation. The fast offset/onset and low irritation to the mucous membranes makes Sevoflurane a preferred anesthetic for mask induction. Sevoflurane had a market revenue of 782.6 million USD in 2018.[3]

1.1.3. Isoflurane

Isoflurane (2-chloro-2-(difluoromethoxy)-1,1,1- trifluoro-ethane) with a boiling point of 48.5ºC is a non-flammable liquid administered by vaporizing. It is a clear colorless stable liquid containing no chemical additives. It can be stored in glass bottles under indirect sunlight for almost 5 years with no change in composition. It has a mildly pungent and musty odor. Isoflurane is administered with another drug, usually Propofol, to induce stable general anesthesia.[4] The use of Isoflurane has decreased in recent times due to its longer induction and recovery time compared to Sevoflurane.

1.1.4.Desflurane

Desflurane (1,2,2,2-tetrafluoroethyldifluoromethyl ether) is a polyfluorinated methyl ethyl ether that is almost identical to Sevoflurane. The complete fluorination greatly reduces its blood solubility coefficient and potency. The low boiling point of Desflurane (23.35^{o}C) requires a highly specialized vaporizer. Desflurane is the most pungent of all the inhaled anesthetics. This property of Desflurane increases the risk of cough, laryngopasm.[5] Hence, despite its quick recovery, it has limited practical use.

1.2.Environmental Implications of Anesthetic Gases

The atmosphere can be subdivided based on its temperature profile. The lowest layer where the temperature decreases with increase in altitude is called the troposphere. The layer above it is called the stratosphere where the temperature increases up to a distance of 50 km. The layer of ozone in the stratosphere often referred to as the stratospheric ozone acts as a shield from the harmful UV radiations of the sun.

This stratospheric ozone layer is damaged by the long living chlorine and bromine free radicals which are released due to human activities. The use of CFCs and Halons were eventually regulated as part of the Montreal Protocol.

A class of halogenated compounds that have been in use in medicine without regulations are the halogenated anesthetic gases mentioned above. The global warming potential of these gases which is defined as the measure of the gas' ability to trap heat when compared to CO_2 over 100-year time period are Sevoflurane=130, Isoflurane=510, Desflurane=2540, N_2O=298 and CO_2=1.[6]

These anesthetics are often exhaled almost as it is by the patient. Their rates of in vivo metabolism are 0.2%, < 0.02%, 5 % for Isoflurane, Desflurane and Sevoflurane respectively and ~20% for Halothane.[7]

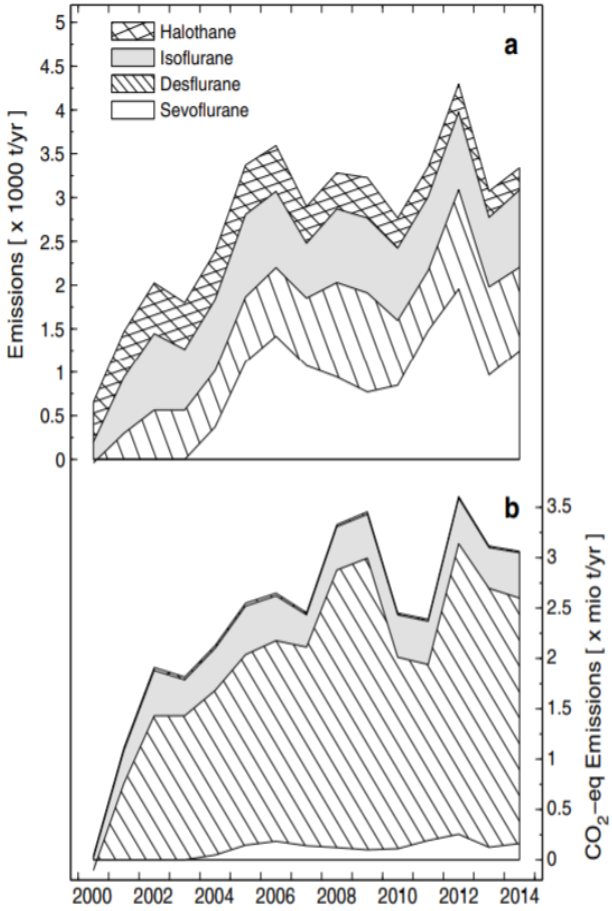

These anesthetics are administered via a system that mixes them with a carrier gas specifically oxygen and nitrous oxide. In addition to the exhaled gases, the anesthetics also escape through leaks in the vaporizer or outdated equipments. Because currently there are no mandatory waste anesthetic gas capture systems, these gases are entirely vented to the outside environment through the ventilation systems.

As of 2009, a typical large US hospital is said to use 1081, 505, and 6 liters of Isoflurane, Sevoflurane and Desflurane respectively.

Figure 1.1: Global emissions trend of modern anesthetic gases[7]

Around 5% of the anesthetic is metabolized by the patient while the remaining anesthetic is released via the ventilation system, untreated into the environment. This growing anesthetic gas usage trend shown in Fig 1.1 predicts a total CO_2 eq emission of 3.16 million t/yr in 2014 alone where the total global carbon dioxide emission was 9.79 giga tonne. This CO_2 eq emission of 3.16 million t/yr in 2014 is equal to almost 33.3% of the emissions from all the Swiss passenger car fleets for that year.[7]

Radiative forcing is a measure of magnitude and importance of a particular factor in altering the

Earth's energy balance. Although these anesthetic gases occur in concentrations million times lower than that of CO_2, they are responsible for a radiative forcing of 0.3 W/m^{-2}. These halogenated organics absorb strongly in the infrared region of the electromagnetic spectrum (600-1400cm^{-1}).

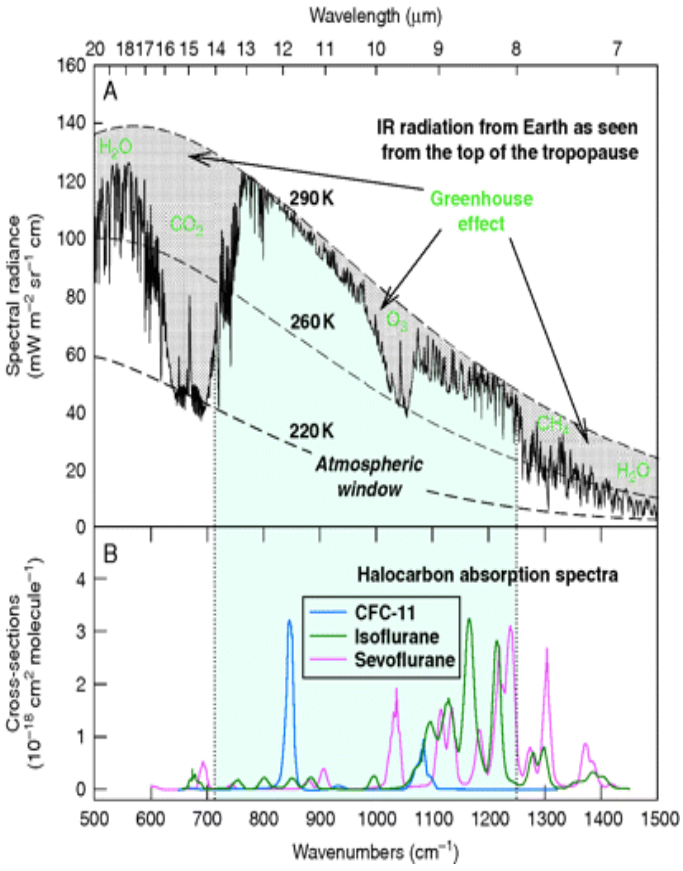

This region also known as the atmospheric window is used by the earth to radiate the excess IR energy back to the outer space. These anesthetics strongly absorb these emitted IR radiations, causing an imbalance in the earth's energy budget as shown in Fig 1.2.[8]

This work when put to practice will help reduce or eliminate these anesthetic gases from being released untreated into the environment thus preventing damage.

Figure 1.2:Anesthetic gases with maximum absorbance in the atmospheric window

1.3.Advanced Oxidation Processes

Advanced oxidation processes (AOPs) were initially proposed for potable water treatment in the 1980s. They predominantly use powerful oxidizing agents like hydroxyl or sulphate radicals. These radicals are different from the standard chlorine oxidants since they have a dual role of degradation

Oxidizing Groups	Relative Oxidation Power
Chlorine	1.00
Hypochlorous Acid	1.10
Permanganate	1.24
Hydrogen Peroxide	1.31
Ozone	1.52
Atomic Oxygen	1.78
Hydroxyl Radical	2.05
TiO2+	2.35

Table 1:Relative oxidizing power of selective oxidizing groups

and disinfection. Although AOPs have been studied in detail for wastewater treatment, they are rarely employed for gas treatments. The $OH^{\bullet}$ radical is a non-selective yet strong chemical oxidant that once produced, attacks nearly all oxidizable organic complexes.

Since the lifetime of the radical is very small it is mostly generated in-situ from hydrogen peroxide, ozone, photo-catalysis or oxidants alongside UV radiation. Attack by the $OH^{\bullet}$ radical can diminish the pollutant concentration from parts per million to as low as parts per billion. Table 1 clearly shows that the relative oxidizing power of the OH^{o} is much higher than the other oxidizing agents.[9] The major advantage of AOPs is allowing simultaneous treatment of multiple contaminants. This occurs due to the presence of highly non-selective but efficient oxidants. There are several types of AOPs that degrade the pollutants, specifically hydroxyl based AOPs, ozone based AOPs, UV based AOPs, fenton based AOPs, sulphate radical based AOPs, and sonolysis.

The current work focuses on three such ways: UV-photolysis, UV-photocatalysis, and UV-ozonation.

1.3.1.UV-Photolysis

Photodegradation generally employs a low or medium pressure mercury lamp emitting strong UV radiations at different wavelengths. There are two pathways for the degradation induced by UV irradiation. One pathway is photolysis whereby the reactant molecules are broken down by absorption

of incident UV photons. This breakdown occurs due to the cleavage of one or more covalent bonds in the molecule due to the absorption of light energy. [10] The other pathway is photo-oxidation where the reactant molecule is excited in the presence of UV light and subsequently results in an oxidation reaction.[10] Photodegradation by UV treatment was first used for wastewater treatment and suggested for waste gas treatment in the early 1990s.[11,12] In the past two decades, UV-photodegradation has gained attention due to its simplicity however its widespread use has been limited due to the higher costs associated with it.

1.3.2.UV-Ozonation

Ozone, when compared to the saturated calomel electrode, has a very strong oxidizing potential of 2.07 V.[13] Ozone (O_3) readily absorbs UV radiations emitted at the 254 nm wavelength producing H_2O_2 as an intermediate, which further decomposes to produce hydroxyl radicals. The reactions below depict the mechanism of pollutant degradation in UV-ozonation:

- $O_3+hv \rightarrow O_2+O$ ……Equation 1
- $O+H_2O \rightarrow H_2O_2$ ……Equation 2
- $H_2O_2 \rightarrow 2OH^o$ ……Equation 3

This process is highly energy and cost consuming. Generating ozone is the most cost consuming part of UV-ozonation.

1.3.3.UV-Photocatalysis:

Hydroxyl radicals can be produced by irradiation in the presence of an appropriate semiconductor

catalyst as depicted in Fig 1.3. Titanium dioxide (TiO_2) and zinc oxide (ZnO) are the most commonly used industrial catalysts.

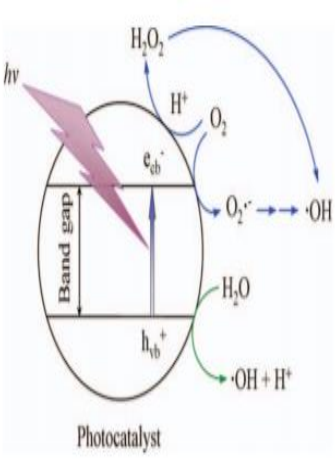

The catalyst particles in the presence of light photons are excited when the incident energy is greater than the band gap energy of the catalyst. This excitation produces valence band holes (hvb^+) with an oxidative capability and conduction band electrons (ecb^-) with a reductive capability.

Figure 1.3: Mechanism of UV-photocatalysis[14]

When the excitation energy is sufficient enough to prevent electron-hole recombination, the holes reach the surface of the catalyst to combine with water molecules to form adsorbed hydroxyl radicals. These OH^{o} radicals leave the bulk to form free radicals that take part in the oxidation of the reactant species as shown below:

- $TiO_2 + h\nu \rightarrow ecb^- + hvb^+$ ……..Equation 4
- $ecb^- + hvb^+ \rightarrow$ heat ……..Equation 5
- $hvb^+ + OH^-_{ads} \rightarrow OH^{o}_{ads}$ ……..Equation 6
- $hvb^+ + H_2O \rightarrow H_2O^+ \rightarrow H^+ + OH^{o}_{free}$ ……..Equation 7

Even though the catalyst used is often non-toxic, cheap, chemically and biologically inert and very efficient in the anesthetic degradation, the recovery of the catalyst is often a major problem and the primary drawback of photocatalysis.

1.4.Scope

The current research work aims at testing the possibility and efficiency of degrading the waste anesthetic gases emitted from medical facilities using selective advanced oxidation processes.

1.5.Relevance

The main motive behind this work was to identify an efficient oxidation technique which can be used as a treatment system to prevent any untreated halogenated anesthetic gas being released into the environment directly. Advanced oxidation processes have gained immense success in treating wastewater; however, not much work has been done in using them in treating anesthetics. Hence, to maintain novelty, three of the most commonly used AOPs were tested primarily with Halothane which was not only cheap and abundantly available but has similar physical and chemical properties as the other three anesthetics. Based on the results obtained, the same experiments were then conducted with the other two anesthetic gases namely Sevoflurane and Isoflurane. The results obtained were normalized for comparison since, for the same inlet volumes of the different anesthetics the concentration obtained in the GC results were different due to variation in their densities, their boiling points, their vaporization rates and their reactivity with the surfaces of the reactors and GC analytical equipment. The anesthetic gas concentrations obtained were analyzed in terms of reaction rates to obtain a deeper insight into the degradation.

1.6.Overview

The introduction and literature review section briefly details the common anesthetic gases in use currently, their environmental implications and gives the reader an insight into the mechanism of the

advanced oxidation processes used in this study. The introduction is followed by a detailed literature review on the various applications of advanced oxidation processes in treated pollutants in liquid and gas streams. It elaborates the influence of each parameter on the degradation efficiency and also broadly outlines similar studies done by other researchers in degrading the anesthetic gases. The materials and methods section talks about the materials used, experimental setup and the analysis techniques used in this study. The experimental section focuses on documenting the results and providing an explanation for the observations. The conclusions and future work talks about the inference from the work done and how best the work can be carried forward for the benefit of the environment.

Anesthetic gases are one of the typical pollutants created in an operation room.[15,16,17] These anesthetic gases are present in the air normally due to leaks in the breathing circuit, respiration by the patient, due to accidental spills or poor practices. Chronic exposure to anesthetic gases can cause kidney diseases, irritation in the mouth, skin and throat and also increase the risk of congenital abnormalities.[15]Anesthetic gas concentrations above the occupational exposure limits are a reality which is primarily caused due to inefficient ventilation systems or poor work practices.[15]

Advanced oxidation is an energy efficient technology that consists of generating oxidizing species that have the potential to convert the pollutants into substances like carbon dioxide and water. Numerous studies have shown that it is feasible to remove pollutants using photocatalytic oxidation.

In the current times, even though there are many studies on the photocatalytic oxidation of aqueous contaminants[18-26] the studies in the gas phase are very limited.[27,28] Even though many kinds of pollutants like alkanes, ketones, aromatics and chlorinated hydrocarbons can be removed from air using photocatalytic oxidation[29-40], their application has been limited due to problems with deactivation of the photocatalyst.[41-49]Hence, immobilizing the catalyst is a key aspect in designing a setup for

photocatalysis.[50,51] TiO_2, due to its high catalytic degradation efficiency, lower cost and non-toxicity is widely used in photocatalysis.[52]ZnO was tested as another potential photocatalyst since it also has high photosensitivity, stability, strong oxidizing power, is non-toxic and has a large band gap. A major reason for choosing ZnO alongside TiO_2 for comparison is their similar band gap energy of 3.26 and 3.33 eV respectively. Many researchers have focused their work in developing non-TiO_2 catalysts with low or similar band gaps as TiO_2such as ZnO, Fe_2O_3, ZnS and, CeO_2.[50,53-57] In some research work, ZnO has shown better degradation for dyes in aqueous solutions than TiO_2.[58-63] Some research work states that dopants have the ability to cause photogenerated electron-hole recombination thus affecting the efficiency of photocatalysis.[52]

Fiberglass cloth has emerged as a promising catalyst support surface since it is lightweight, has a low cost and is highly stable against UV light.[64,65] It can also be folded and cut into many shapes.

The performance of photocatalytic oxidation can be studied in two forms: process parameters (air velocity, light intensity, amount of catalyst) and environmental parameters (pollutant initial concentration, moisture). The influence of these factors has been extensively studied in Literature.[66-72]

Just like the other advanced oxidation processes, photodegradation was first considered for waste water treatment and later found more suitable for waste gas treatments in 1990s.[11,12] Photodegradation gained much popularity in the last two decades in contrast to photocatalysis due to the formation of intermediates on the catalyst surface that subsequently reduce the catalytic activity with time.[73,74]

Most of the studies have been performed on everyday home and office pollutants like toluene and benzene while very little attention has been paid to treat the specific hospital pollutants.[75] The selective research that has been done on treating anesthetic gases is focused on using photocatalytic oxidation to study only one particular anesthetic gas.[75,76,77] To the best of the author's knowledge, no research work has been conducted to compare the anesthetic gas degradation efficiency of three advanced oxidation processes namely UV-photolysis, UV-ozonation and UV-photocatalysis.

The objective of this work was to evaluate the performance of three advanced oxidation processes: photolysis, ozonation, and photocatalytic oxidation in degrading three anesthetic gases: Halothane, Isoflurane, and Sevoflurane. The performance of photocatalytic oxidation was studied by varying the pollutant inlet concentration, incident light wavelength, power of the light source, type of catalyst, type of catalyst support surface, catalyst surface area illuminated, reactant inlet concentration, amount of catalyst used and the moisture content.

OBJECTIVES OF THE CURRENT RESEARCH

Since anesthetic gases are found to affect the environment adversely, the current research work aims to

1. Design a reactor and set up a batch system to carry out the designed experiments
2. Compare the efficiency of three advanced oxidation processes in degrading the anesthetic gas
3. Test the influence of the type of catalyst on the anesthetic gas degradation rate using UV-photocatalysis
4. Test the efficiency of UV-photocatalysis in degrading the anesthetic gas by varying the catalyst support surface.
5. Test the influence of incident light source wavelength on the anesthetic gas degradation rate
6. Test the influence of the power of the light source on the anesthetic gas degradation rate
7. Test the effect of catalyst area illuminated by the light source on the anesthetic gas degradation rate
8. Determine the anesthetic gas degradation rate at various inlet concentrations
9. Determine the anesthetic gas degradation rate at various amounts of catalyst loading
10. Determine the influence of moisture on the degradation rate of the anesthetic gas

2. MATERIALS AND METHOD

2.1.Chemicals:

AEROXIDE TiO_2 P25 was purchased from Evonik in the form of a nanopowder with a primary particle size of 21 nm as established from analysis by TEM and a surface area of 35-65 m^2/g as established from analysis by BET.[78] It was used as purchased without modification. Zinc oxide in the form of a 99.9% metal basis with a -200 mesh powder size purchased from Alfa Aesar was used without any further treatment. FORANE (isoflurane, USP) was purchased from Baxter Corporation in 100 mL amber colored glass bottle. Halothane was purchased from Sigma Aldrich in 125 mL amber bottles. Sevoflurane was purchased from AbbView Corporation. A sample of Desflurane was provided by Class 1 Inc. All the anesthetic liquids purchased were used without any further treatment.

2.2.Photocatalytic Reactor:

The photocatalytic oxidation experiments were performed in a 3.8 L (46.736 cm length x 10.16 cm diameter) annular reactor constructed of black ABS plastic and operated in a batch mode (Fig 2.1). The non-removable end of the reactor was covered thrice with duct tape to minimize the leaks. The removable end had a two or four pin lamp holder fixed on its inside. The rear end of the holder was taped firm to minimize the leaks. This annular reactor was chosen for its combination of simple geometry, low pressure drop and good accessibility to light. Even though this type of reactor is not designed for high air flow rates they are useful in testing the kinetic parameters.[79] The reactor used for these experiments was equipped with a sampling septum on the top center that allowed for injection and sampling of the anesthetic gas. The contents of the reactor were recirculated using a Cole Parmer

Masterflex peristaltic pump equipped with a 60 cm length of 17 Norprene tubing with a 6.4mm inner diameter. A piece of 370 cm long polytetrafluoroethylene (PTFE) tubing was used for recirculation with the pump rate set at 500 ml/min. This flow rate meant that one full volume of the reactor would be circulated in approximately 7.6 min. The media and the lamp were housed inside the reactor. Three different light sources were used for the experiment. One 18W 254 nm UVC lamp with dual fluorescent tubes (Phillips TUV PL-L/4P series) each tube having a diameter 39 mm and length of 325 mm was used. A 9W 254nm UVC lamp with dual fluorescent tubes (Phillips TUV PL-S/2P series) and a 9W 365 nm UVA lamp with dual fluorescent tubes (Phillips PL-S/2P series) both having a tube diameter of 28 mm and length of 210 mm were also used. The light sources were connected to an external control source to turn the power on/off when required. Residual reactants and degradation products in the reactor and on the photocatalytic media were removed by flushing compressed air with 11% relative humidity through and over each component for 60 min before each experiment.[80]

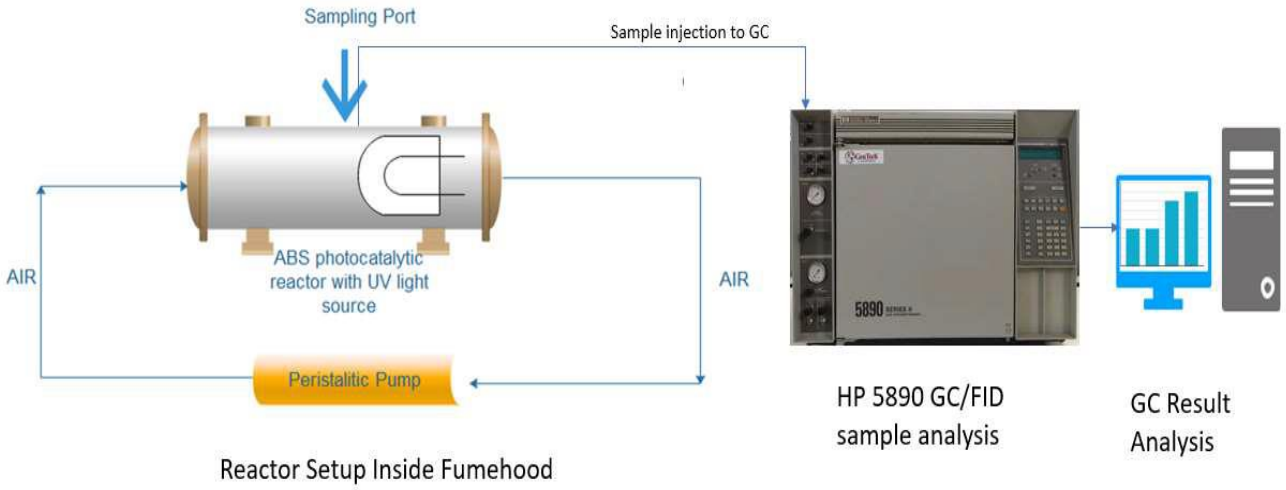

Figure 2.1: Schematic representation of the photocatalytic reactor

The photocatalytic media used were prepared by deposition (painting with a brush) of the catalyst powder prepared in a water suspension with a composition of 0.17 g TiO_2/ml of DI unless otherwise

mentioned, onto a polished 30 cm wide × 25cm long x 1 mm thick aluminum support that was subsequently dried overnight at ambient conditions. This process was repeated until the required amount of catalyst was deposited on the support surface as determined by measuring the change in the dry weight.

2.3.Fabricating Media with Different Support Surfaces

Here the main goal was to compare the photocatalytic results obtained, using the closed-loop reactor, with (i) a flat aluminum sheet (ii) a fiberglass cloth mesh and (iii) a fiberglass cloth mesh supported on the aluminum sheet, with each medium coated with the same amount of TiO_2.This ensured that each material was tested under similar appropriate conditions and the comparison was not biased.

In case of the flat aluminum sheet, the medium was prepared as mentioned in Section 2.2.In the second case, a fiberglass cloth mesh of the same size as that of the flat aluminum sheet, 30 × 25 cm, was used as a support surface for TiO_2. The cloth was initially weighed and the required amount of TiO_2 and water suspension was coated onto the cloth until the required change in the dry weight was attained. The catalyst coated cloth was dried overnight at ambient conditions before being tested.

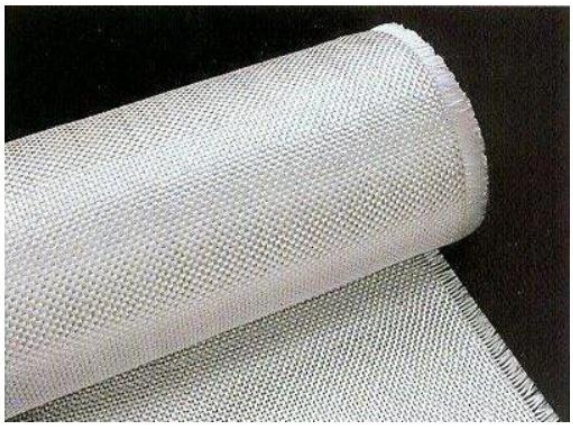

Figure 2.2: Fibreglass cloth mesh used as a catalyst support

The fiberglass cloth mesh fixed on the flat alumina sheet with plastic clips was tested as the third support surface. The combination of fiberglass cloth and the aluminum sheet were initially weighed and coated with the required amount of catalyst suspension until the desired weight change was observed. This setup was dried overnight at ambient conditions and tested the following day.

2.4.Sampling and Analytical Methods

The anesthetic gases throughout the experiments were quantified using a gas chromatograph (HP5890 Series II) with a 30m long 0.53mm in diameter RTX502.2 capillary (Restek, Pennsylvania) column as shown in Fig 2.3. The GC is equipped with a split/splitless injector, a FID (flame ionization detector) and an ECD (electron capture detector). Hydrogen and air were used as the detector gases with a flow range of 29 ml/min and 310 ml/min respectively. Nitrogen was used as the makeup gas. The flow rate through the column was set to 6-7 ml/min. The oven was set to a static temperature of 60^{o}C with no ramp up.

The RTX 502.2 column was often exposed to multiple gases and impurities during experiments. Running an air blank often showed a few peaks in the chromatogram resulting from residual contaminants not eluting from previous experiments. Hence, before beginning each day's experiments the column was baked at 210^{o}C for 30 min to drive off the residuals from the column.

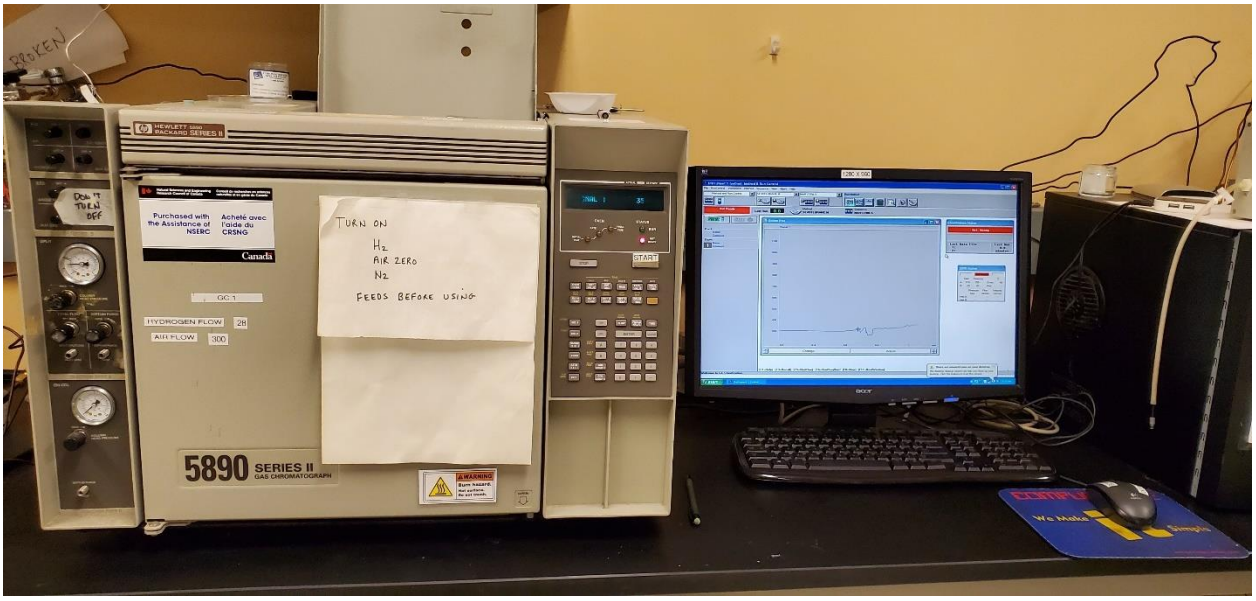

Figure 2.3: HP5890 series II gas chromatograph used to quantify the anesthetic samples

The peaks in the gas chromatograph were sufficiently separated with retention times of 0.54 for Desflurane, 0.56 min for Sevoflurane, 0.62 min for Isoflurane and 0.75 min for Halothane. The peaks in the gas chromatograph were easily identifiable since no experiments were conducted with a mixture of two or more anesthetic liquids.

2.4.1.GC Calibration

Before conducting any experiments, the GC was calibrated with the anesthetic gas to be tested using the following methods.

2.4.1.1.Air Blanks

Before any sample injection for calibration, 500 µl of room air was injected as a blank to determine the column residual level. The resulting area counts were used as a baseline for the calibration curve.

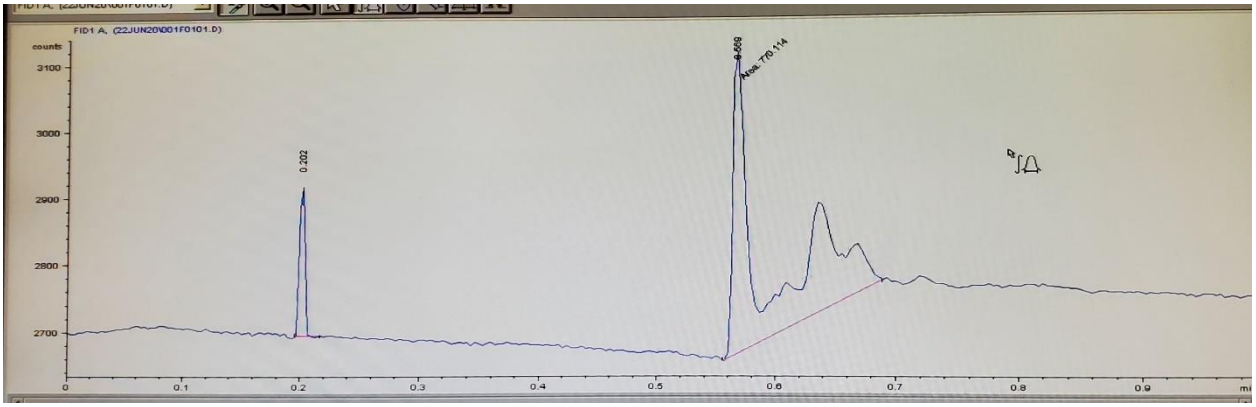

Figure 2.4: Air blank showing background noise in the absence of any sample

Air blanks were also run midway in the experiment to determine the amount of carry-over anesthetic adhered, if at all, to the teflon tip of the sample injection plunger. To avoid carry-over, the syringe was flushed multiple times and the teflon plunger was placed near the FID heater to volatilize any carry-over anesthetic gas.

2.4.1.2.Halothane Calibration Data

Calibration of the anesthetic gas was performed to provide the relationship between the area count and the mass of the anesthetic injected as a sample. Based on this relationship, the area count, and eventually the concentration of the anesthetic gas injected as a sample, was determined by the GC software. The anesthetic liquid volume being injected into the reactor was chosen in such a way that experimental gas area counts were sufficiently within the calibration curve to prevent over estimation.

To obtain a calibration curve, a known volume of 0.5 µl of Halothane was injected into a pre-silanized glass bulb of 250 ml volume containing air. Air oxidation was determined to be insufficient to degrade the Halothane within the time frame of the calibration. However, calibration was usually performed within a 30 to 60-minute time period. The bulb contents were allowed to mix at room temperature for 10 minutes after which five different known volumes of the anesthetic gas mixture from the bulb were

collected and their area counts measured using the GC. The results depicting the variation in the FID and ECD area counts with the Halothane amount injected are presented in Figure 2.5 and 2.7. Figure 2.6 depicts the Halothane calibration as observed in the FID of the GC computer.

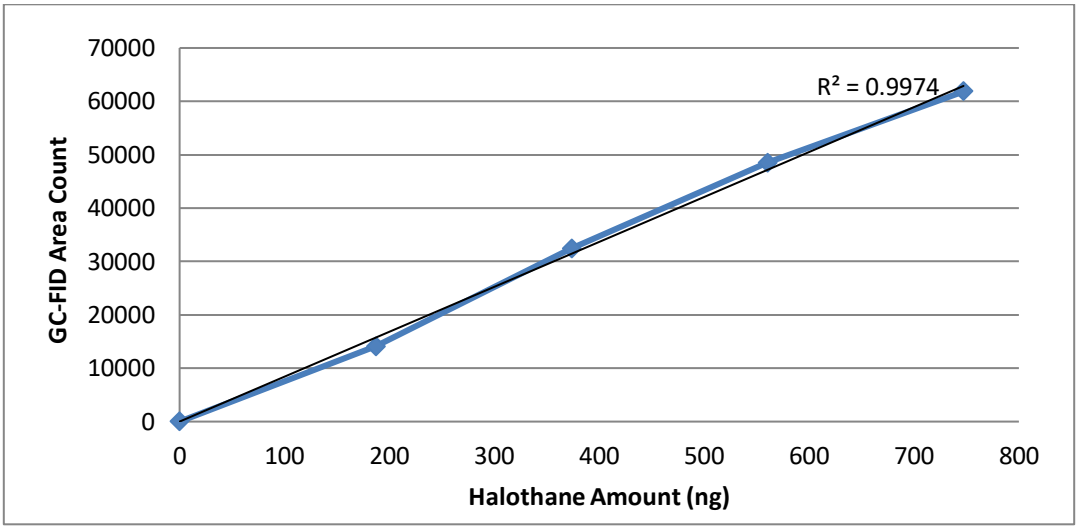

Figure 2.5: Change in the GC-FID area count with increase in the injected Halothane sample mass

The area counts for the blank at the retention time of the anesthetic gas with a well flushed syringe were only 5 to 10% of that of the first standard.

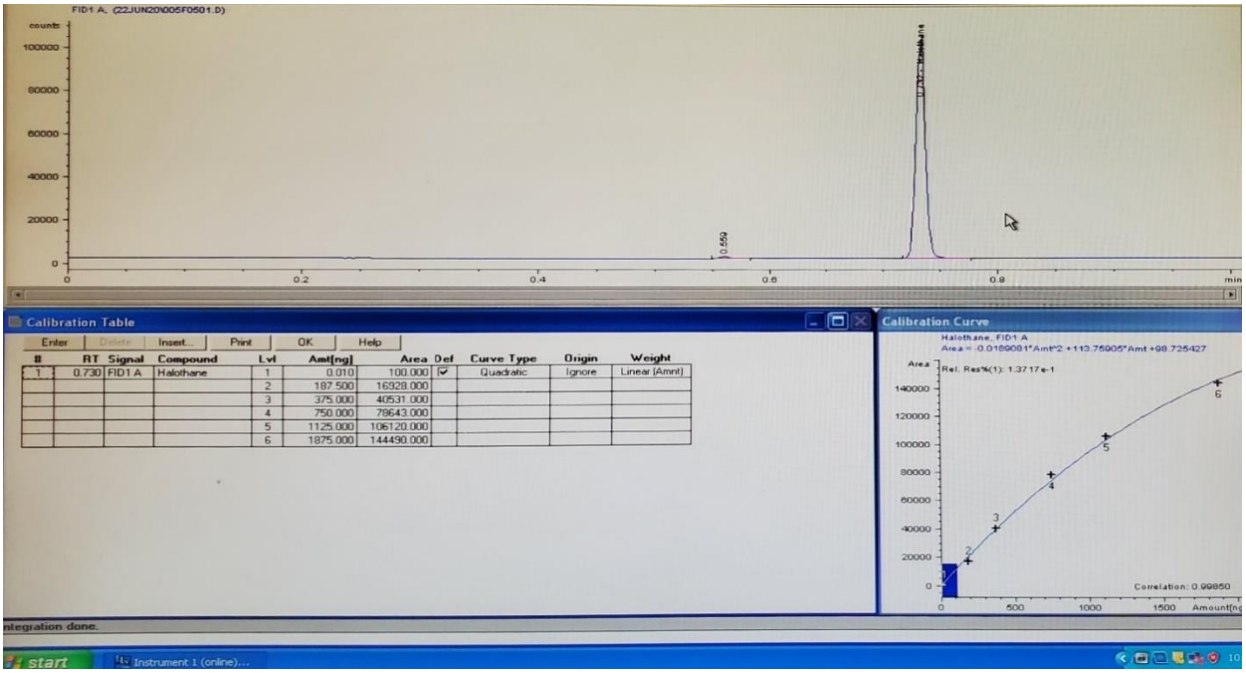

Figure 2.6: Halothane calibration as observed on the FID of the GC computer

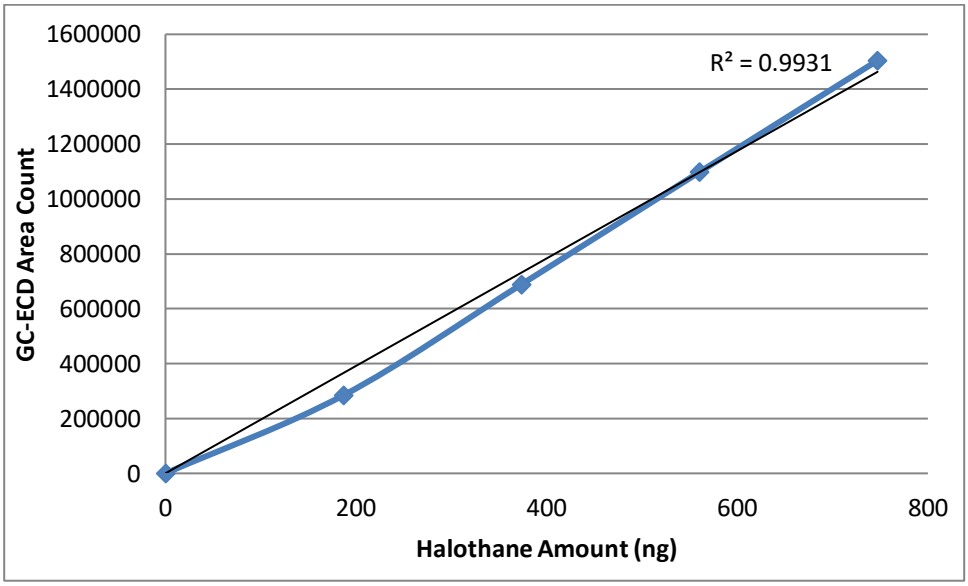

Figure 2.7: Change in the GC-ECD area count with increase in the injected Halothane sample mass

The electron capture detector is recommended for highly electronegative compounds such as halogenated compounds. The ECD is known to be 100-1000 times more sensitive towards these

compounds than the FID. Due to its sensitivity it is often used for measuring highly dilute solutions where the resulting area counts aren't as high as the ones depicted in Fig 2.7.

Since the sample concentrations being tested weren't very low and the FID gave reasonable results, the ECD was not needed for its sensitivity and the GC-FID was subsequently used for all further anesthetic gas quantifications.

2.4.1.3.Isoflurane and Sevoflurane Calibration

For the calibration of Isoflurane and Sevoflurane, 0.5 µl of the anesthetic in liquid form was injected into the 250ml silanized glass bulb and allowed to volatilize. A silanized bulb was used to minimize any wall effects. Various known volumes of the resulting anesthetic gas were sampled from the bulb and analyzed using the FID. The resulting area counts were plotted against the injected mass of anesthetic gas to populate the calibration curve of the anesthetic gas. This calibration curve was used to then measure the unknown concentrations of the anesthetics in the experimental samples. The results are depicted in Figures 2.8 and 2.10. Figure 2.9 and 2.11 depict the calibration of Sevoflurane and Isoflurane as observed on the FID of the GC computer.

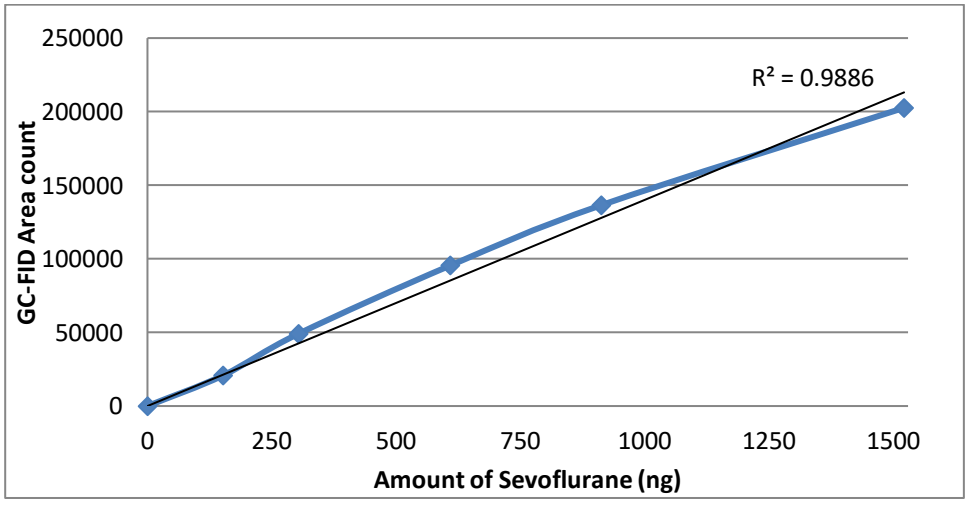

Figure 2.8: Calibration curve for Sevoflurane

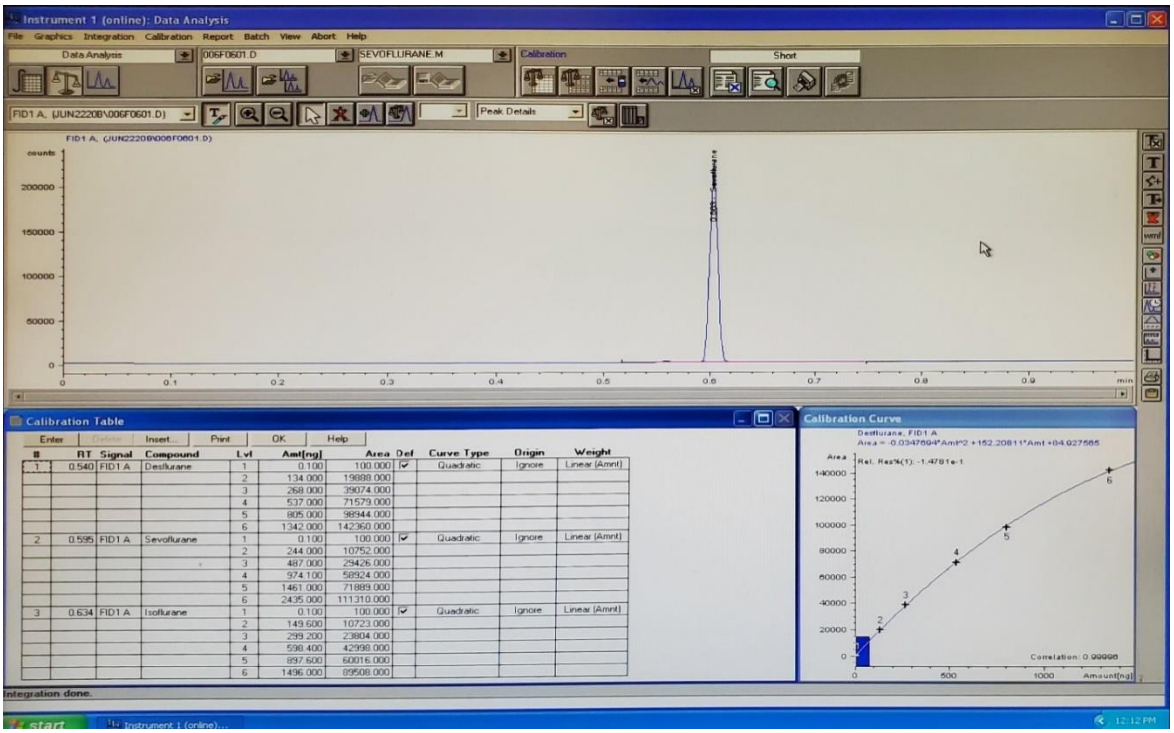

Figure 2.9: Sevoflurane calibration as observed on the FID of the GC computer

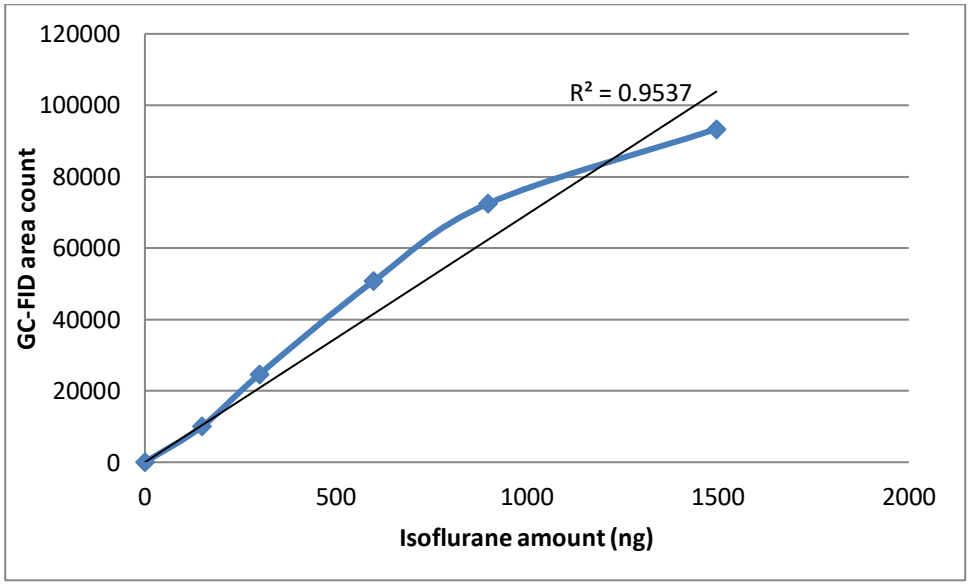

Figure 2.10: Calibration curve of Isoflurane

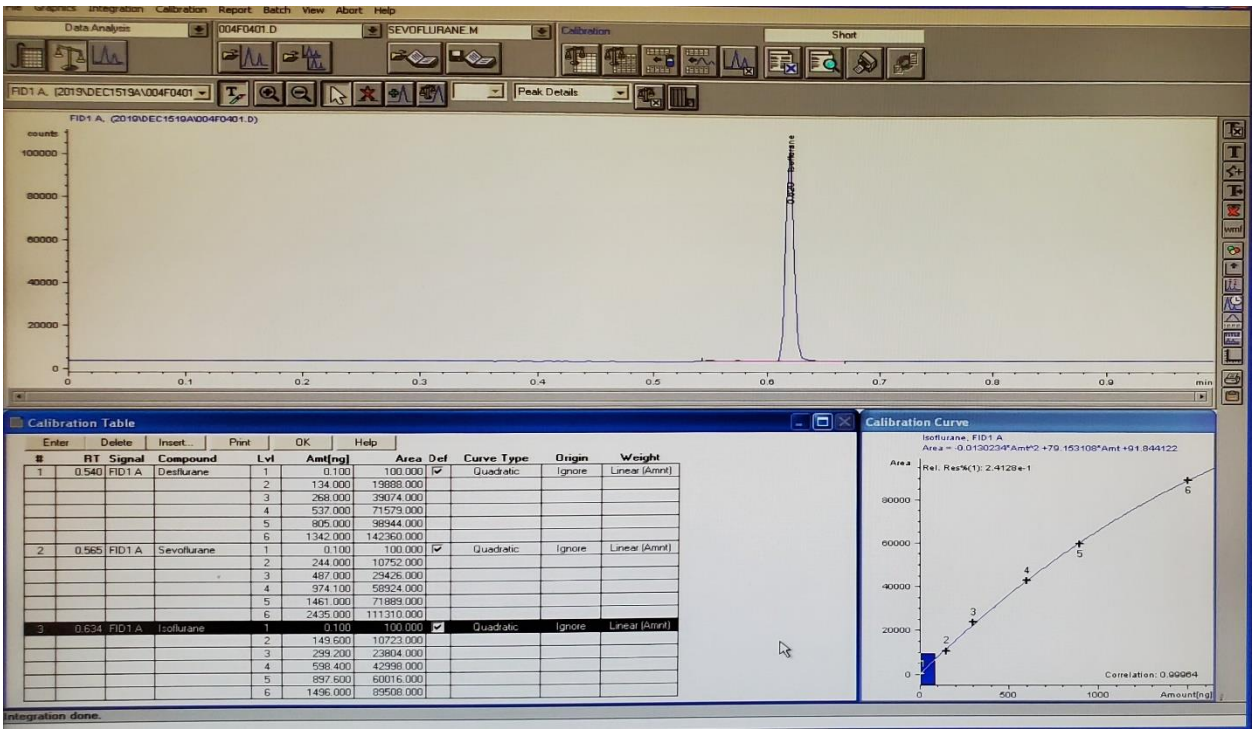

Figure 2.11: Isoflurane calibration as observed on the FID of the GC computer

2.4.1.4.Desflurane Calibration

The calibration curve for Desflurane was difficult owing to its extreme volatility at room temperature. Desflurane boils at 23.5ºC, very near to the room temperature. During the calibration using the liquid Desflurane, it was observed that as soon as the liquid was extracted from the bottle, it vaporized. If injected into the glass bulb, sampled and analyzed there was no Desflurane peak observed at 0.54 min retention time or subsequent sampling times. The next step was to extract 50 µl of the head space from the Desflurane container into the glass bulb. Even though a bit of Desflurane was detected in the chromatograph, the area counts dropped drastically over time suggesting loss of Desflurane to either the walls or the teflon plungers.

As a final resort, the Desflurane sample, glass bulb, and the syringe were frozen placed in the freezer.

Liquid volumes were extracted from the bottle and immediately injected into the bulb inside the freezer and analyzed using the GC. The Desflurane concentration again dropped drastically over time. It was then decided that no accurate calibration could be performed using Desflurane and any further attempts were made simply to mark the peak retention time. No further studies were carried out using Desflurane. The resulting area counts were plotted against the time to monitor the gas stability as shown in figure 2.12.

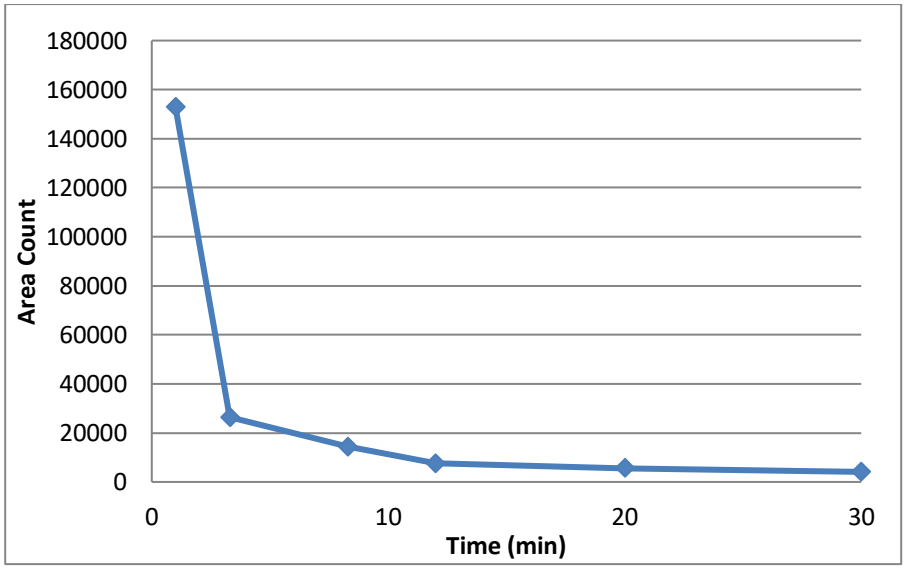

Figure 2.12: Change in the area counts for Desflurane over the time of 30 min

2.4.2.Wall Effects and Leaks

The ABS photocatalytic reactor was made in-house and had a removable threaded end cap. Leaks due to lose fittings or loss in concentration due to absorption on the reactor walls is a common problem in the air phase experiments. Hence preliminary trials also called as dark reactions were carried out for all the anesthetic gases to determine the contribution of leaks in the system and the wall effects. The wall effects and leaks measured were considered as the T_0 concentration for the subsequent tests.

For these tests, 5 µl of the anesthetic liquid was injected via the injection septum on the top of the reactor, allowed to volatilize and analyzed. The resulting anesthetic gas concentrations measured are depicted in Fig 2.13, 2.14 and, 2.15.

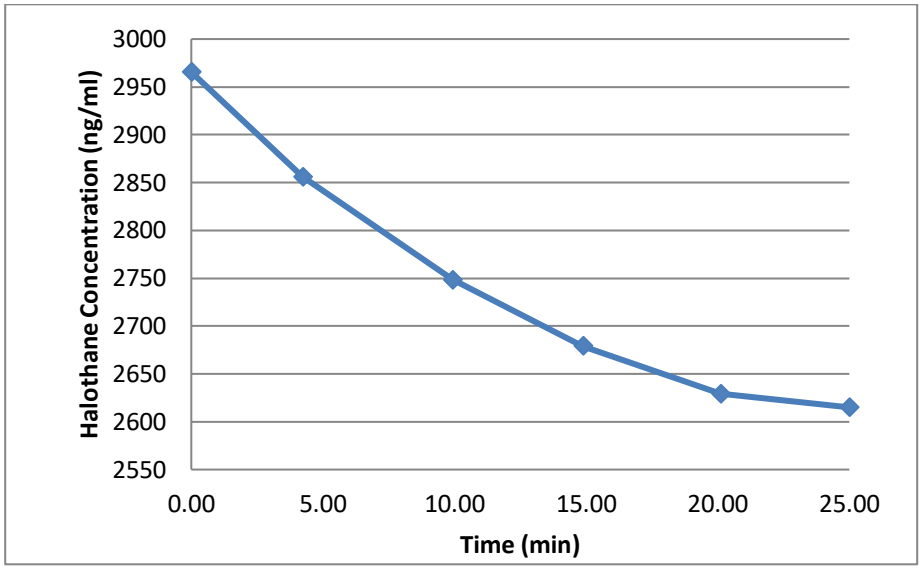

Figure 2.13: Change in the Halothane concentration due to wall effects and leaks over a time of 25 min

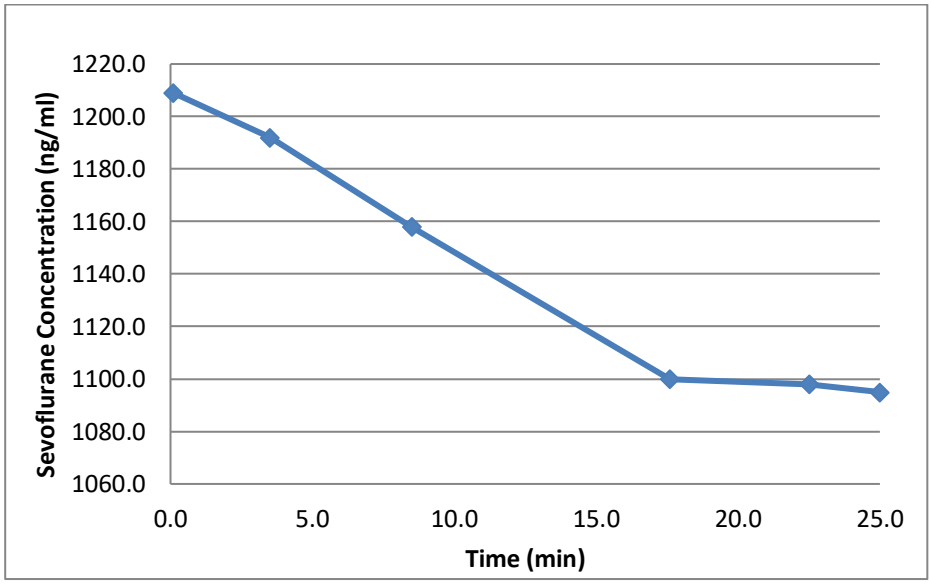

Figure 2.14: Change in the Sevoflurane concentration due to wall effects and leaks over a time of 25 min

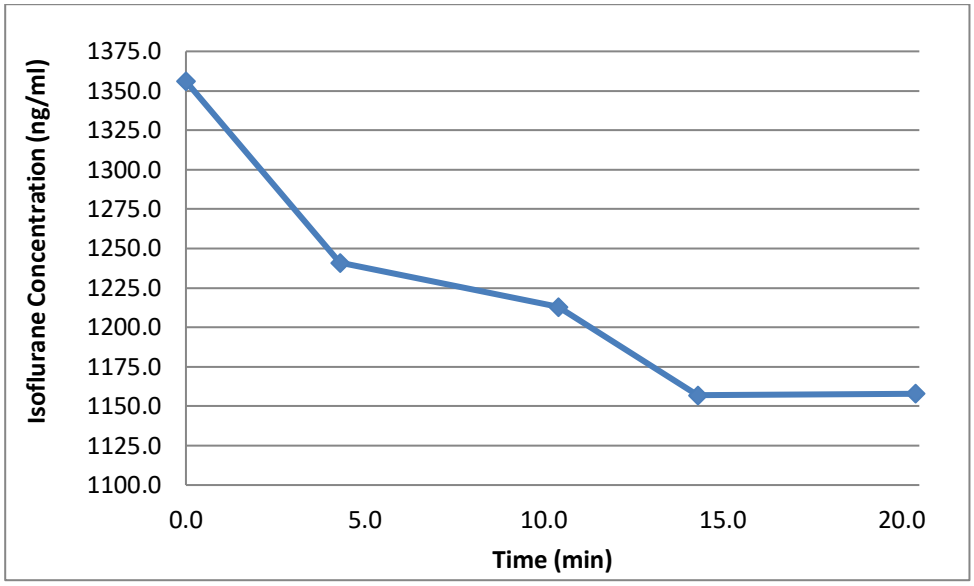

Figure 2.15: Change in the Isoflurane concentration due to wall effects and leaks over a time of 20 min

It was observed that the loss due to leaks and wall effects were consistent (within the experimental limits) for all the three anesthetic gases tested. Around 13% of the anesthetic gas was lost to the surroundings during the dark reactions in 20 min. Wall effects were considered stabilized and a constant loss rate was achieved after 20 min when the change in anesthetic gas concentration was less than 0.1%.

To further test the wall effects and leaks, various volumes of Halothane (10µl, 15µl and 25 µl) were injected into the photocatalytic reactor to measure the wall effects and loss due to leaks. It was noted that a maximum of approximately 15% of the anesthetic was lost to the surroundings before reaching stabilization in 30 min as depicted in Fig 2.16.

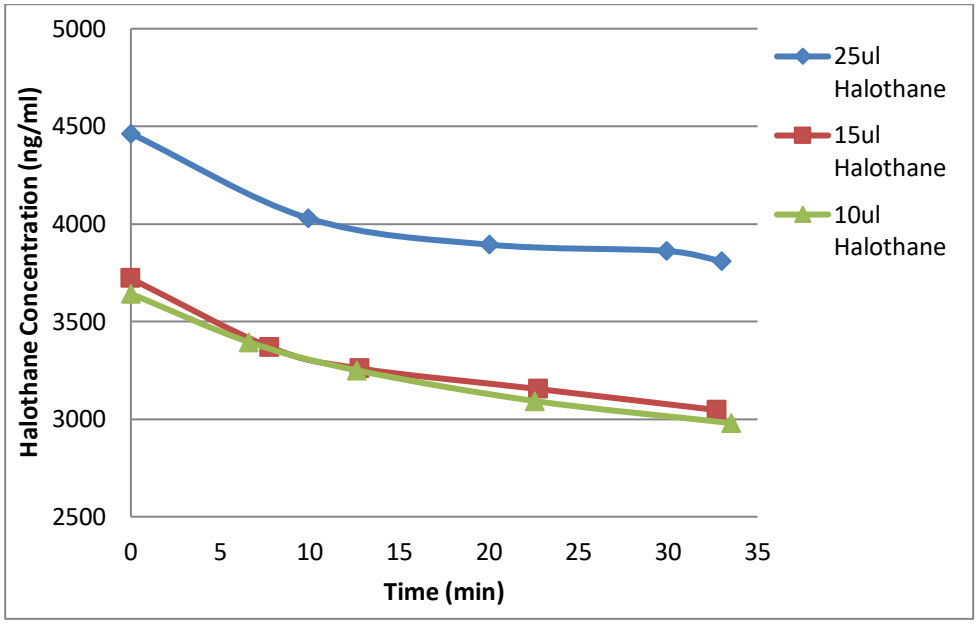

Figure 2.16: Variation in the wall effects with the inlet volume over the time of 35 min

2.4.3.Absorption on the Catalyst Surface:

Before measuring the decrease in anesthetic gas concentration due to UV-photocatalysis, the loss in anesthetic gas due to absorption on to the catalyst surface was measured. This loss measured was compared with the loss due to the dark reaction to determine the exact amount of anesthetic gas being absorbed onto the catalyst. This was taken as a T_0 concentration for UV-photocatalysis. This will be explained in Section 4.1.3.

2.4.4.Measuring the Absorption Spectrum of the Anesthetic Gases

The HP 8452 Diode Array Spectrophotometer shown in Fig 2.17 was used to measure the absorption spectrum of ozone and the anesthetic gases. A wavelength region of 200-820 nm was available for

measurement using this spectrophotometer. Olis GlobalWorks software was used as a user interface to communicate with the device. Each sample was collected in a 10 cm pathlength x 1.8 cm diameter cuvette and scanned for the absorbance three times in the interval of 0.01s. The resultant absorbance spectrum obtained was converted into a excel graph and analyzed further.

Figure 2.17: HP 8452 Diode Array Spectrophotometer used to measure the absorption spectrum of ozone and the anesthetic gases

2.4.5.Ozone Generator

A VTTL 2 - Ozone Generator by OZOMAX Inc as shown in Fig 2.18 was used to generate ozone with compressed air set to a minimum flow rate of 6 cfm as a feed using the corona discharge method. The maximum setting was used to produce ozone and the concentration of ozone generated was measured as mentioned in Equation 8 and 9.

1. $T = 10^{-\varepsilon bc} = 10^{-A}$ (where A is the absorbance at 254 nm) ……...Equation 8

2. Conc (molecules/cm^3) = LN(T)/(absorption cross-section of ozone* b), where b = cell pathlength in cm ……...Equation 9

Figure 2.18: Ozone generator

2.4.6. Testing for Byproducts of UV-Photocatalysis

The 18W UV lamp running the length of the reactor was fixed in the lamp holder. The walls of the reactor were lined with the TiO_2 coated sheet. Five (5) µl of liquid Isoflurane was injected via the septum and allowed to volatilize. The peristaltic pump was used to ensure uniform concentration throughout the reactor. Once the concentration had stabilized, the UV lamp was switched on and the Isoflurane concentration was measured and analyzed. It was observed that the GC-FID did not show any new peaks during the degradation testing of Isoflurane and Sevoflurane other than the background noise as shown in Fig 2.19 and 2.20.

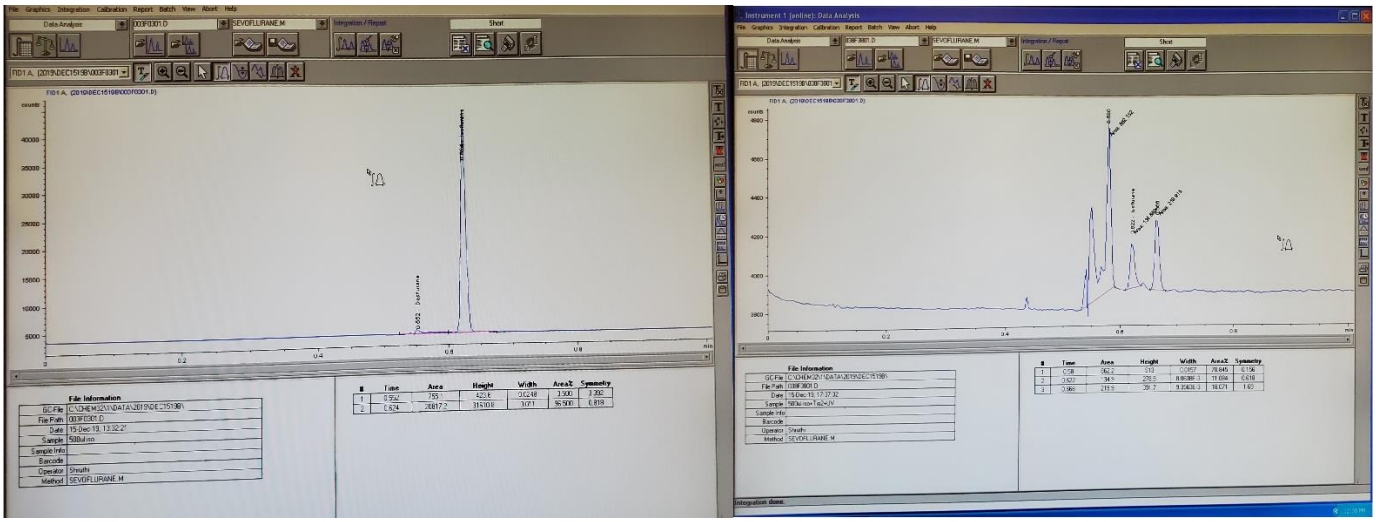

Figure 2.19: Chromatograms depicting peaks observed before (left) and after (right) the Isoflurane degradation

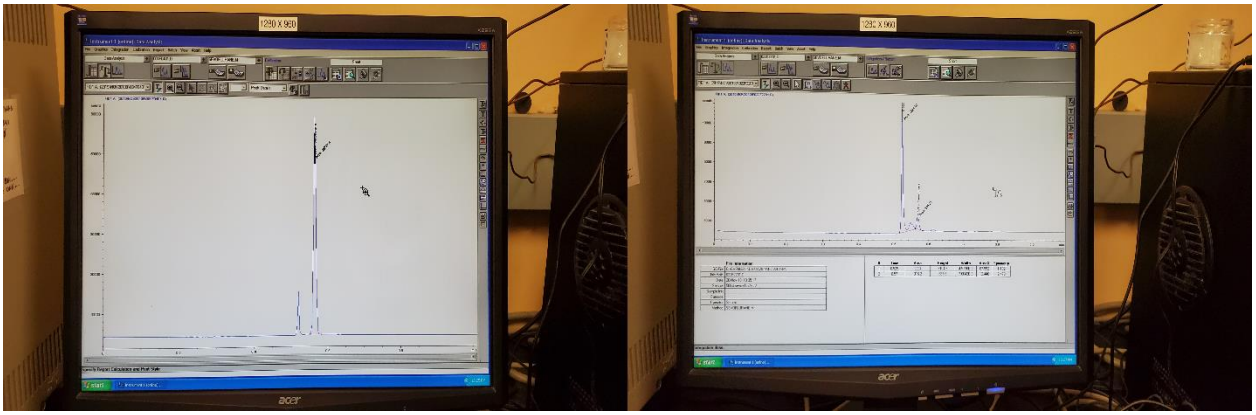

Figure 2.20: Chromatograms depicting peaks observed before (left) and after (right) the Sevoflurane degradation

The expected byproducts for the photocatalytic oxidation based on the literature review for Sevoflurane and Isoflurane are HF, HCl, CO_2, Compound A (CF_2=C(CF_3)-O-CH_2F), pentafluoropropanol. Of the 5 compounds HF, HCl and CO_2 cannot be detected by the GC-FID. Previous work hints at compound A might be a precipitate which again cannot be measured by GC. [109] Pentafluoropropanol is the only byproduct which is volatile and has C-H bonds, hence can be detected by the GC-FID however, since its sensitivity towards the FID isn't known, no precise conclusions can be drawn about the after-degradation peaks observed in Fig 2.19.

Based on the literature review, a new procedure for testing any potential water soluble samples using Ion Chromatography was drafted. The major challenge with analyzing the samples directly was that they were gaseous in nature. Two different techniques were incorporated to collect the samples for anion testing specifically for the water-soluble HF and HCl using ion chromatography with a detection limit of 0.1 mg/l.

First, the contents of the reactor after complete degradation were passed through a bubbler containing

30 ml DI using air as shown in Fig 2.21. The aim of the test was to capture the water-soluble degradation products from the reactor in the bubbler DI which could then be used for IC testing. It was required to keep the air flow rate to a minimum to ensure sufficient contact time and prevent the bubbler from over bubbling.

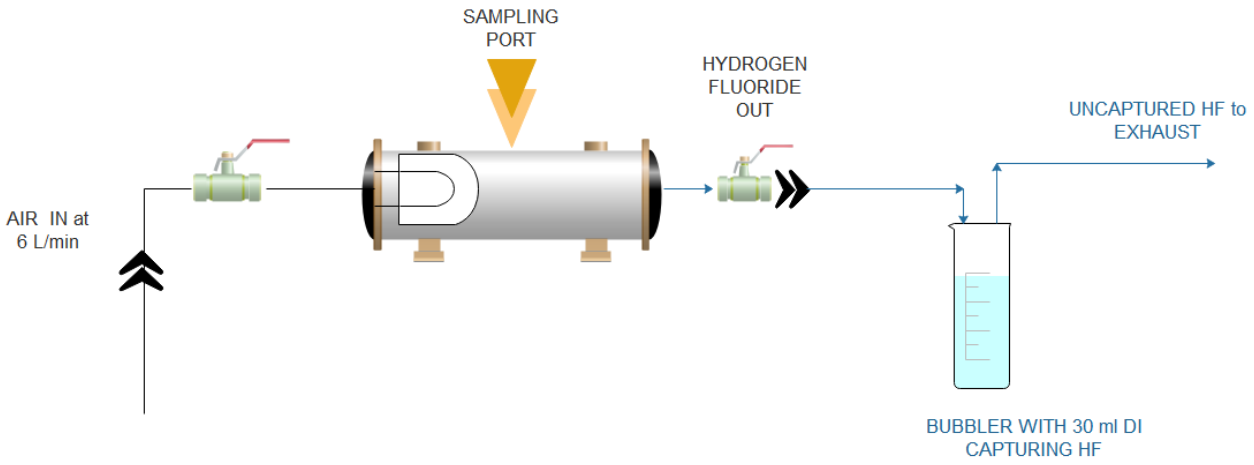

Figure 2.21: Sample collection setup for testing of byproducts from photocatalysis of Isoflurane

However, it was observed that the bubblers did not bubble at air flow rates below 6 L/min. The most probable reason for it being, leaks in the reactor probably at joints. For a reactor volume of 3.8 L it meant almost 40 seconds bubbling which was not sufficient for proper contact. Such high flow rates also compromised the bubbler capture efficiency.

Theoretically, if all of the Isoflurane inside the reactor had degraded to HCl and all of it was captured then 1.48 mg of chlorides (as shown in the appendices) was expected in the bubbler sample. However, the IC results obtained for the bubbled sample estimated a total of 0.00063 mg of fluorides and 0.01 mg of chlorides for the samples tested with the DI containing 0.00026 mg of fluorides and 0 mg of chlorides. The mass of fluorides detected by IC were much lower than the detection limit. Hence this

setup was not appropriate for sample collection since the high air flow rates into the bubbler reduced the capture efficiency of the bubbler and hence was abandoned.

Second, before starting the experiment, the walls of the reactor were washed with DI and the wash water was collected in a vial for testing. When the UV experiment was complete and the Isoflurane had completely degraded, the UV lamp was switched on for an additional 30 min to encourage desorption of any gas adhered to the reactor walls. After 30 min, the lamp was switched off and the catalyst sheet was washed sufficiently using DI in an attempt to simply remove the top layer off the surface and, collect it in a plastic vial. The sheet was then removed, and the same procedure was performed with the reactor walls. A sample of the DI used for reactor wash was also collected to be tested as a blank.

A major challenge observed with the catalyst surface wash water was that it was highly turbid due to the presence of TiO_2 particles. It was filtered using various pore sized filter papers and syringe filters (0.25 to 0.45 µm). It was even centrifuged to see if the supernatant could be used for IC. However, it was confirmed that even the supernatant was highly turbid, and it could not be analyzed using IC. Hence the catalyst wash sample was disregarded.

Hence, the reactor wall wash samples before and after the photocatalysis were only conducted to obtain a rough estimate of the possible byproducts from the UV-photocatalysis of Isoflurane and Sevoflurane.

2.4.6.1.Safety Procedures while Experimenting with Isoflurane and Sevoflurane

Past experimental work and literature review has shown that degradation of Isoflurane and Sevoflurane

produces hydrogen fluoride or hydrogen chloride. This hydrogen fluoride or hydrogen chloride when in contact with water forms the respective acid. HF acid is highly corrosive and fuming in nature, although this is highly dependent on its concentrations. It is extremely harmful to the ocular tissues and concentrations as low as 5 ppm is known to cause eye irritations. It also acts as an irritant to the mucosa of the upper and lower respiratory tract and one of its most common toxicities is its ability to penetrate through the skin into bones and replace the calcium present with fluoride.[81]

While capturing the anions with the bubbler setup, the theoretical mass of the maximum HF or HCl that may be produced if all of the reactant was to degrade (Sevoflurane/Isoflurane) was estimated. The amount of DI in the bubbler was altered to ensure that no more than 0.1% of the acid solution was being formed inside the bubbler to mitigate any risks while handling the bubbler.

The below actions were taken before handling any possible HF/HCl (g) or HF/HCl (l) sources:

1) Lab coat to cover the body
2) Disposable gloves with nitrile gloves on top secured with tape to the lab coat sleeve to prevent any direct skin exposure
3) Covered shoes to prevent harm during accidental spills
4) All equipments (tongs, scissor, bubblers and connections) once used were neutralized with a 10% $NaHCO_3$solution overnight followed by a rinse with DI followed by tap water.
5) The gloves once exposed to potential HF/HCl (g) or HF/HCl (l) were neutralized with a 10% $NaHCO_3$solution followed by DI and final rinsed with tap water.
6) The pH of the reactor wash sample was measured as soon as it was collected.
7) Calcium gluconate cream was made available to treat any accidental exposure to HF.

To decontaminate any exposed surfaces:

1) Once the reactor had been bubbled through or washed for sample collection, all the connections were removed and soaked in 10% $NaHCO_3$ solution followed by a rinse with DI.
2) The reactor was then de-assembled, and the non-electric ends and the body of the reactor were soaked in 10% $NaHCO_3$ while the electric end of the reactor was wiped clean with a sponge soaked in 10% $NaHCO_3$.
3) The above cleaning was followed by tap water wash followed by a DI rinse.
4) After cleaning, a fresh stream of air was passed through the reactor and sampled to ensure no traces of anesthetic were detected on the GC.

3.RESULTS AND DISCUSSION

3.1.Reproducibility

In order to ensure the validity of the conclusions deduced from each experiment, all the experiments were conducted three times on different days with the same setup. To ensure reproducibility, all the experiments were conducted with the same sampling instruments.

The error in the area counts as measured by the GC-FID when it was calibrated with 5 µl of Isoflurane is shown in Fig 3.1.

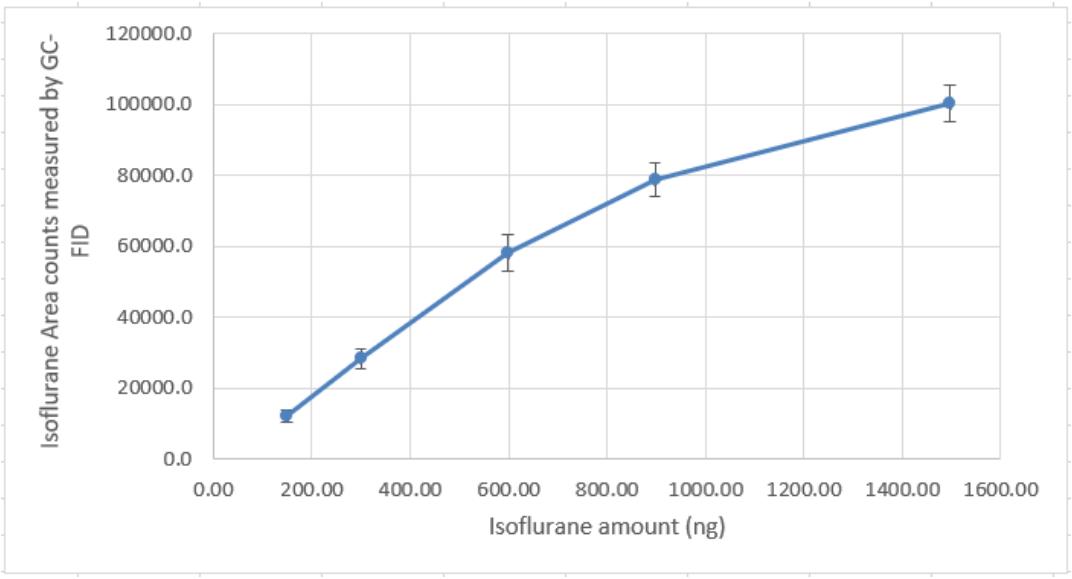

Figure 3.1: The error in area counts as measured during calibration of Isoflurane

The percentage error in the Isoflurane concentration when analysed at various times in the absence of any external factors sampled from the reactor on three different days is shown in Figure 3.2.

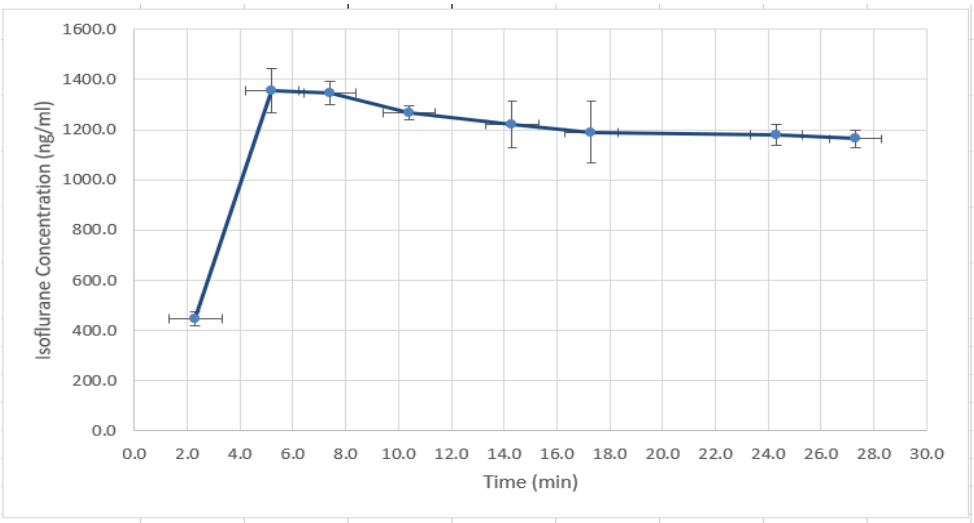

Figure 3.2: The variation in concentration in the absence of any external factor as measured with Isoflurane at various times

An error of 11 % (max) was observed at almost 17 min because, of the three trials done to study the wall effects of Isoflurane, in one trial the Isoflurane concentration fluctuated for almost 21 min after which it eventually decreased until the wall effects were saturated. Meanwhile for the other 2 trials the concentration had stabilized at almost 7 min after which it started to drop due to leaks.

The error in the Isoflurane concentration measured in the presence of UV light as sampled from the reactor is shown in Fig 3.3.

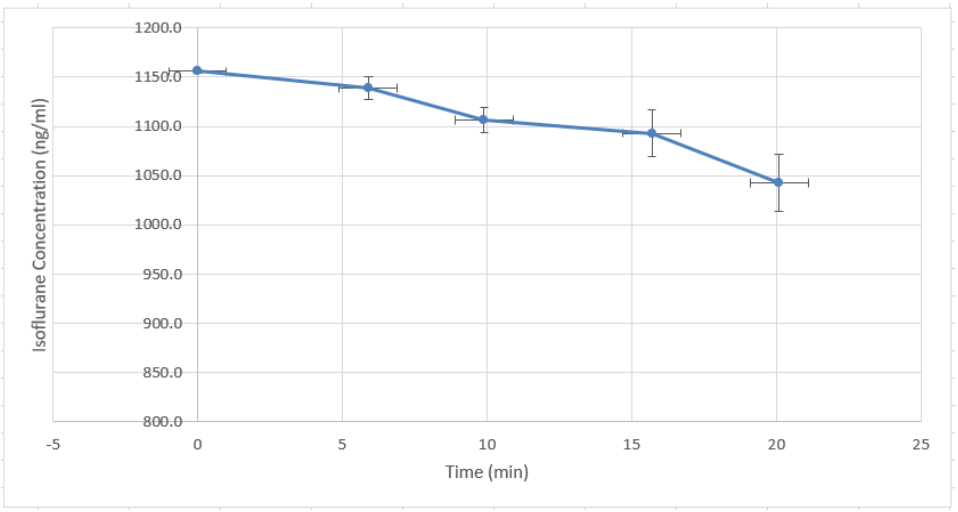

Figure 3.3: Variation in the Isoflurane concentration when measured during its UV-photolysis

A maximum error of 2.1 % was observed in the Isoflurane concentrations during photolysis over the multiple runs.

There were variations in the anesthetic gas concentrations measured throughout the sets of experiments even though efforts were made to try and keep the concentration as similar as possible. The variation in the anesthetic gas concentrations measured throughout the sets of experiment can be due to following reasons:

1. Variation in the anesthetic injection volume – A 10µl GC auto sampler syringe was used to inject 0.5 µl of the liquid sample. Due to its small orifice there was often air bubbles pulled in along with the sample. Even though efforts were taken to remove every single air bubble during sampling, there were times when the air bubbles were difficult to remove hence, the volume of actual sample injected into the reactor was tested using the pullback method which was different with each experiment by almost 0.2 µl. In the pullback method the syringe was flushed with the sample several times to wet the barrel and plunger. The required volume of sample was then drawn into the syringe. The needle was removed from the sample and the plunger was pulled back to induce a pocket of air as a marker. The volume occupied by the air bubbles inside the syringe was subtracted from the total sample volume inside the syringe. The sample was then injected into the bulb and the plunger was pulled back to determine the remaining sample volume inside the syringe. The remaining sample volume was subtracted from the inlet sample volume measured to obtain the precise injected volume.

2. The gas samples were taken using a Hamilton 500 µl GC gas tight syringe. Even though the samples when collected from the reactor were measured precisely, there were instances where carry-over occurred from injection to injection because the anesthetic gas from the previous injection would adhere to the teflon plungers of the syringe. Hence, subsequent concentrations

could have been higher than what was being taken out of the reactor, although it is believed this was less than 10% and was generally more of an issue at low concentrations. To minimize this effect, after each injection the teflon plunger was placed near the FID heater to volatilize any anesthetic adhered to the plunger.

3. The variation in the anesthetic gas concentration observed can be due to the injection method being followed during the experiments. The liquid anesthetic was injected via the septum on the top after which it is allowed to volatilize and circulated uniformly using the pump. This liquid falling inside the reactor might come in direct contact with either the reactor walls which were less absorbing or the more absorbing catalyst sheets which were lined against the reactor walls. Since the number of molecules of the catalyst at any point on catalyst sheet cannot be the same always, the extent of absorption of the liquid anesthetic entering the reactor by the catalyst molecules varied.

4. With time the wall effects have the ability to passivate. Hence at the very beginning there might have been greater percentage of anesthetic loss to wall effects which over the continuous use of the reactor might have diminished due to saturation.

5. Since it was a time-based experiment, the concentrations varied with change in time. Since not all samples for different experimental sets were taken at exactly the very same minute, changes in the resulting concentrations occurred. Therefore, the error for time and volume were combined and compared in Fig 3.2 and 3.3.

3.2.Comparing the Efficiency of Three Advanced Oxidation Processes in Degrading the Anesthetic Gas

Three advanced oxidation processes namely UV-photolysis, UV-ozonation and UV-photocatalysis were tested to determine their Halothane degradation efficiency.

3.2.1.UV-Photolysis

Five (5) µl of the liquid Halothane was injected into the reactor and allowed to volatilize. In the absence of any external factors the Halothane concentration was measured and analyzed in 500 µl volumes for a total time of 42 min until the wall effects were stabilized and constant leak rate was achieved. The 18 W UV light source was then switched on and 500 µl of the gas mixture from the reactor was sampled and the concentration of Halothane was measured using the GC as shown in Fig 3.4.

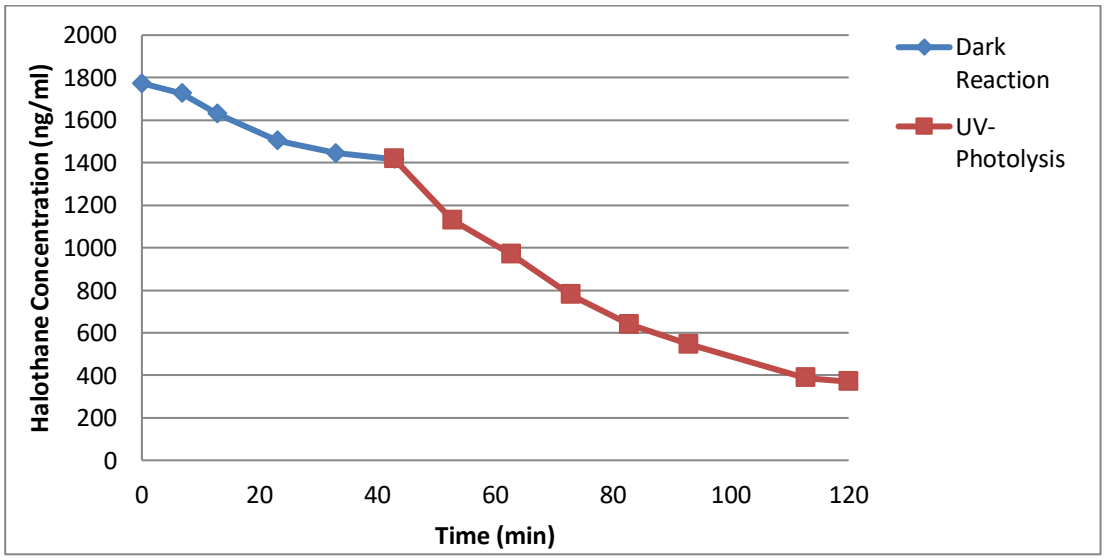

Figure 3.4: Change in the Halothane concentration with time in the absence and presence of UV light

With 1773 ng/ml of Halothane, in the absence of an appropriate excitation source (dark reaction),

Halothane was lost at a rate of ~ 9 ng/ml/min to leaks and wall effects. The decrease in the Halothane concentration was almost uniform at the start of the experiment but, eventually stabilized with time indicating stabilization of wall effects and constant leak rate. When the rate of decrease had dropped below 2 ng/ml/min, the light source was switched on.

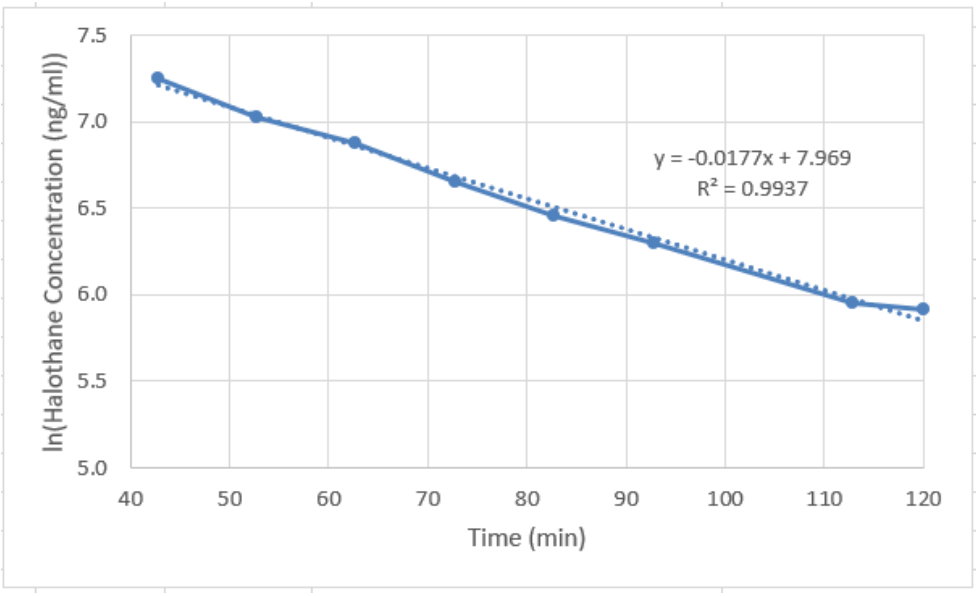

Figure 3.5: First order decay plot of Halothane concentration with time in the presence of UV light

The first order decay plot of Halothane in the presence of UV light was completely linear as shown in Fig 3.5. With 1400 ng/ml of Halothane, the rate of decrease of Halothane had increased to ~13 ng/ml/min in the presence of UV light source. However, the decrease eventually stabilized at around 70 min post irradiation. Overall, a 20% decrease during the dark reaction was recorded when compared to a 54% decrease in the presence of UV light over a time period of 40 min.

This increase in degradation rate can be attributed to Halothane's slight yet notable absorbance in the 254 nm range. An attempt to measure the absorbance was made by injecting 5 µl of Halothane inside the reactor and allowing it to volatilize. The resulting mixture was then flushed through a 10 cm UV

cuvette with air.

The absorption cross section of Halothane decreases from $1.25x10^{-18}$ cm^2/molecule at 204 nm to $4.5x10^{-20}$ cm^2/molecule at 254 nm.[84] At 254 nm, an absorbance of 0.013 was recorded for 2280 ng/ml of Halothane with a 10 cm cuvette as shown in Fig 3.6. For the 1400 ng/ml of Halothane that was present inside the reactor before the UV light was turned on, an absorption fraction of 0.0045 was calculated (as shown in the Appendices). Hence with the 18W lamp which emitted $3.33x10^{22}$ photons in 70 min at 254 nm, only $1.5x10^{20}$ photons is expected to be absorbed by the Halothane based on the absorption fraction calculated.

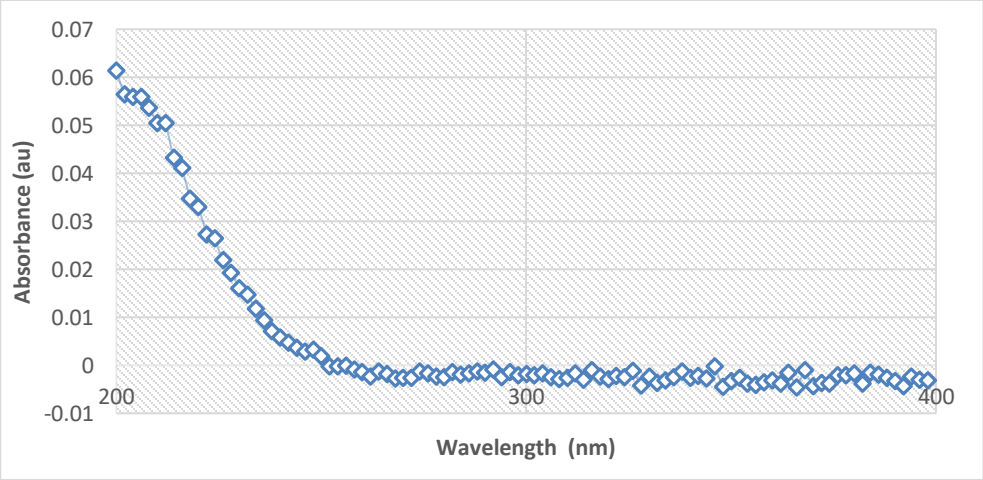

Figure 3.6: UV absorption spectrum 2280 ng/ml of Halothane measured in a 10 cm cuvette using the spectrophotometer

The UV spectrum of Halothane obtained during the current work showed a maximum absorbance at around 204 nm after which the peak started to flatten. This UV spectrum obtained is similar to the ones found by other researchers in the region of 187 – 300 nm where Halothane was found to show a maximum absorbance at 204 nm and eventually reduced to a minimum at 290 nm.[82,83] There was an additional absorbance peak observed at ~170 nm when the UV spectrum was measured between 160-300 nm wavelength as shown in Fig 3.7. [84]

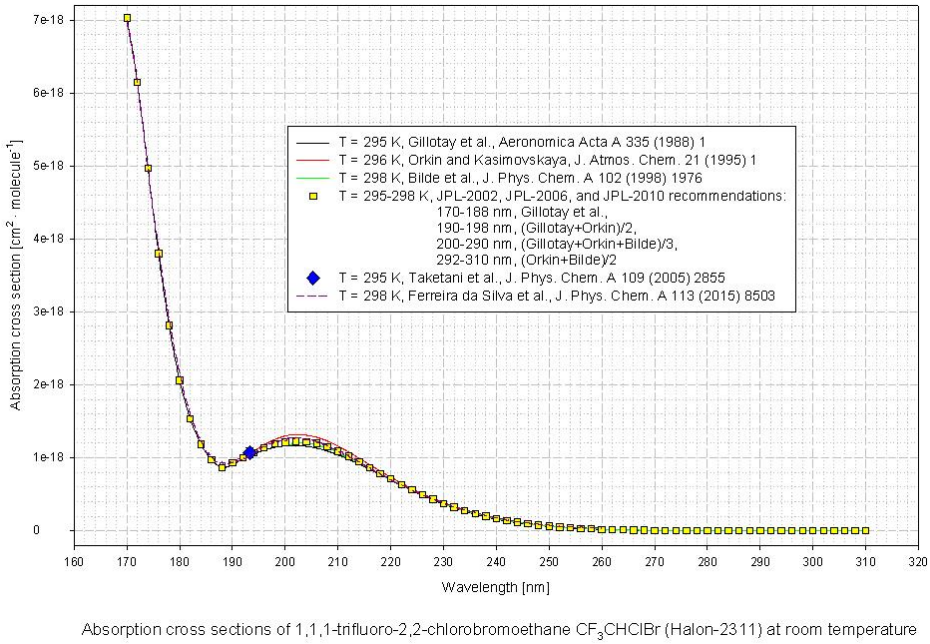

Figure 3.7: Absorption cross section of Halothane at room temperature showing an absorbance peak at ~ 170 nm.[84]

3.2.2.UV-Ozonation

The Ozomax ozone generator was used as a source of ozone for the experiments. To measure the amount of ozone produced, the ozone was generated for approximately 10 minutes, then a sample of the ozone output was collected in a 10 cm UV cell and a UV spectrum of the ozone in the cell was recorded with the spectrophotometer.

At 254 nm (the ozone peak centre), the absorption cross-section of ozone used was 1159×10^{-20} cm^2/molecule.[85] Based on the absorbance obtained from the UV spectrum of ozone it was estimated that 2315.8 ng/ml of ozone (1163 ppm) entered the reactor (as shown in the Appendices).

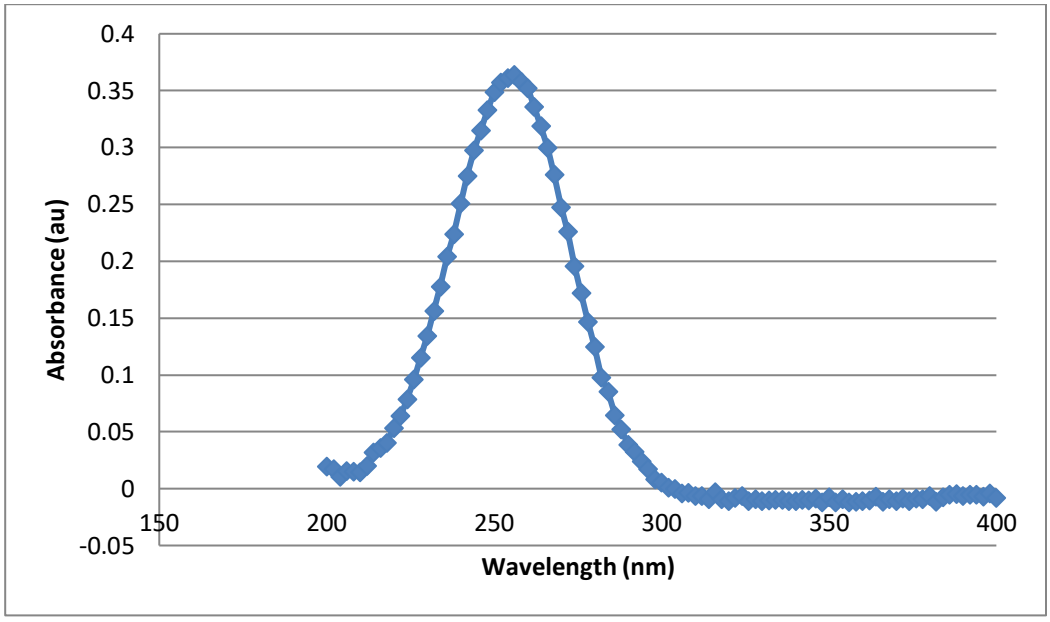

Figure 3.8: UV absorption spectrum of ozone as measured in a 10 cm cuvette using the HP8452 spectrophotometer

The UV spectrum obtained from the experiments as shown in Fig 3.8 is in complete agreement with the ones obtained by other researchers.[86] Ozone shows a maximum absorbance at 254 nm wavelength after which it starts to drop to almost 0 au at around 290 nm.

The ozone generated was then flushed through the reactor to replace the air for 10 minutes then, the ozone generation was discontinued, and the reactor was closed. Halothane measuring 5µl was then injected into the reactor, allowed to volatilize and then a gas sample was collected. The concentration was allowed to stabilize till the rate of decrease in Halothane concentration dropped to 3 ng/ml/min. The 18W UV lamp was then switched on and the concentration decrease was monitored by periodically analyzing 100 µl samples from the reactor using the GC as shown in Fig 3.9.

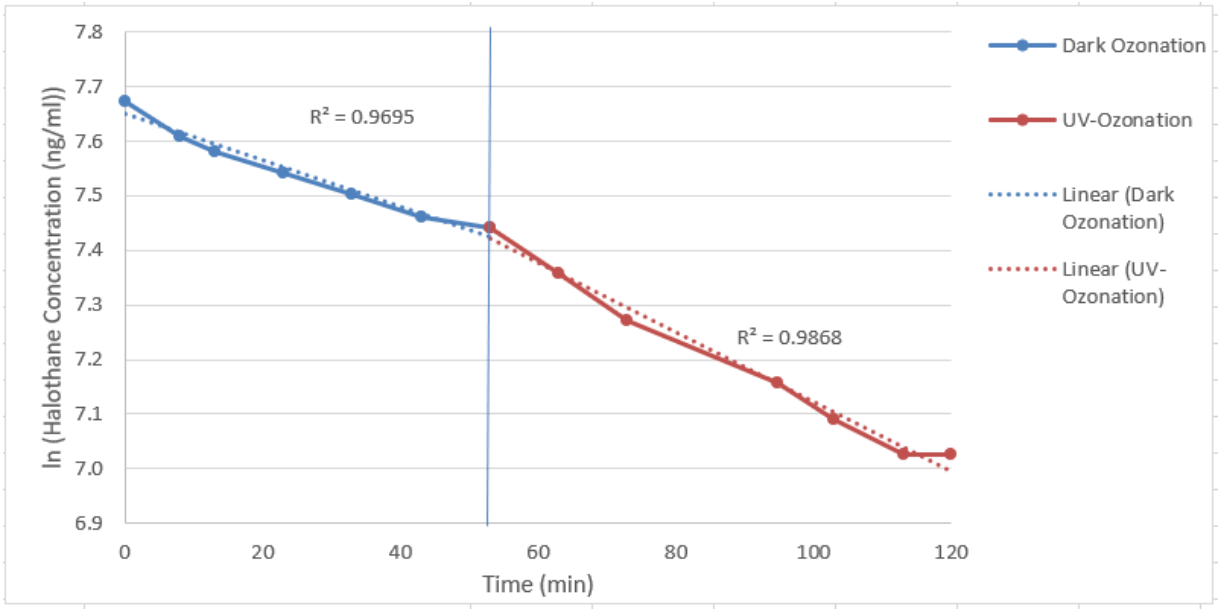

Figure 3.9: Change in Halothane concentration in the presence of ozone followed by decrease in Halothane when subjected to ozone and UV light

During the dark ozonation in the presence of 2150.7 ng/ml of Halothane as shown in Fig 3.9, the decrease in the concentration was almost linear as evident from the R^2 value. It was observed that no appreciable interaction occurred between Halothane and ozone in the absence of a light source. The loss in Halothane concentration was ~ 8.1 ng/ml/min in 50 min, which was almost equal the decrease observed in the case of dark reaction in photolysis (~ 8.9 ng/ml/min) as depicted in Fig 3.4. It can be concluded that this loss was primarily due to wall effects and leaks in the reactor.

With 1705.8 ng/ml of Halothane, it was observed that the rate of decrease in the concentration after turning on the UV light was ~ 8.7 ng/ml/min in 60 min which was not much different from the rate of decrease in the absence of UV light (~ 8.1 ng/ml/min). The wall effects brought a reduction of 482 ng/ml with 1773 ng/ml of Halothane, photolysis brought a reduction of 780 ng/ml with 1415 ng/ml of Halothane in 60 min as depicted in Fig 3.4, while UV-ozonation reduced 1705.8 ng/ml of Halothane by 522 ng/ml in the same time.

A possible reason for the slightly improved degradation efficiency of UV-photolysis in comparison to UV-ozonation may be due to the less efficient degradation of Halothane through OH^o radical. The absorption cross-sections of Halothane and ozone at 254 nm are $4.24x10^{-20}$ and$1.5x10^{-17}$ cm^2/molecule respectively.[84] With an almost 300 times greater absorbance area count, ozone absorbs more than 99% of the incident photons if present in equal amounts with Halothane. In this case 1163 ppm of ozone was present with only 30 ppm of Halothane hence, both halothane and ozone compete for the incident photons. Ozone may absorb more photons, but it appears not to really produce oxidizing agents, likely due to a lack of moisture inside the reactor. When irradiated with UV light, the ozone inside the reactor dissociates to form O_2 and O atom which can either recombine or the nascent oxygen atom (O) might combine to produce O_2 in the absence of moisture. Hence, due to absorption of 99.99% of the incident photons by ozone, this combined with Halothane's very low absorption coefficient leads to insufficient photons to produce a measurable change.

The formation of oxidizing agents such as the hydroxyl radical (OH^o) and superoxide radical (O_2^{o-}) occurs when ozone is irradiated in the presence of water with the air. Since the compressed air used has only 11% humidity, this appears to have been insufficient to produce enough OH^o radicals to introduce any change when compared to UV-photolysis.

3.2.3.UV-Photocatalysis

The UV-photocatalytic degradation efficiency of Halothane was tested using TiO_2 catalyst. The reactor walls were lined with the catalyst coated support sheet and 5µl of the liquid anesthetic was injected into the reactor. The resultant gas was sampled in 500µl volumes from the reactor and analyzed until equilibrium was reached indicating saturation of Halothane absorption onto the catalyst surface and a

constant leak rate. Once the reduction rate had dropped below 3 ng/ml/min, the 18 W UV light was switched on and 500µl of the gas was sampled from the reactor and analyzed using the GC-FID until all the Halothane had been degraded as can be seen from the data in Figure 3.10.

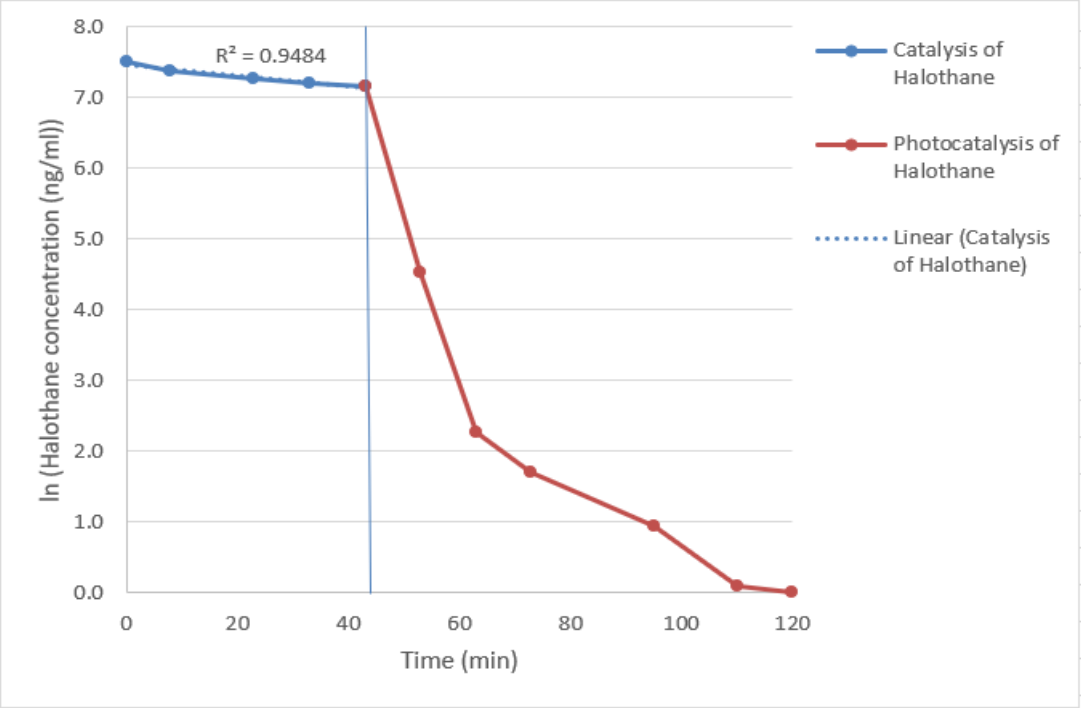

Figure 3.10: Change in the Halothane concentration with time due to wall effects, leaks and absorption on to the TiO_2 surface followed by the change in concentration when subjected to UV-photocatalysis

In the case of dark photocatalysis, the increase in the concentration reduction rate when compared to the dark reaction during photolysis was due to a combination of wall effects, leaks and absorption on to the TiO_2 surface. A concentration of 562 ng/ml of Halothane from a total concentration of 1810.7 ng/ml was lost during the dark photocatalysis when compared to a loss of 362 ng/ml during the dark reaction in photolysis. The decrease in Halothane concentration in the case of UV-photocatalysis was not linear as can be seen from Figure 3.10. The photocatalysis of the anesthetic gas was assumed to be apparently first order whereas the actual anesthetic gas degradation was due to both photolysis and photocatalysis

in the presence of UV light. With a starting concentration of 1295.7 ng/ml, the rate of decrease was 125 ng Halothane/ml/min within the 1st 10 min of UV irradiation, which accounted for 93% of the total Halothane degradation. The rate of decrease then dropped to ~8 ng/ml/min for the next 10 min probably due to the limited availability of the reactant or reduced activity of the catalyst surface and finally stabilized to around 0.2 ng/ml/min for the remaining duration of the experiment.

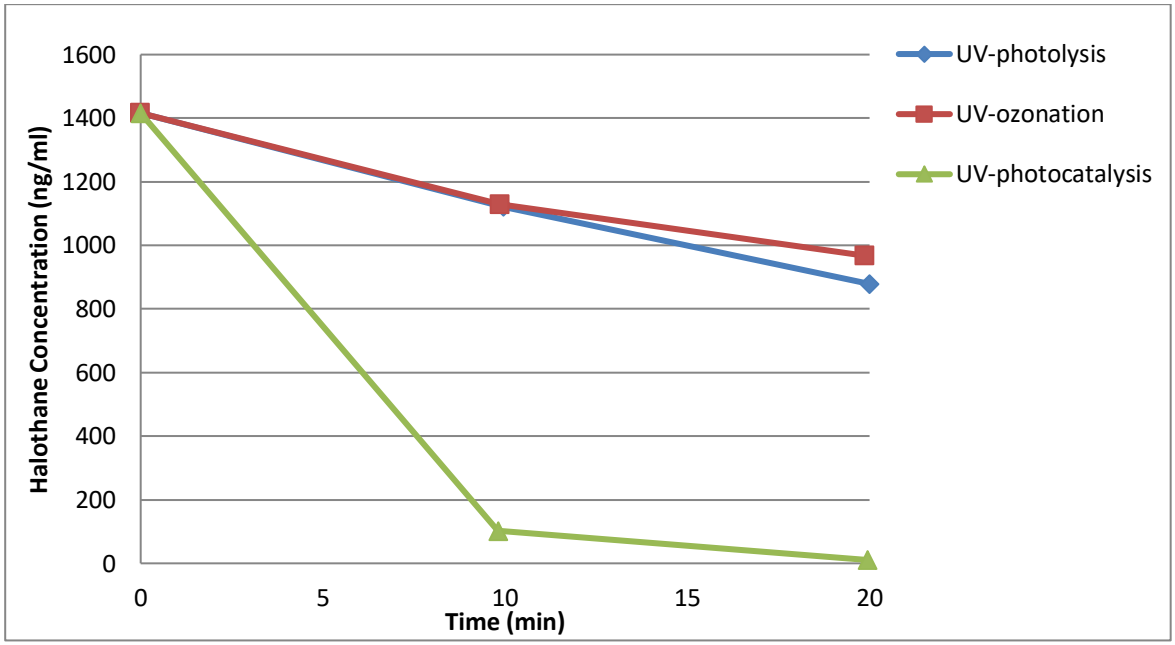

Figure 3.11: Halothane degradation efficiency of three AOPs namely UV-ozonation, UV-photolysis and UV-photocatalysis.

Fig 3.11 compares the Halothane degradation efficiency of the three AOPs over 20 min. UV-photocatalysis achieved ~99.9% Halothane degradation compared to a degradation of ~ 35% for both UV-ozonation and UV-photolysis. The presence of the catalyst improved the degradation efficiency since in the presence of UV light, TiO_2 acts to produce hydroxyl radicals which accelerate the anesthetic degradation.

UV-ozonation of Halothane did not yield significantly different results than UV-photolysis. This was

likely due to the scavenging of most of the light by ozone owing to its greater absorption cross-section and higher concentration than that of halothane.

To establish if this same phenomenon would occur with Isoflurane and Sevoflurane, the UV absorption spectrum was recorded as was done with Halothane. The recorded UV spectrum for Isoflurane and Sevoflurane is shown in Fig 3.12 and 3.13.

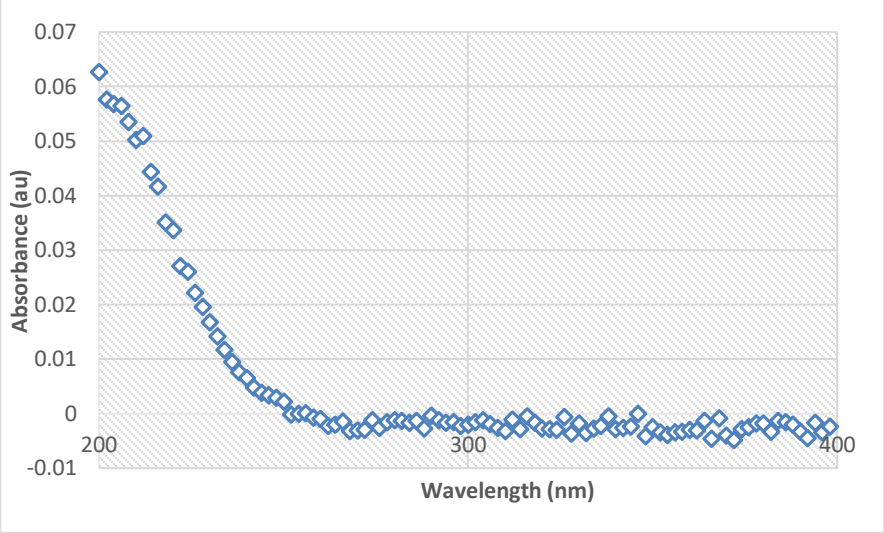

Figure 3.12: UV absorption spectrum of 1200 ng/ml of Isoflurane

The UV absorption spectrum recorded for Isoflurane showed a maximum absorbance at ~ 200 nm as shown in Figure 3.12 with an absorption cross section of 2.61×10^{-21} cm^2/molecule.[84] A similar absorbance curve depicting maximum absorbance of Isoflurane at 200 nm had been obtained by other researchers.[83]

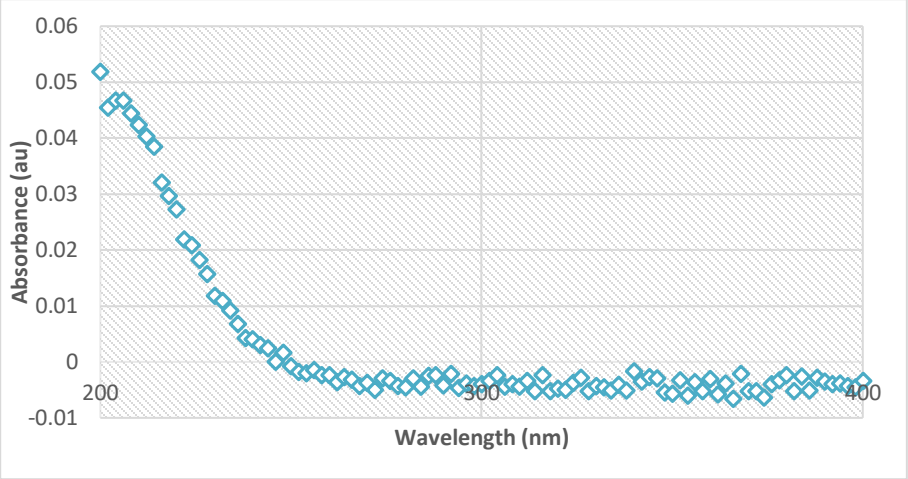

Figure 3.13: UV absorption spectrum of 1567 ng/ml of Sevoflurane

Unlike the UV absorption spectrum obtained by other researchers which suggest that Sevoflurane does not absorb in the UV region[83], the UV spectrum obtained in the current research as shown in Fig 3.13 depicts a similar absorbance pattern for Sevoflurane with an absorption cross section of 1.331×10^{-20} cm^2/molecule.[84] The theoretical absorption cross sections for these two anesthetic gases were compared with ozone. Since their absorption cross-sections were smaller in magnitude than Halothane (2.6×10^{-21} and 1×10^{-20} respectively),[84] their behaviour when subjected to ozonation was presumed to be similar if not lower than Halothane. Hence, further tests with these gases were carried out only using UV-photolysis and UV-photocatalysis.

Once UV-photocatalysis was determined to be the preferred degradation technique among the ones tested, the logical next step was to determine the preferred catalyst to be used.

3.3.Effect of the Type of Photocatalyst Used on the Anesthetic Gas Degradation Rate

The efficiency of ZnO and TiO_2as a photocatalyst in degrading Halothane and Sevoflurane was compared in this experiment.

The reactor walls were lined with the catalyst coated support sheet and 5µl of the anesthetic liquid was injected into the reactor and allowed to volatilize. The contents of the reactor were mixed using the peristaltic pump. The resultant gas was sampled until equilibrium was reached, indicating no further absorption onto the catalyst surface and a constant leak rate. The 18 W light source was then switched on and, 500µl of the gas was sampled at intervals over 20 min and analyzed using the GC-FID as depicted in Fig 3.14 and Fig 3.15.

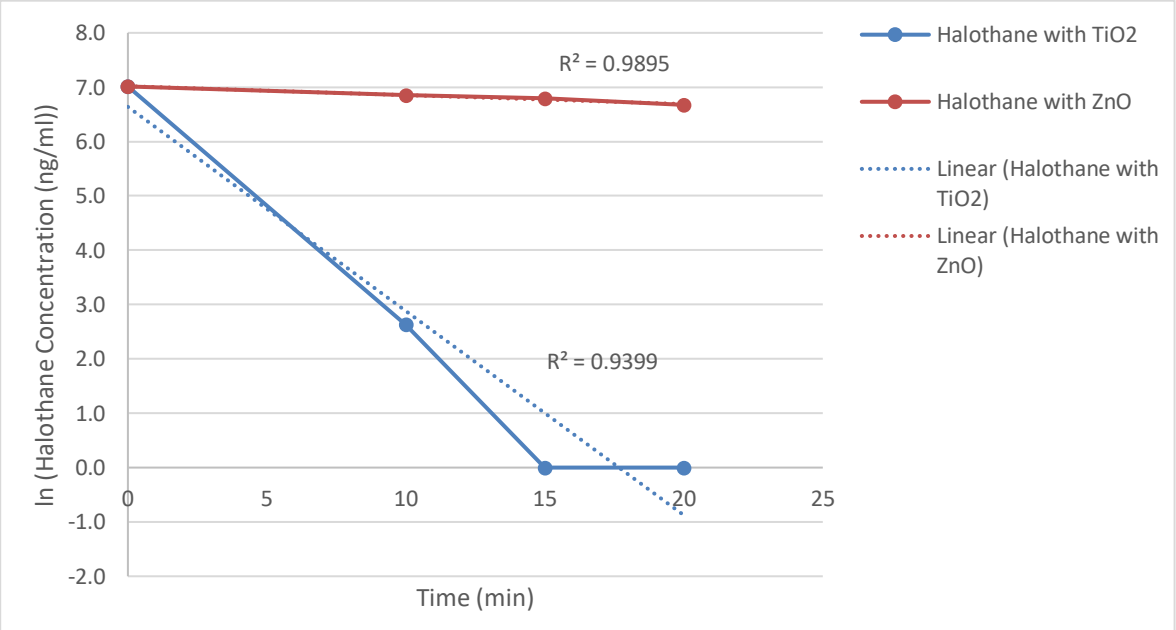

Figure 3.14: Change in the Halothane concentration when subjected to UV-photocatalysis the presence of TiO_2 and ZnO

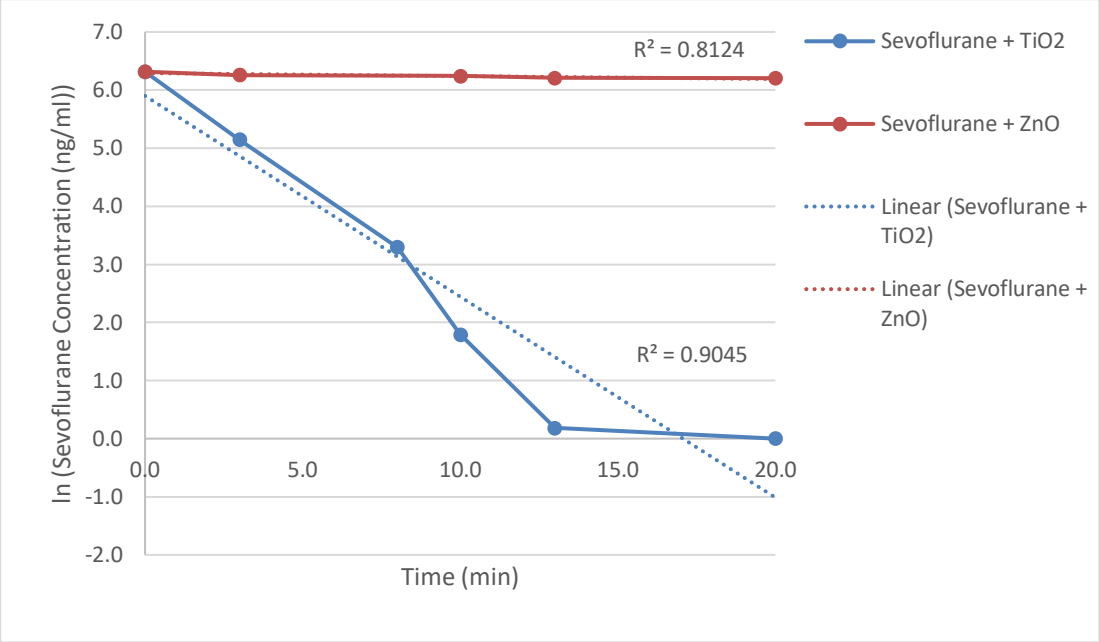

Figure3.15: Change in the Sevoflurane concentration when subjected to UV-photocatalysis the presence of TiO_2 and ZnO

The experiments clearly indicated that TiO_2 was more efficient in oxidizing both Halothane and Sevoflurane in the presence of UV light than ZnO where the rate of decrease was rather insignificant.

During the dark photocatalysis, in the presence of TiO_2 and ZnO, both Halothane with an initial concentration of 1111.4 ng/ml (33.5% and 26.2%) and Sevoflurane with an initial concentration of 553 ng/ml (22.2% and 20%) absorbed almost equally on the respective catalyst surfaces. This suggested that they had almost a similar affinity to the catalysts tested.

The degradation rate in the case of Sevoflurane and Halothane with ZnO and UV was insignificant. This suggested that both Halothane and Sevoflurane did not degrade significantly with ZnO as a photocatalyst.

With a starting concentration of 1111.4 ng/ml, the rate of decrease of Halothane with TiO_2 and UV was

drastic, with a loss of 1100 ng/ml in the first 10 min of irradiation accounting for a 98.7 % loss of Halothane. Due to the depletion of the reactant (~13 ng/ml) or accumulation of byproducts or reaction intermediates on the catalyst surface the rate of reaction slowed down to 2.8 ng/ml/min afterwards. A similar trend was observed in the case of 553 ng/ml of Sevoflurane with a loss of almost 500 ng/ml in the first 10 min of irradiation. This decrease however stabilized after 10 min by which time 98.9% of the Sevoflurane had already degraded.

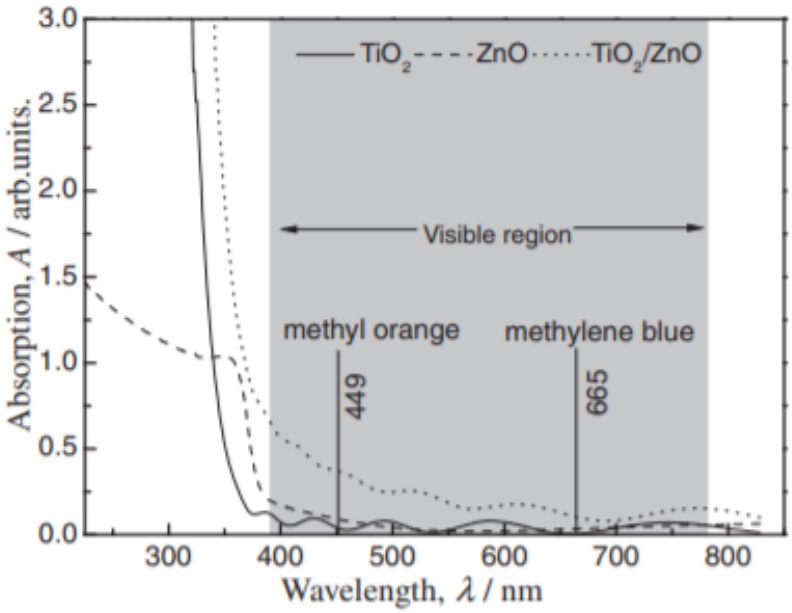

Figure 3.16: UV/Vis absorbance spectrum of TiO_2, ZnO and TiO_2/ZnO.[87]

Even though TiO_2 and ZnO have almost similar band gaps of 3.33 and 3.26 eV respectively, the UV-Vis absorbance spectrum of TiO_2 and ZnO films clearly shows that TiO_2 has a much larger absorbance than ZnO at 254 nm as shown in Fig 3.16[87]. Since the reference does not talk about the individual concentrations or the path length of the cell while measuring the UV spectrum of ZnO and TiO_2, we presume that the UV spectrum recorded for ZnO and TiO_2 in Fig 3.14 was carried out in the same UV cell and with similar concentrations. Not many electron hole pairs would have been formed in the case

of ZnO with the incident light at 254 nm due to its lower absorption cross section thus limiting the production of OH^{o} radicals. This possibly is the reasons for the limited anesthetic degradation rate of ZnO. The difference in the form of catalyst particles used: TiO_2 in the form of nanopowder and ZnO in plain powder form can also possibly influence the amount of catalyst surface area available during UV-photocatalysis.

Experiments conducted with ZnO and TiO_2 by other researchers on photocatalysis of selective impurities in water have given similar results as obtained in this experiment.[88-91] TiO_2 had shown greater degradation efficiency in the UVC region when compared to ZnO. TiO_2 was found more efficient in the acidic environment while ZnO was efficient in the alkaline region for the removal of poly vinyl chloride from aqueous solutions.[88] ZnO nanopowder was less efficient in degrading textile wastewater when compared to TiO_2 at 254 nm due to its lesser purity.[89] ZnO was observed to be more efficient in degrading estrone from wastewater than TiO_2 only in the UVA region (315-400 nm), while in the UVC (100-280 nm) region TiO_2 was more efficient in degrading estrone present in water (compound often used in treating the membranes after being used for reverse osmosis) than ZnO. This change in efficiency can be possibly attributed to ZnO's greater absorbance than TiO_2 in the UVA region.[90]

3.4.Influence of the Incident Light Source Wavelength on the Anesthetic Gas Degradation Rate

Illumination was provided by a 9W 254 nm and a 365 nm UV lamp for comparing the effect of different UV wavelengths on the anesthetic gas degradation rate. This setup was used in the absence of the catalyst sheet for UV-photolysis as shown in Figure 3.17 and in the presence of catalyst TiO_2 coated

aluminum sheet for photocatalysis as shown in Figure 3.18.

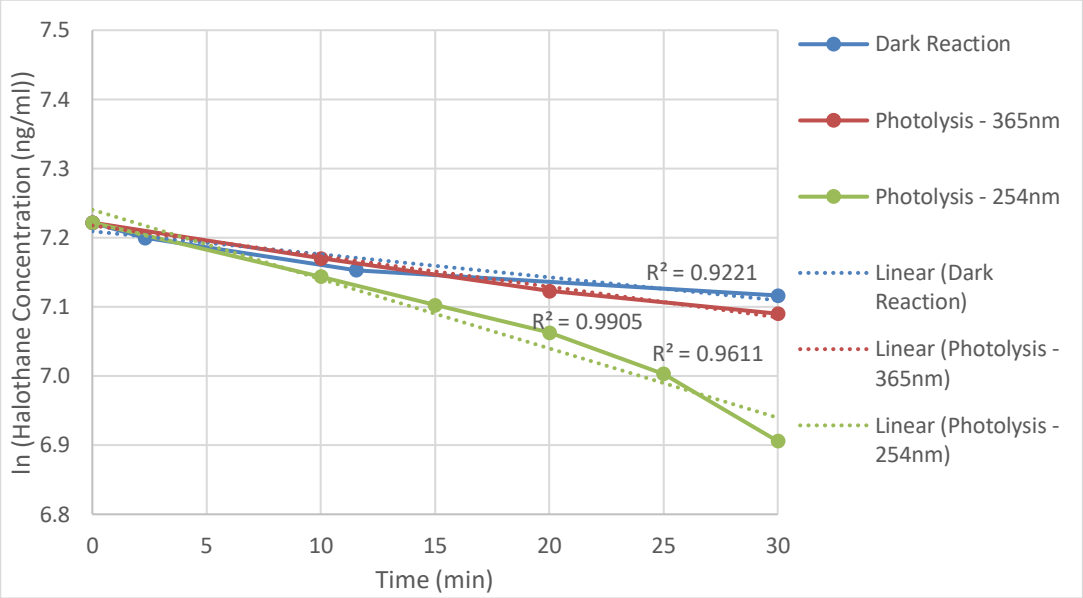

Figure 3.17:Influence of the incident light wavelength on the Halothane degradation rate in the absence of the photocatalyst

In the absence of any UV irradiation, the rate of degradation of 1300 ng/ml of Halothane due to wall effects and leaks was ~ 7.5 ng/ml/min. With 1368.9 ng/ml of Halothane, in the presence of the 365 nm light source, the degradation rate slightly increased to ~ 8.3 ng/ml/min. However, in the case of the 254 nm light source with the same Halothane concentration, ~ 12 ng/ml/min of decrease was observed. In the time of 30 min for which each of these experiments was conducted, 225 ng/ml of Halothane was lost due to leaks, 249 ng/ml was lost due to leaks and photolysis with the 365 nm UV light source and 360 ng/ml was lost due to leaks and photolysis with the 254 nm light bulb. An overall decrease of 12.3% and 27% was observed during the photolysis of 1368.9 ng/ml of Halothane in the presence of 365 nm light source and 254 nm light source respectively in 30 min.

The 9W 254 nm light source produces 3.83×10^{18} photons/sec while the 365 nm lamp produces

$5.50x10^{18}$ photons/sec. The absorption cross section of Halothane decreases from $4.5x10^{-20}$ cm^2/molecule at 254 nm to $<1.20x10^{-23}$ cm^2/molecule (approximately) at 365 nm.[84] Hence with these absorption cross sections in 30 min at 254 nm, $1.58x10^{19}$ molecules of Halothane will absorb $3.04x10^{19}$ photons and at 365 nm Halothane will absorb $1.17x10^{16}$ photons (as shown in the appendices). Since much lower photons are absorbed by Halothane at 365 nm than at 254 nm, UV photolysis at 254 nm was much more profound than at 365 nm.

To test the influence of the incident light wavelength on UV-photocatalysis of Halothane, the reactor wall was lined with the TiO_2 coated aluminum sheet. Five (5) µl of the liquid Halothane was injected into the reactor, allowed to volatilize and then sampled till stabilization. Once the Halothane concentration was found to be stable, the light source was switched on to test the degradation efficiency as plotted in Figure 3.18.

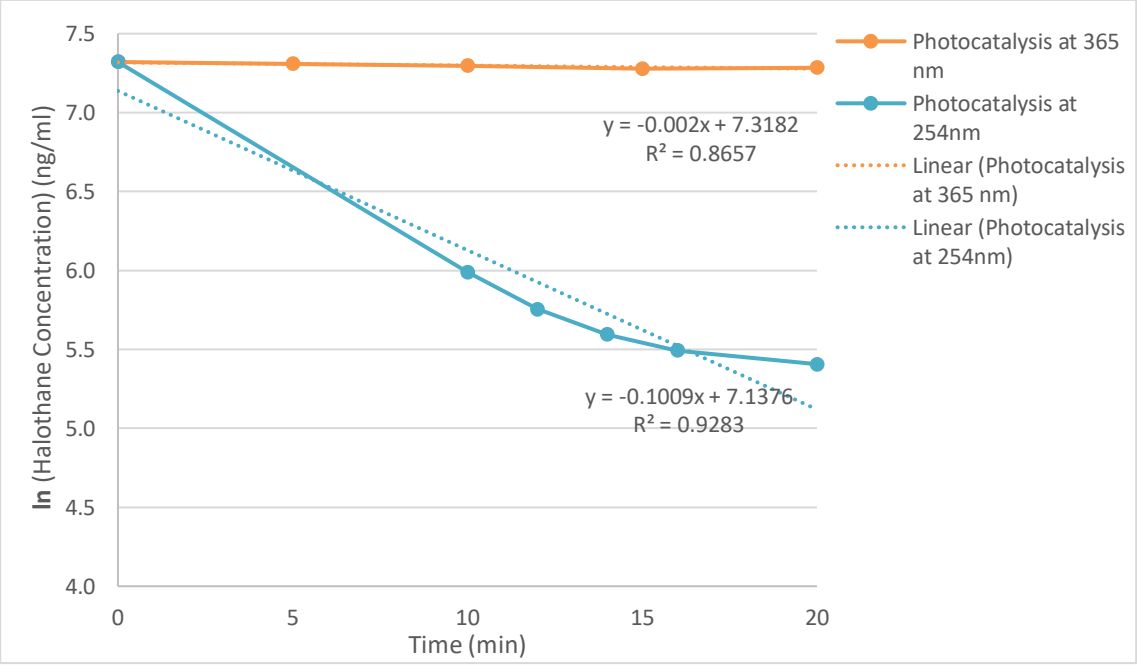

Figure 3.18: Change in the Halothane concentration with time when subjected to photocatalysis with two different incident light wavelengths

In the presence of 1511 ng/ml of Halothane, with the 365 nm light source, the change in Halothane concentration with time was negligible during photocatalysis with a decrease of 3% in 20 min. The 1st order decay curve plotted in Fig 3.18 is almost a linear fit in the case of UV-photocatalysis with 254 nm light source with a reaction rate coefficient of 0.1 min^{-1} indicating that the rate of reaction is dependent purely on the reactant concentration. Just like in the other experiments conducted above, the rate of degradation was extremely high in the first 10 min with a loss of 111.1 ng/ml/min of Halothane accounting for 74% of the total degradation. A total degradation of 85% was recorded during photocatalysis with the 254 nm light source.

The 9W 254 nm light source produces $3.83x10^{18}$ photons/sec while the 365 nm lamp produces $5.50x10^{18}$ photons/sec. According to the UV spectrum in Fig 3.16 the absorbance of TiO_2 at 254 nm is almost three times the absorbance at 365 nm. Hence TiO_2 will probably absorb 99% more photons at 254 nm than at 365 nm thereby, producing more OH^o radicals which will accelerate the photocatalysis of Halothane. The greater absorbance of TiO_2 at 254 nm coupled with the relatively greater absorption cross section of Halothane at 254 nm when compared to 365 nm possibly contribute to the greater photocatalytic degradation rate of Halothane at 254 nm when compared to 365 nm.

3.5.Influence of the Power of the Light Source on the Anesthetic Degradation Rate

From the results obtained in Section 3.4, it was evident that the light source output at 254 nm was more efficient in degrading Halothane. The next step was to determine the influence of the power of the light source on the anesthetic degradation rate by comparing the results for the 9W and 18W lamps.

The reactor after being flushed with compressed air was fed with 5µl liquid Halothane. Once the

Halothane had volatilized and the concentration had stabilized the UV light source was switched on for 30 min to monitor the decrease in the Halothane concentration.

The influence of the power of the UV bulb was also tested using photocatalysis. The photoreactor was once again flushed with the compressed air. The reactor walls were lined with the same amount of TiO_2 for both the light sources. Five µl of Halothane was injected into the reactor, allowed to volatilize and the peristaltic pump was switched on to ensure uniform mixing within the reactor. Once the Halothane concentration was found to be stable, the UV light source was switched on to monitor the decrease in the Halothane concentration. Figure 3.19 compares the Halothane degradation efficiency of the 9 W light source with a length of 210 mm against the 18W UV light source with a length of 325 mm in terms of photolysis and photocatalysis.

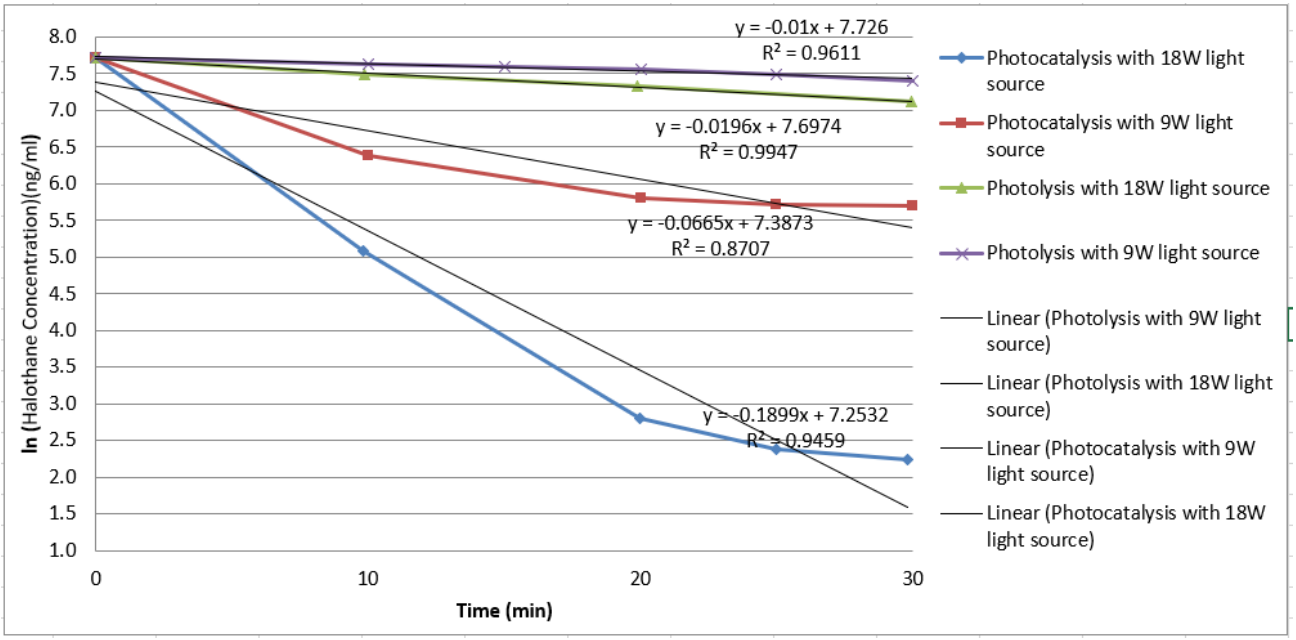

Figure 3.19: 1st order decay plot of Halothane under the influence of 9W and 18W UV light source

The 1st order decay plot of Halothane is not perfectly linear in all the four cases as observed from their R^2 values. For the photolysis of 2224.6 ng/ml of Halothane, a loss of 32 ng/ml/min with the 18W UV

lamp and a loss of 19 ng/ml/min with the 9W UV lamp were recorded with a degradation of 45% and 27% respectively in 30 min. For the photocatalysis of 2224.6 ng/ml of Halothane, a loss of 110.4 ng/ml/min in 20 min with the 18W UV lamp and a loss of 95.4 ng/ml/min in 20 min with the 9W UV lamp was recorded. A total degradation of 87% and 99.8% was achieved, when subjected to photocatalysis with the 18W and the 9W lamp respectively in 30 min.

For the duration of the experiment, the 18W lamp emitted $1.38x10^{22}$ photons while the 9W lamp emitted $6.89x10^{21}$ photons assuming 33.3% of the supplied energy was converted into light. The photoreactor contained $2.59x10^{19}$ molecules of Halothane, hence based on the absorption cross section of Halothane, with the 18W lamp $9.86x10^{19}$ photons will be absorbed by the 2224.6 ng/ml of Halothane and with the 9W lamp the same amount of Halothane will absorb $4.92x10^{19}$ photons Assuming quantum yield=1, the measured absorption spectrum of Halothane was accurate, the conversion in the lamp is accurately 33.3% and the absorption characteristics of the anesthetic do not vary once inside the reactor, a complete degradation of Halothane during photolysis with the 9W lamp is expected since, the amount of photons absorbed by the Halothane in the presence of the 9W lamp source is greater than the total number of Halothane molecules present inside the reactor. In such a scenario, Halothane acts as a limiting agent and the excess photons produced and absorbed in the presence of the 18 W lamp source do not add much value. However, this is not in accordance to what was observed during the photolysis experiment since, at the end of 30 min unreacted Halothane was observed inside the reactor. Hence one or more of the assumptions are incorrect. The excess photons generated by the 18 W lamp could potentially interact with more Halothane to cause a greater photodegradation during photolysis if there were a lot more halothane molecules to interact with.

In the case of photocatalysis, the catalyst sheet has $3.4x10^{22}$ molecules of TiO_2, these excess electron hole pairs generated from the 18W light source interact with a greater amount of TiO_2 molecules to

further generate $OH^{\bullet}$ radicals that increase the degradation rate of Halothane. Another probable reason for increased degradation is the varying length of the 2 light sources used. Since the 18W lamp ran the length of the reactor, the entire catalyst sheet was illuminated by the incident photons and hence participated in the degradation, however, the 9W lamp barely covered 70% of the catalyst sheet hence the contribution of the remaining 30% of the catalyst sheet in the degradation would have been limited.

The reaction rate coefficients in case of photolysis with the 9W and the 18W UV light source were 0.01 min^{-1} and 0.02 min^{-1} respectively. In the case of photocatalysis, the reaction rate constant initially started with 0.13 $min^{-1}$and 0.26 min^{-1} with the 9W and 18W lamp, however, in the next 30 min the reaction rate dropped by 46 % and 30% to 0.07 min^{-1} and 0.18 min^{-1} respectively.

Even though no reaction intermediates were detected on the GC during the photocatalysis, a possible buildup of by products or reaction intermediates such as HF, HCl and HBr on the photocatalyst can reduce the degradation rate. In the case of the 9W UV lamp, the reactor still had sufficient Halothane to be degraded after 30 min of treatment, hence catalyst poisoning, deactivation or lack of oxidizing radicals due to reduced photon generation is a probable reason for the drop in the reaction rate constant.

Literature suggests similar results were obtained with degrading Eosin Y (stain used in histological studies) in water, where the rate of degradation dropped from 93 to 82 % when the lamp power was reduced from 16 W to 6 W with ZnO as a photocatalyst.[92] Review also suggests that the single pass removal efficiency of Isoflurane increased consistently with an increase in the light intensity from 1 – 4 $mW.cm^{-2}$ in a closed loop multi pass reactor with TiO_2 as a catalytic medium.[75]

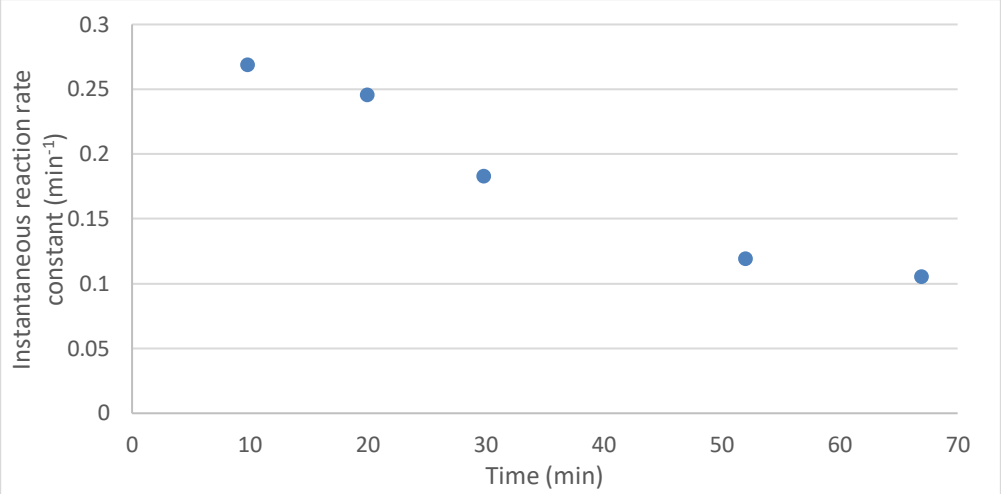

Figure 3.20: Variation of reaction rate with time for Halothane in the presence of 18W UV lamp

The instantaneous reaction rate constants for the photocatalysis of Halothane decreased with time as shown in Fig 3.20. This suggests that OH^{o} radicals are the primary contributors in the oxidation of Halothane. However, no literature is currently available to obtain a deeper insight into the Halothane chemistry.

The above studies have clearly shown that UV-photocatalysis with TiO_2 and an 18W 254 nm UV lamp was a more effective technique among the ones tested to degrade the anesthetic gases being emitted from the health care facilities directly into the environment.

3.6.To Test the Influence of Catalyst Area Illuminated on the Anesthetic Gas Degradation Rate

Since the 18W UV lamp source ran the entire length of the reactor, the relatively smaller 9W UV lamp with a length of 210 mm was used to test the influence of the catalyst surface area illuminated on the anesthetic gas degradation rate. To rule out the possibility of blind spots i.e. a possibility of selective

catalyst sites not receiving the emitted photons, thus preventing them from participating in the photocatalysis, the test described below was performed.

Two media containing equal amounts of TiO_2 catalyst, one extending to the length of the UV lamp (21 cm x 25 cm) and the other extending to the length of the reactor (30 cm x 25 cm) were fabricated. These catalyst coated sheets were lined against the reactor walls. Five (5) µl of Halothane were injected via the inlet septum and allowed to volatilize. After the concentration had stabilized, the UV lamp was turned on. The resulting gas concentrations measured using the GC is presented in Fig 3.21.

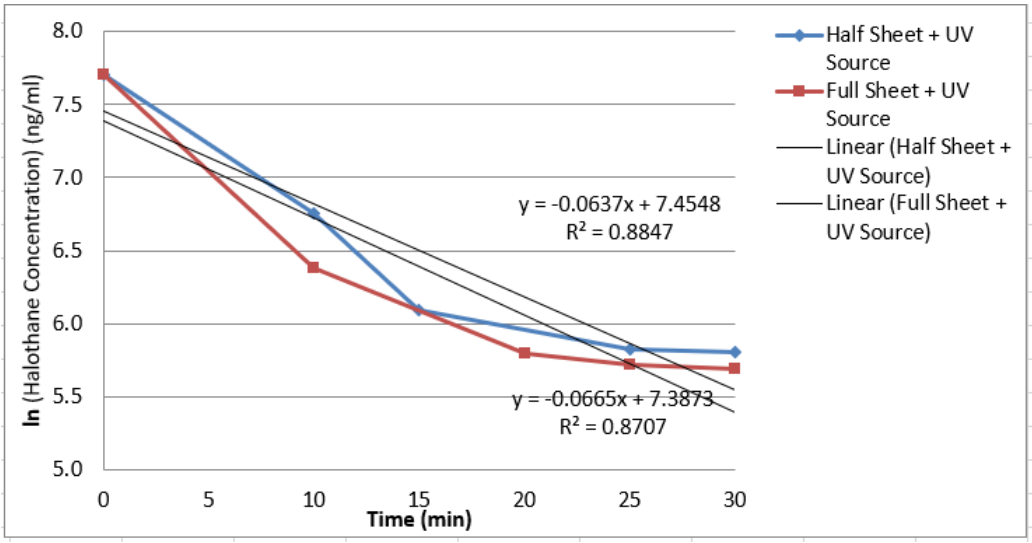

Figure 3.21: First order decay plot of Halothane under the influence of varied catalyst illuminated area

The first order decay plot of Halothane in the presence of 2 different illuminated catalyst surface area was not completely linear, as evident from their R^2 values. In both the cases, with an initial concentration of 2224.6 ng/ml, the maximum loss of Halothane occurred in the first 10 min of the illumination. In the case of the full-length catalyst sheet, Halothane was lost at a rate of 163.7 ng/ml/min, while in the case of the half catalyst sheet it was lost at a rate of 136.7 ng/ml/min in the first 10 min. After this the reaction rate had slowed down due to either limited reactant availability or

reduced catalyst activity. An overall decrease of 85.12% and 86.7% was observed during the photocatalysis in the presence of the half and the full catalyst sheet respectively. The reaction rate constants for the first 10 min in both the cases were 0.095 and 0.13 min^{-1}respectively.

It was evident that the possibility of a part of the catalyst sheet not being activated due to lack of incident light could be ruled out as a significant factor in influencing the anesthetic degradation rate when the power of the light source was varied.

3.7.The Influence of Type of Catalyst Support Surface on the Anesthetic Gas Degradation Rate

The three different support surfaces (fiberglass mesh, flat aluminum sheet, fiberglass mesh supported on aluminum sheet) were coated with a same amount of aqueous mixture of powdered TiO_2 (0.17 g TiO_2/ml H_2O) and dried overnight in ambient air. The reactor walls were lined with the full flat aluminum sheet or the aluminum sheet supporting the fiberglass mesh. The third catalyst test support surface namely the fiberglass mesh was supported on the light source using closure seals by wrapping it three times around the light source. This was done to ensure that the TiO_2 molecules came in sufficient contact with the photons being generated from the light source first for the formation of electron hole pairs.

The photocatalytic degradation was tested with 5 µl of halothane and the 9W 254 nm light source. The resultant degradation measured is plotted in Fig 3.22.

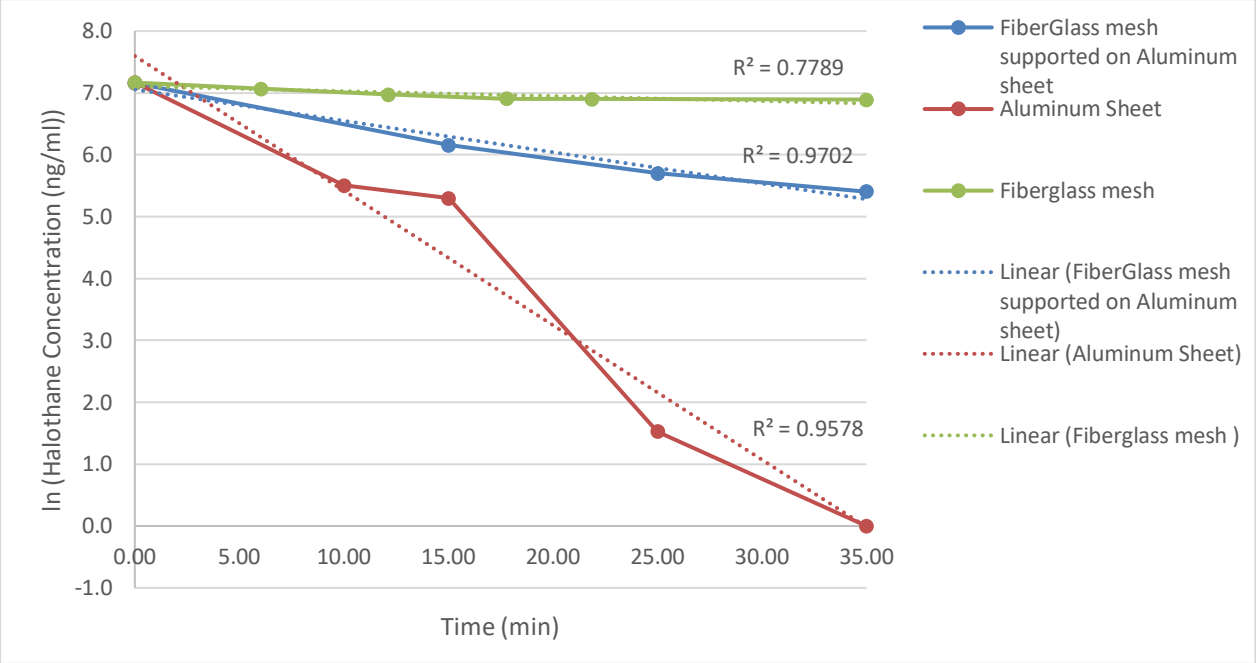

Figure 3.22: Concentration vs time profile during the photocatalysis of halothane in the presence of various support surfaces

In the absence of a light source, the loss in the Halothane concentration over 20 min in the presence of the three support surfaces due to wall effects, leaks and absorption on to the catalyst surface was almost approximately 13% for all when compared to a 9.4 % loss due to the wall effects and leaks alone.

In the presence of 1297.5 ng/ml of Halothane, the TiO_2 coated on the fiberglass mesh degraded 24% of the Halothane in 35 min. The rate of decrease in the first 10 min of the photocatalysis was 20.5 ng/ml/min which reduced to 10.9 ng/ml/min in the next 8 min, and finally dropped to 0.5 ng/ml/min over the final 17 min.

In the presence of 1288 ng/ml of Halothane, the TiO_2 coated on fiberglass cloth supported on the aluminum sheet degraded 80% of the Halothane in 35 min. In the first 10 min of the photocatalysis, the rate of decrease was 68.8 ng/ml/min followed by a drop to 21.2 ng/ml/min in the next 8 min and finally dropped to 7.5 ng/ml/min for the final 17 min.

In the presence of 1297.5 ng/ml of Halothane, the TiO_2 coated on the aluminum sheet support degraded 99.9% of the Halothane in 35 min. The degradation started with loss of 105 ng/ml/min in the first 10 min. The rate then slowed down to 15.15 ng/ml/min in the next 8 min.

In summary the fiberglass mesh alone degraded Halothane by 24% in comparison to the 80% degradation by the fiberglass mesh fixed on the aluminum sheet and 99.6% by the aluminum sheet alone in 35 min.

The primary reason for the difference in degradation rate was due to the structure of the support surface. Since the fiber glass cloth was highly porous, depositing the required amount of catalyst onto the surface became highly challenging, requiring multiple coats of the catalyst suspension. This combined with the setup where the fiberglass mesh was wrapped thrice over the UV lamp reduced the number of TiO_2 molecules that came in direct contact with the emitted photons and the Halothane. The catalyst layer closest to the UV lamp would have formed the OH^o radicals however, the OH^o radicals would have to travel through the other two layers to be able to come in contact with the Halothane. On the other hand, the outermost catalyst layer in contact with the Halothane will not be in a position to generate the required amount of hydroxyl radicals since the incident photons being emitted from the light source will need to travel through the other layers thus limiting its degradation efficiency when compared to the fiberglass mesh supported on the aluminum sheet or the aluminum sheet alone.

The difference in the degradation rate between the fiberglass mesh supported on the aluminum sheet and the aluminum sheet by itself is probably due to the fibrous nature of the fiberglass cloth. Due to its nature, there are high chances that the catalyst water suspension while being coated on the fiberglass mesh supported on the aluminum sheet was absorbed into the inner layers of the mesh. Since photocatalysis is a surface reaction, it is essential for the Halothane molecules to come in contact with

the surface generated hydroxyl radicals in order to degrade. Due to the absorption of the catalyst, even though the required change in the dry weight was observed during catalyst deposition not all of the TiO_2 molecules were available on the surface of the mesh to absorb the incident photons and generate the expected amount of hydroxyl radicals. In the case of the aluminum sheet by itself, since no such inner layer absorption of the catalyst molecules into the sheet was possible, all the deposited TiO_2 molecules were available on the surface of the catalyst support to produce the expected amount of hydroxyl radicals. The nature of the catalyst support surface namely polished or rough can also influence the actual catalyst surface area available for interaction with the anesthetic gas molecules.

For the following experiments, flat aluminum sheet was used as the catalyst support surface unless otherwise mentioned.

3.8.The Influence of the Amount of Catalyst Used on the Anesthetic Gas Degradation Rate

Support surfaces fabricated with consecutive coats of various amounts of TiO_2 catalyst on the aluminum sheet were lined against the reactor walls. Five (5) µl of Halothane was injected into the inlet septum and allowed to volatize. After the concentration was found to stabilize, the 18 W 254 nm UV light source was switched on. The resulting gas concentrations measured are plotted in Fig 3.23.

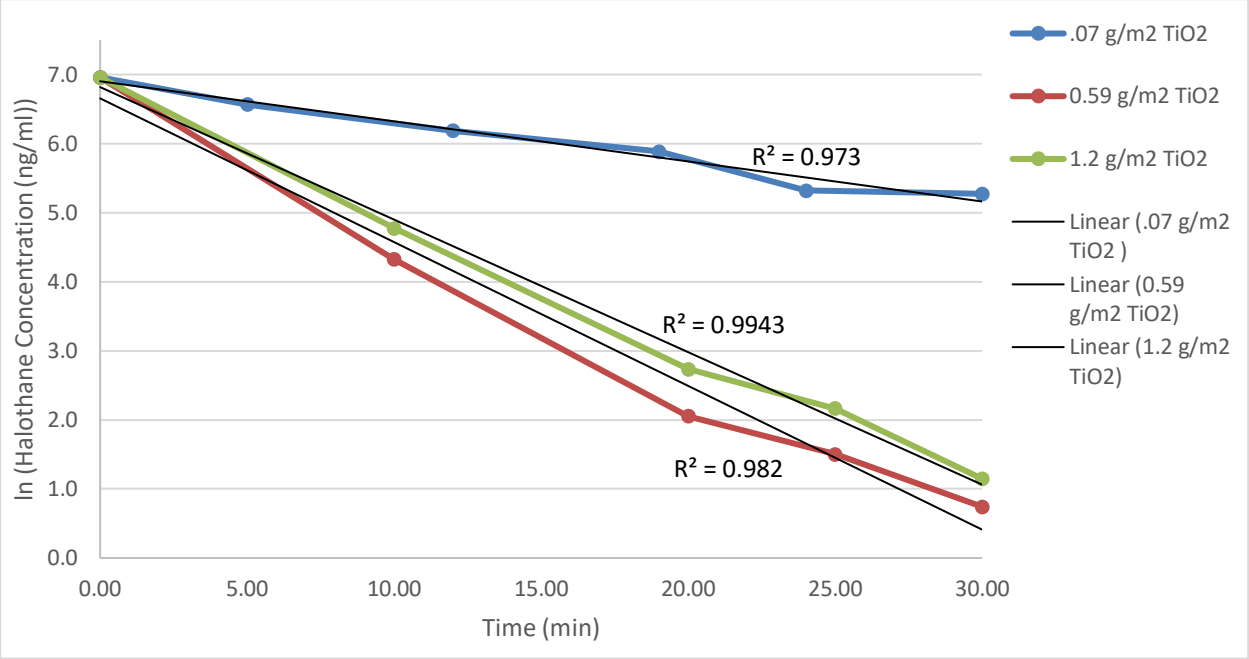

Figure 3.23:Variation in the Halothane concentration with change in the catalyst loading

It can be concluded from the results that an increase in the catalyst loading resulted in an increase in the Halothane degradation rate up to a specific amount. Beyond that specific amount, there was a range of catalyst loading where the degradation rate remained the same. Any further increase in the catalyst loading beyond this range reduced the Halothane degradation rate. This was in complete agreement with the observations found in the literature.[93-98]

It was observed from the experimental results that in the presence of 1052.3 ng/ml of Halothane, the catalyst loading of 0.07 g/m^2 degraded Halothane at the rate of 35.19 ng/ml/min in the first 20 min of the irradiation. However, with the same initial Halothane concentration, the catalyst loading of 0.59 g/m^2 degraded Halothane at the rate of 54.3 ng/ml/min and the catalyst loading of 1.2 g/m^2 degraded Halothane at the rate of 51.8 ng/ml/min in the first 20 min of the irradiation. In 30 min of the irradiation, 84%, 99.8% and 96% of the initial Halothane had been degraded by the three different catalyst loading respectively.

Increasing the TiO_2 loading increased the number of active sites available, which increased the amount of hydroxyl radicals produced. For a fixed Halothane inlet concentration, only a fixed amount of catalyst sites will be occupied. The reactor contained $2.59x10^{19}$ molecules of Halothane. A catalyst loading of 0.07 g/m^2 contained $3.77x10^{21}$ molecules of TiO_2, the catalyst loading of 0.59g/m^2 contained $3.32x10^{22}$ molecules of TiO_2 and the catalyst loading of 1.2 g/m^2 contained $6.86x10^{22}$ molecules of TiO_2. As mentioned before, UV-photocatalysis is a surface reaction however all the catalyst sheets used in this experiment were fabricated with consecutive coats meaning not all of the deposited TiO_2 particles were available on the surface of the catalyst sheet to absorb the incident photons. The catalyst loading of 0.59 g/m^2 degraded more of the Halothane when compared to the catalyst loading of 0.07 g/m^2 probably due to presence of greater number of surface TiO_2 molecules. When the loading was increased beyond 0.59 g/m^2, the excess catalyst active sites either remained unoccupied or the support was so heavily loaded that it led to agglomeration of catalyst particles which limited the amount of light that could be absorbed, hence a lower degradation was observed with the catalyst loading of 1.2 g/m^2.

3.9.The Effect of Anesthetic Gas Inlet Concentration on Its Degradation Rate

The most efficient catalyst loading of 0.59g TiO_2/m^2 on the same aluminum support surface was used to in order to test the change in anesthetic gas degradation rate with change in its inlet concentration.

The catalyst sheet was prepared as previously mentioned. The reactor was flushed with compressed air and the walls were lined with the photocatalyst medium. Four different volumes of Halothane (5 µl, 10µl, 15 µl, 25 µl) were injected via the septum and allowed to volatilize. The peristaltic pump

connected to the ends of the reactor was switched on to continuously mix the contents inside the reactor. Once the inlet concentration had stabilized, the 18W UV light source was switched on and the decrease in Halothane concentration was measured by analyzing 500 µl samples using the GC as plotted in Fig 3.24.

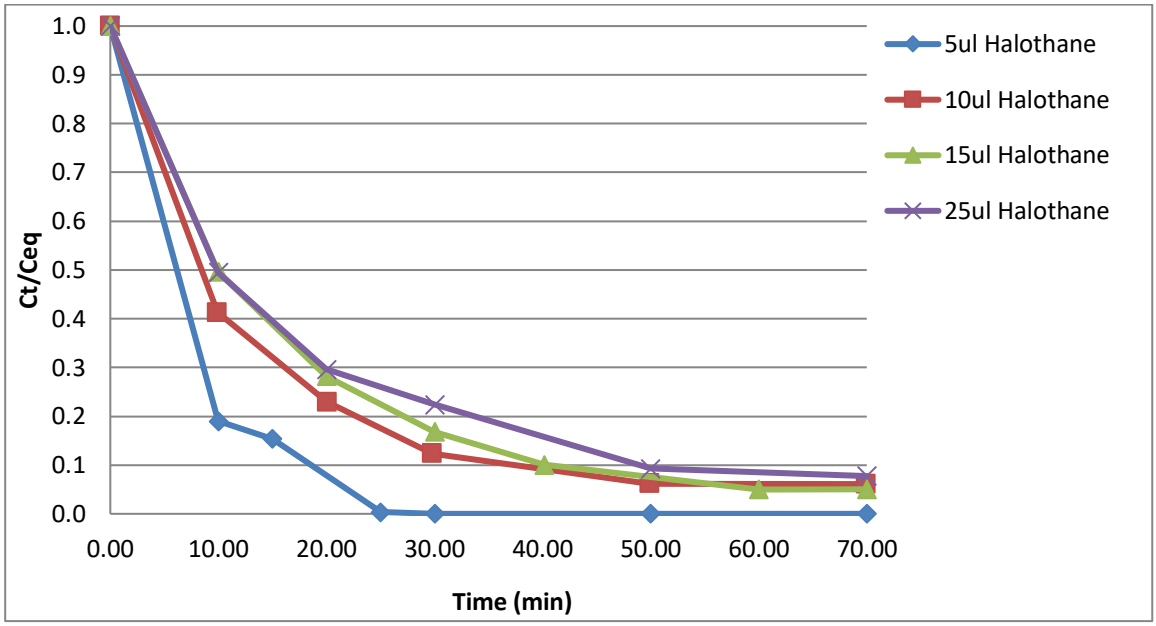

Figure 3.24: Degradation profile of Halothane at various normalized inlet concentrations

It was clearly evident that the catalyst loading used in the experiment was efficient in degrading Halothane at various inlet concentrations, but the degradation efficiency reduced with increase in the inlet concentration. Our results are similar to those reported in literature as examples state that the photocatalytic degradation rate of methylene blue dropped from 87 to 40% as the initial concentration was increased from 25 to 100 mg/l in the presence of ZnO as the photocatalyst.[92] Similarly, it was observed that during the degradation of toluene in the presence of TiO_2, with the increase in concentration from 20 to 100 ppm the removal efficiency dropped from 37 % to 27%.[99]

In the presence of 0.59 g TiO_2/m^2 of the support surface, 100%, 87.6%, 83.2% and 77.6% degradation

in 30 min was observed with 5 µl, 10µl, 15 µl, 25 µl of Halothane respectively. With 5 µl of Halothane a degradation rate of 105.13 ng/ml/min was observed in the first 10 min of the irradiation. For the same time a degradation rate of 76.83 ng/ml/min, 65.34 ng/ml/min and 65.1 ng/ml/min was observed with 10µl, 15 µl, 25 µl of Halothane respectively. In case of the higher volumes (10 µl, 15 µl, 25 µl), the degradation rate eventually stabilized after 50 min suggesting that no more oxidizing radicals were available to degrade the Halothane molecules.

The injected volumes of 5 µl, 10µl, 15 µl, 25 µl correspond to $2.86x10^{19}$, $5.72x10^{19}$, $8.58x10^{19}$ and $1.43x10^{20}$ molecules of Halothane respectively. The catalyst loading of $0.59g/m^2$ contained $3.32x10^{22}$ molecules of TiO_2. Even though the number of molecules of TiO_2 on the whole is much higher than the number of molecules of Halothane, the number of surface TiO_2 molecules varies widely since each catalyst sheet was prepared with successive coats to achieve the required loading. Hence, with the change in number of surface TiO_2 molecules the number of hydroxyl radicals generated will also change thus, affecting the Halothane degradation rate. Another possible reason for decrease in degradation is increased absorption of incident photons at higher reactant volumes, which reduced the number of photons available for the catalyst molecules to generate hydroxyl radicals.

During the experiment it was observed that for higher inlet volumes like 15 µl and 25 µl, reactant concentrations were not stable during the experiments to be measured accurately. This can be attributed to the method of injection used throughout this work. At greater volumes say 15 µl or 25 µl, more liquid anesthetic absorbs directly on to either the catalyst sheet or the reactor walls when injected via the septum. With the contents of the reactor being continuously mixed using the pump, some of this absorbed anesthetic comes off at different times causing an unexpected increase in the anesthetic gas concentration when measured using the GC. However, this effect is not profound at lower anesthetic liquid volumes (5µl, 10 µl) since they have a faster equilibration and volatilization rate.

Considering all the above factors, the catalyst loading of 0.59g TiO_2/m^2 was considered to be appropriate to achieve maximum degradation for lower Halothane concentrations.

3.10.The Effect of Moisture on the Anesthetic Gas Degradation Rate

To test the influence of moisture, standard room air with an estimated 30% relative humidity based on the humidity in the lab was used instead of the usual compressed air which had a low relative humidity level of 11%. The catalyst sheet was prepared as previously mentioned. The reactor was flushed with room air by leaving one end of the peristaltic pump tube open outside the fumehood and into the room in a such way that the room air was pulled in and circulated through the reactor when the peristaltic pump was switched on. Once the reactor had been flushed with sufficient room air, the reactor was closed and, the reactor walls were lined with the catalyst sheet. The desired volume of Halothane (5 µl) was injected via the septum and allowed to volatilize. The peristaltic pump was connected to both the ends of the reactor and was switched on with a flow rate of 500 ml/min to mix the gases inside the reactor. Once the inlet concentration had stabilized, the 18 W 254 nm UV light source was switched on and the decrease in the Halothane concentration was measured by analyzing 500 µl samples using the GC as shown in Figure 3.25.

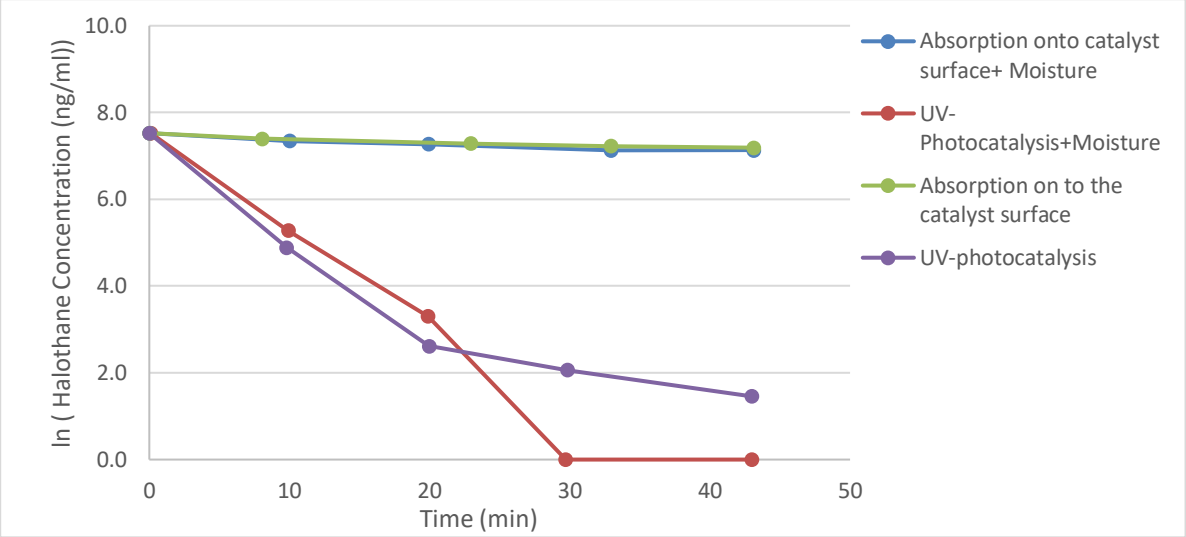

Figure 3.25: Time concentration profile of Halothane in the presence of catalyst and moisture

With an initial concentration of 1852.8 ng/ml of halothane, the rate of decrease of Halothane due to absorption and wall effects increased from 16.3 ng/ml/min to 20.8 ng/ml/min in 20 min when the reactor was flushed with moist air. When the same concentration of Halothane was subjected to UV-photocatalysis, an insignificant increase in the degradation rate from 91.7 ng/ml/min to 92.01 ng/ml/min in the first 20 min of irradiation was measured, when the compressed tank air was replaced with the moist air.

There are conflicting results reported with effect of moisture on the degradation rate. Selective literature with other pollutants observes an increase in the rate of degradation of the reactant with increase in the moisture content up to a limit. Any further increase in the moisture content reduces the degradation rate.[100-102] For example, the degradation rate of toluene increased with increase in humidity up to 35% due to formation of additional hydroxyl radicals, however, the rate decreased for any further increase in humidity due to competitive catalytic adsorption.[103] On the contrary, the degradation rate of ethanol decreased when the relative humidity was increased from 10% to 60% in an open loop reactor

equipped with TiO_2.[104] Similarly, the single pass removal efficiency of Isoflurane decreased with increase in the relative humidity from 20 – 80 % with an inlet concentration of 0.5 ppm, I=4.5 $mW.cm^{-2}$ in a closed loop multi pass photoreactor equipped with TiO_2.[75]

Introducing moisture not only increases the hydroxyl ion concentration but also suppresses the electron hole combination.[105] However, increased moisture content acts as a competitor for adsorption on to the catalyst surface thus limiting the degradation efficiency.

Since the catalyst medium was coated with a suspension of 5 gm of TiO_2 in 30 ml DI, it already had $1x10^{24}$ molecules of water. After the overnight drying, even if 99% of the water molecules had evaporated, the sheet would have still had sufficient water molecules to interact with all of the available TiO_2 to produce 10^{22} hydroxyl radicals which will then completely oxidize all of the $2.59x10^{19}$ molecules of Halothane present inside the reactor. The catalyst medium was self-sufficient in the required water molecules hence, any further addition of moisture either via the air stream or the catalyst media would have probably not increased the degradation rate significantly.

3.11.UV-Photocatalysis of Isoflurane

The study with Halothane clearly proved that UV-photocatalysis with TiO_2 at 254 nm was the most promising advanced oxidation process for breaking down the waste anesthetic gases being released into the environment as compared to the other processes tested.

The 18W 254 nm UV lamp running the length of the reactor was fixed in the lamp holder. The walls of the reactor were lined with the catalyst coated aluminum sheet. Five (5) µl of the liquid Isoflurane was injected via the septum and allowed to volatilize. The peristaltic pump was turned on to mix the

contents of the reactor. Once the concentration had stabilized, the UV lamp was switched on and the Isoflurane concentration was measured. The results are presented in Fig 3.26.

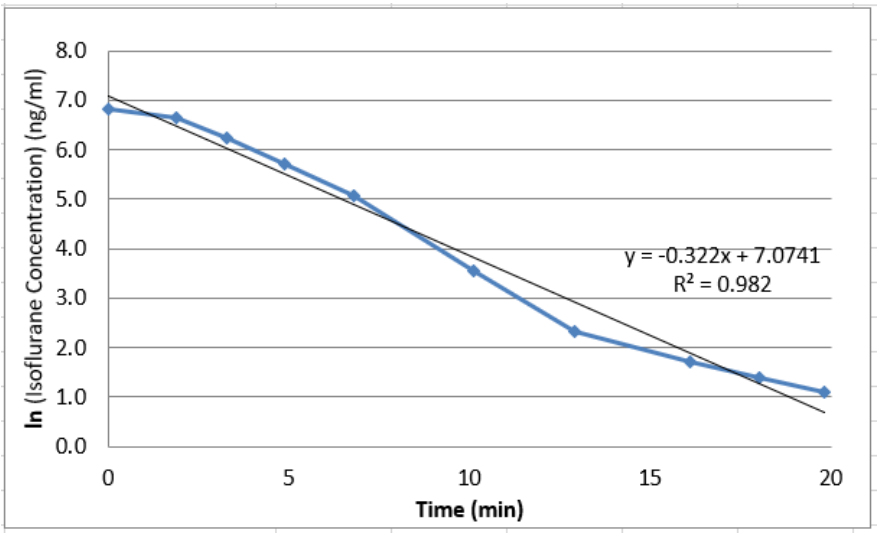

Figure 3.26: First order decay plot of Isoflurane when subjected to UV-photocatalysis

As can be observed in Fig 3.26, at an initial concentration of 911 ng/ml, 99.8% of the Isoflurane had degraded in 20 min with a degradation rate of 87.6 ng/ml/min in the first 10 min of the irradiation and a degradation rate of 3 ng/ml/min over the remaining 10 min of the reaction.

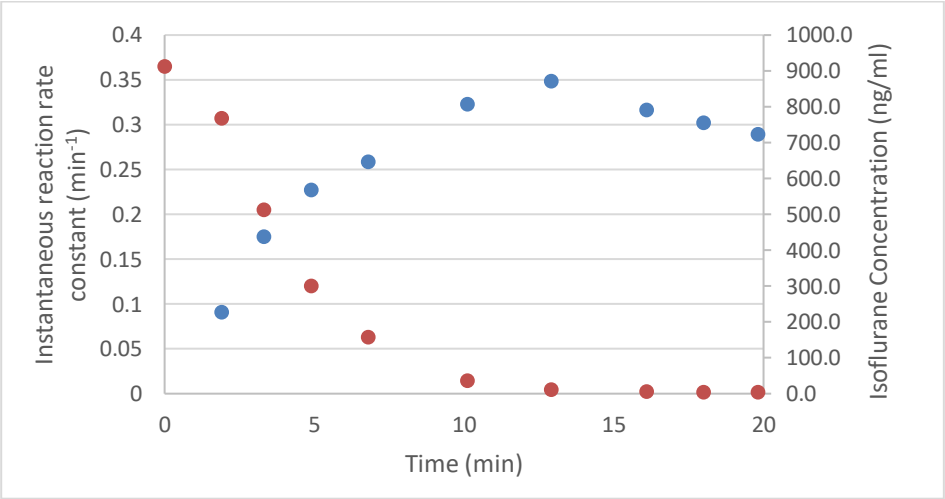

Figure 3.27: Change in the instantaneous reaction rate constants and the Isoflurane concentration when subjected to UV-photocatalysis

It could be concluded that degradation of Isoflurane proceeds in 3 phases, at the beginning the instantaneous reaction rate constant is low (0.091 min^{-1}), with time it increases and achieves a maximum (0.35 min^{-1}) and then finally the instantaneous reaction rate trends downward with time (0.29 min^{-1}) as shown in Fig 3.27. However, the instantaneous reaction rates during the UV-photocatalysis of Halothane as shown in Fig 3.20 trended downwards with time from the beginning of the UV irradiation. A probable reason for this difference can be attributed to the limited number of halogens in Halothane ($C_2HBrClF_3$) when compared to Isoflurane ($C_3H_2ClF_5O$) which may contribute to a different molecular structure, which can influence the halogen abstraction by the hydroxyl radicals during UV-photocatalysis.

The process of degradation begins with generation of OH^{o} radicals from the TiO_2 surface due to formation of electron-hole pairs. With the passage of time, the instantaneous reaction rate constants increase suggesting a faster degradation of Isoflurane which is possible if additional oxidizing agents have been produced. The attack of OH^{o} radicals on Isoflurane generates Cl^{o} radicals which further initiate a chain degradation reaction. With time, the instantaneous reaction rate constant starts to drop probably due to depleting reactant concentration or inactivity of the catalyst resulting from the accumulation of reaction intermediates or by-products on to the catalyst surface.

This unique chain degradation mechanism has been studied in literature extensively for trichloroethylene (TCE)[106,107] and perchloroethylene[92,94]. It was agreed that TCE undergoes a chain degradation mechanism in the presence of OH^{o} and Cl^{o} radicals.[95-97] Literature also points out a similar degradation curve when Isoflurane was degraded photo catalytically in a 420 L closed loop multi pass reactor.[75]

3.11.1.Testing for Byproducts of Photocatalysis of Isoflurane

Before starting the experiment, the walls of the reactor were washed with DI and the wash water was collected in a vial for testing. Once Isoflurane had completely degraded, the UV lamp was switched on for 30 min to encourage release of any contaminants adhered to the reactor walls. After 30 min, the lamp was switched off and the reactor was opened. The catalyst sheet was removed, the walls of the reactor were washed with DI and, the wash water was collected in a vial and tested for their chlorine and fluorine ion concentration using ion chromatography. A sample of the DI used was also tested for its various anion concentrations. The IC results of the samples tested are shown in Fig 3.28, 3.29, 3.30, 3.31, 3.32 and 3.33.

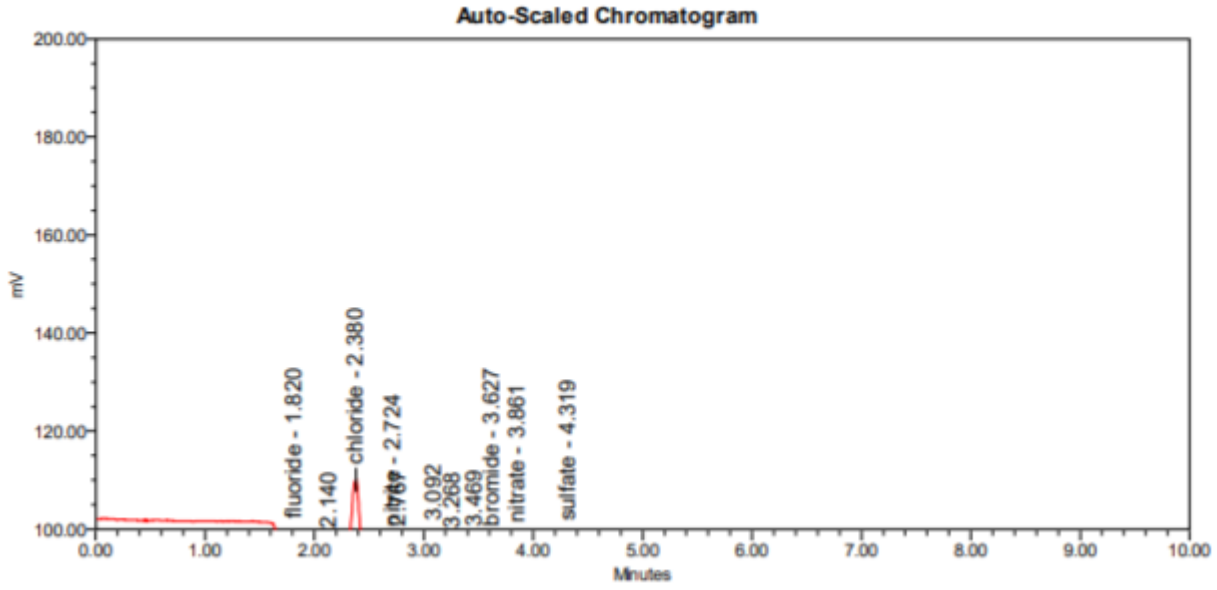

Figure 3.28: IC chromatogram of the reactor wall wash sample before the photocatalysis

Peak Results

	Name	RT	Area	Height	Amount	Units
1	fluoride	1.820	2426	1516	0.027	mg/L
2		2.140	43155	2511		
3	chloride	2.380	80487	15263	1.434	mg/L
4	nitrite	2.724	33946	2158	0.806	mg/L
5		2.767	30502	2124		
6		3.092	18814	2832		
7		3.268	6031	990		
8		3.469	17649	1009		
9	bromide	3.627	4885	860	0.218	mg/L
10	nitrate	3.861	7457	991	0.256	mg/L
11	sulfate	4.319	4067	714	0.108	mg/L
12	phosphate	8.715				

Figure 3.29: IC result of the reactor wall wash sample before the photocatalysis

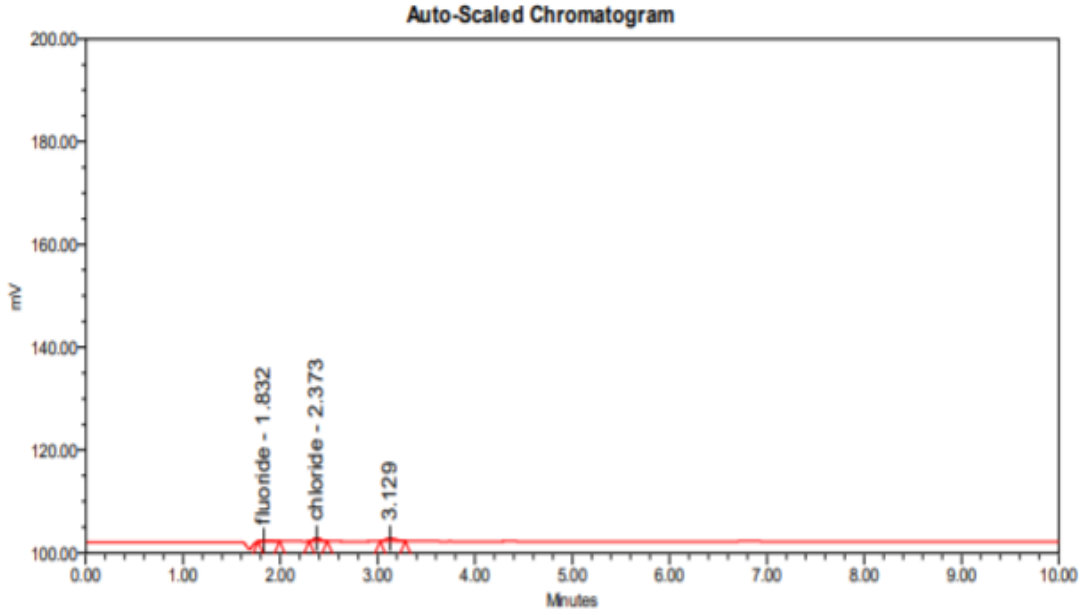

Figure 3.30: IC chromatogram of the DI sample used for reactor washing

Peak Results

	Name	RT	Area	Height	Amount	Units
1	fluoride	1.832	1201	175	0.013	mg/L
2	chloride	2.373	3116	668	0.056	mg/L
3	nitrite	2.601				
4		3.129	4077	634		
5	bromide	3.659				
6	nitrate	3.909				
7	sulfate	4.386				
8	phosphate	8.715				

Figure 3.31: IC result of the DI sample used for reactor washing

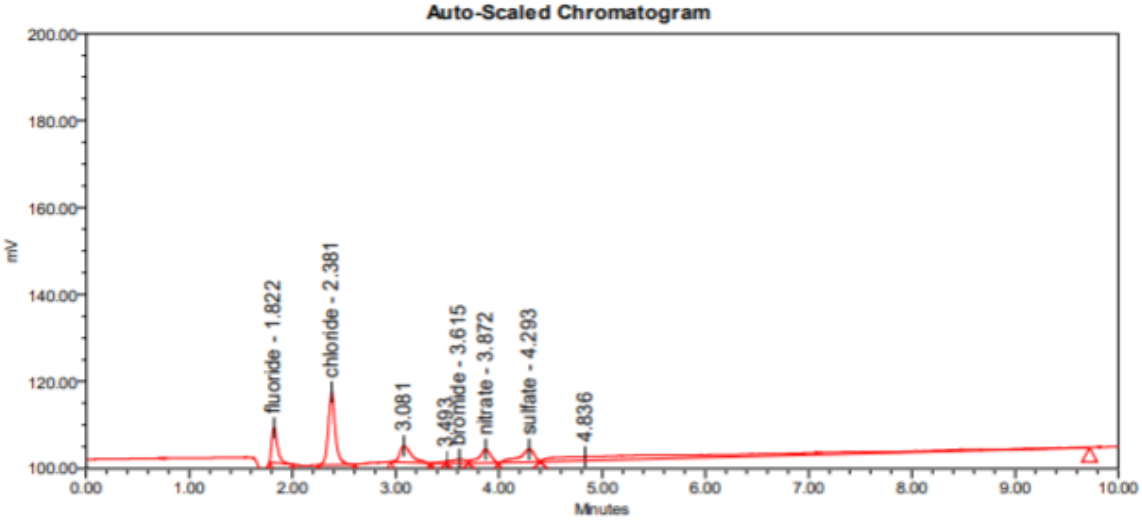

Figure 3.32: IC chromatogram of the reactor wall wash sample after the oxidation of Isoflurane

Peak Results

	Name	RT	Area	Height	Amount	Units
1	fluoride	1.822	30721	8026	0.341	mg/L
2	chloride	2.381	78510	16789	1.399	mg/L
3	nitrite	2.601				
4		3.081	29735	3744		
5		3.493	2118	456		
6	bromide	3.615	8968	909	0.400	mg/L
7	nitrate	3.872	24810	3124	0.850	mg/L
8	sulfate	4.293	30370	2995	0.802	mg/L
9		4.836	139486	916		
10	phosphate	8.715				

Figure 3.33: IC result of the reactor wall wash sample after the oxidation of Isoflurane

The IC reported a mass of 0.02 mg of fluorides from the reactor walls before the reaction in comparison to the 0.00026 mg of F^- ions contained by the DI used for washing and, the 0.06 mg of fluorides from the reactor walls sampled after the degradation. This suggested an increase of 0.041 mg of fluoride ions produced in the reactor during the degradation of Isoflurane. Similarly, the IC reported a mass of 0.09 mg of chloride ions from the reactor walls before the reaction in comparison to the 0 mg contained by the DI used for washing and 0.4 mg of chloride ions from the reactor walls sampled after the degradation. This suggested an increase of 0.31 mg of chloride ions produced in the reactor during the degradation of Isoflurane. Theoretically, if all of the 911 ng/ml of Isoflurane that was present inside the reactor before turning on the UV was to degrade completely based on Equation 10, then 0.68 mg of chloride ions are expected to be produced in the reactor during the degradation. However, the possibility of these ions absorbing on to the catalyst surface is really high, but since the catalyst sheet wash was highly turbid its anionic composition could not be analyzed by the IC.

$C_3H_2ClF_5O + H_2O \rightarrow C_3F_5OH + HCl + H_2O$ ……..*Equation 10*

Literature suggests that reaction of Isoflurane with the hydroxyl radicals proceeds via abstraction of the H atom which leads to the formation of $CF_3C(\bullet)ClOCHF_2$ radical. It calls out a possible degradation mechanism of Isoflurane in the presence of hydroxyl radicals leading to the formation of pentafluoropropanol as a major product in addition to chlorodifluoroacetalydehyde, acetic acid, formic acid, formaldehyde, acetaldehyde as other byproducts in the presence of TiO_2.[75]

$C_3H_2ClF_5O + OH^\circ \rightarrow C_3F_5OH + Cl^\circ + H_2O$ ..……*Equation 11*

Of these potential byproducts, the GC-FID with the column installed could possibly detect the pentafluoropropanol but not the aldehydes. There were no significant additional peaks observed in the chromatogram after the UV irradiation suggesting that either it is improbable that any detectable amount of pentafluoropropanol was formed or that is did not have sufficient C-H bonds to be sensitive to the GC.

This chlorine free radical obtained as shown in Eq (11) further attacks the Isoflurane in a chain reaction which eventually stops with either no Isoflurane remaining to be acted upon or reduced catalytic activity due to accumulation of byproducts onto the catalyst surface. This reaction mechanism is in line with our observation of an increase in the chloride ion concentration after the reaction.

3.12.UV-Photocatalysis of Sevoflurane

The 18W 254 nm UV lamp running the length of the reactor was fixed in the lamp holder. The walls of the reactor were lined with the catalyst coated sheet. Five (5) µl of liquid Sevoflurane was injected via the septum and allowed to volatilize. The peristaltic pump was used to promote uniform concentration throughout the reactor. Once the concentration had stabilized, the UV lamp was switched on and the

Sevoflurane concentration was measured and analyzed as shown in Fig 3.34.

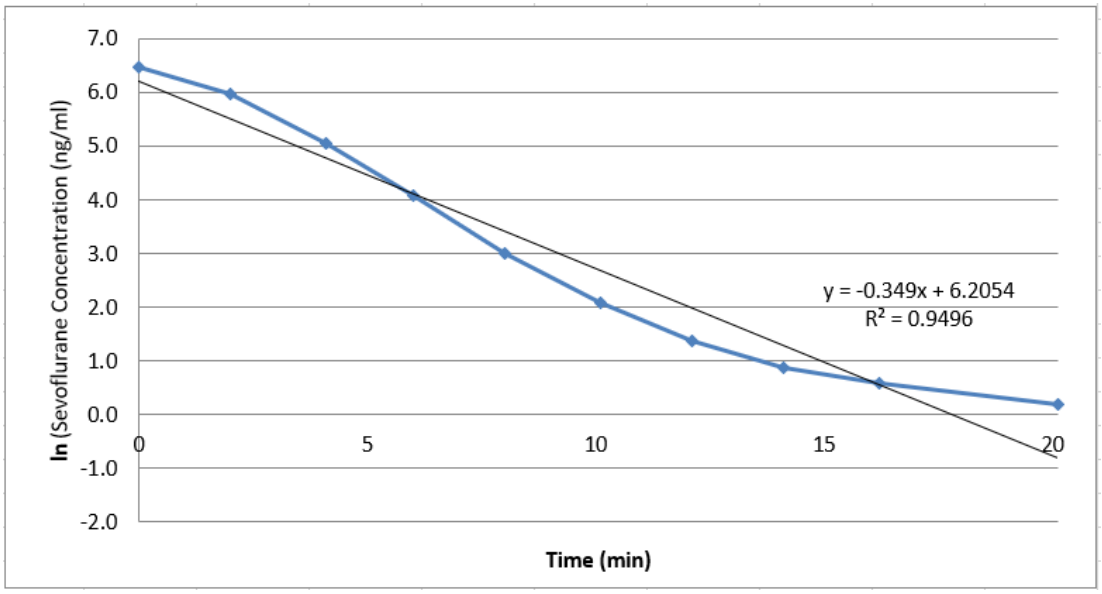

Figure 3.34: First order decay curve of Sevoflurane when subjected to photocatalysis in the presence of TiO_2

With an initial concentration of 847 ng/ml, a 99.8% decrease in the Sevoflurane concentration was observed with a rate of decrease of 63.2 ng/ml/min the first 10 min of the irradiation and 0.5 ng/ml/min over the remaining 10 min when subjected to photocatalysis in the presence of TiO_2.

The 1st order decay curve fit the linear curve at some points, the plot of the instantaneous reaction rate constants at various time intervals was slightly different to the ones obtained in the case of Isoflurane as shown in Fig 3.35. The instantaneous reaction rate constants started with 0.25 min^{-1} for Sevoflurane and 0.0842 min^{-1} for Isoflurane, after which they increased with time but the Sevoflurane reaction rate decreased more sharply after it reached its maximum to 0.31 min^{-1}when compared to the reaction rate of 0.29 min^{-1} for Isoflurane.

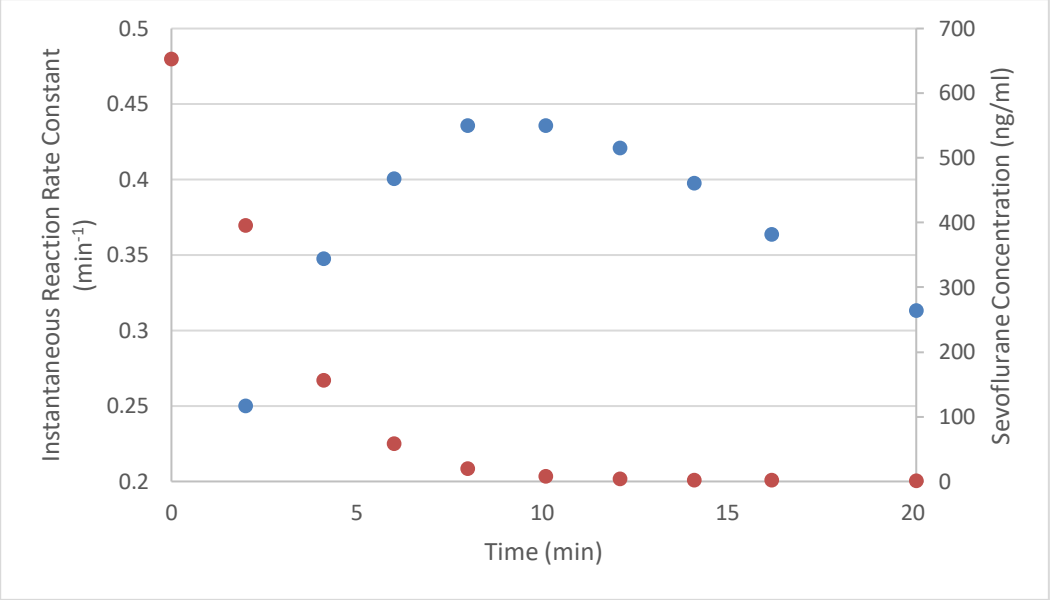

Figure 3.35: Variation of instantaneous reaction rate constants and the concentration with time during the photocatalysis of Sevoflurane

During the photocatalysis of Sevoflurane and Isoflurane, all the parameters such as the catalyst concentration, anesthetic gas concentration and the amount of water used for the medium preparation were kept constant hence the same amount of hydroxyl radical production is expected during both the experiments. However, the only difference is that Sevoflurane lacks chlorine while Isoflurane doesn't. The available oxidizing species in addition to the existing hydroxyl radicals that can possibly cause the chain degradation mechanism during the photocatalysis of Sevoflurane is F^- radicals. Since the F^- radicals have a greater oxidizing power than the chloride radicals, they possibly oxidized Sevoflurane at a higher rate because of which in the first 10 min of the irradiation ~ 98% of the Sevoflurane was oxidized, after which the reaction rates dropped due to limited reactant availability.

3.12.1.Testing for Byproducts of Photocatalysis of Sevoflurane

The testing for oxidation intermediates or byproducts of Sevoflurane was performed similarly to that of Isoflurane as described in Section 3.11.1. The samples collected were analyzed for the free ion concentration of fluorides and chlorides using the IC. The IC results of the samples tested are shown in Fig 3.36, 3.37, 3.38, 3.39, 3.40 and 3.41.

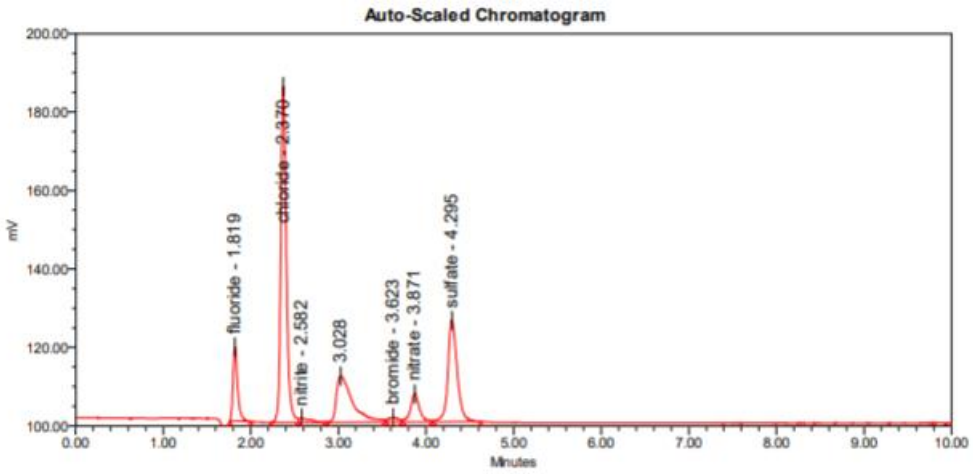

Figure 3.36: IC chromatogram of pre reaction reactor wall wash sample

Peak Results

	Name	RT	Area	Height	Amount	Units
1	fluoride	1.819	68733	18895	0.765	mg/L
2	chloride	2.370	378042	85676	6.656	mg/L
3	nitrite	2.582	9724	1105	0.231	mg/L
4		3.028	150248	11743		
5	bromide	3.623	9813	1195	0.438	mg/L
6	nitrate	3.871	51561	7151	1.759	mg/L
7	sulfate	4.295	190985	25874	4.900	mg/L
8	phosphate	8.715				

Figure 3.37: IC result of pre reaction reactor wall wash sample

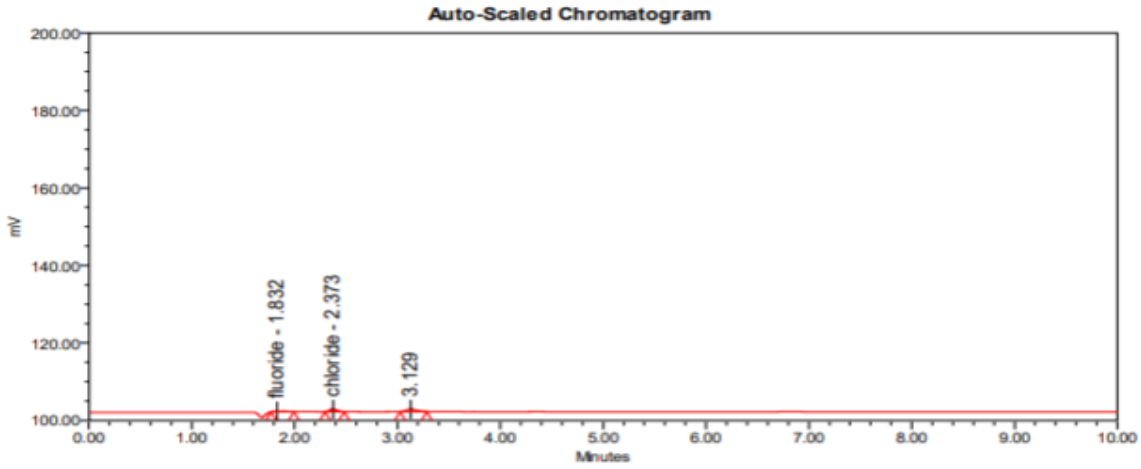

Figure 3.38: IC chromatogram of DI used for reactor wash

Peak Results

	Name	RT	Area	Height	Amount	Units
1	fluoride	1.832	1201	175	0.013	mg/L
2	chloride	2.373	3116	668	0.056	mg/L
3	nitrite	2.601				
4		3.129	4077	634		
5	bromide	3.659				
6	nitrate	3.909				
7	sulfate	4.386				
8	phosphate	8.715				

Figure 3.39: IC result of DI used for reactor wash

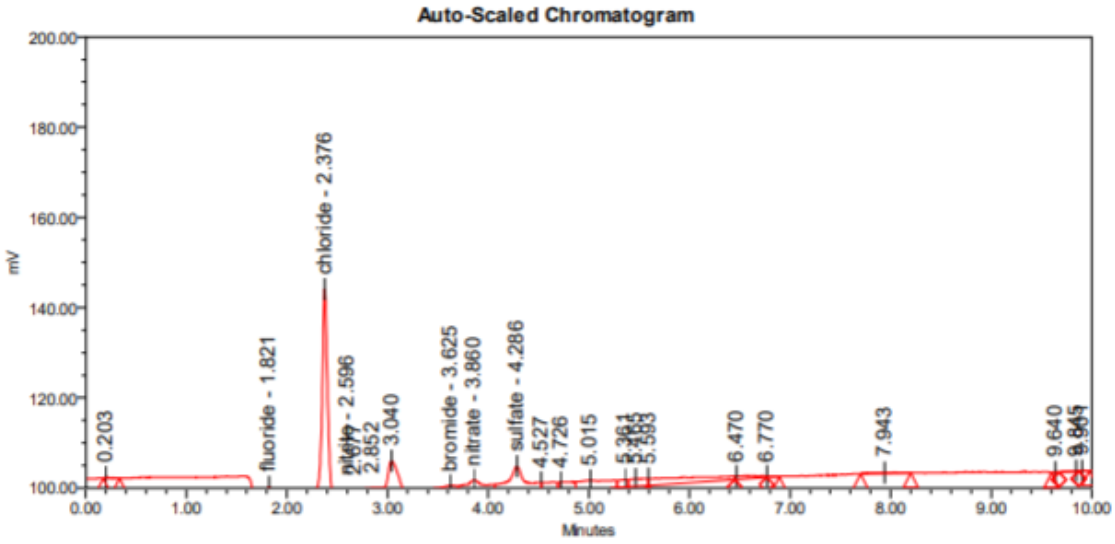

Figure 3.40: IC chromatogram of post reaction reactor wall wash

Peak Results

	Name	RT	Area	Height	Amount	Units
1		0.203	695	212		
2	fluoride	1.821	1797	1273	0.020	mg/L
3	chloride	2.376	260188	48267	4.603	mg/L
4	nitrite	2.596	23270	3173	0.553	mg/L
5		2.677	16756	3249		
6		2.852	47682	3357		
7		3.040	76103	9203		
8	bromide	3.625	67478	2938	2.973	mg/L
9	nitrate	3.860	62108	3829	2.115	mg/L
10	sulfate	4.286	89313	6174	2.333	mg/L
11		4.527	21317	2231		
12		4.726	21094	2030		

Figure 3.41: IC result of post reaction reactor wall wash

The IC reported a mass of 0.0062 mg of fluorides from the reactor walls before the reaction in comparison to the 0.00026 mg of F^- ions contained by the DI used for washing and, the 0.0084 mg of fluorides from the reactor walls sampled after the degradation. This suggested an increase of 0.002 mg

of fluoride ions produced in the reactor during the degradation of Sevoflurane. Theoretically, if the injected Sevoflurane was to oxidize completely into $CO_2$and HF only based on Equation 12 then, 1.81 mg of HF is expected if all of the created HF was captured and measured.

$2C_4H_3F_7O + 5O_2 + 4H_2O \rightarrow 8CO_2 + 14HF$ …….*Equation* 12

The increase in fluoride ion concentration post photocatalysis suggests the presence of free fluoride radicals which would have been generated during the oxidation of Sevoflurane with OH^{o}. These fluoride ions produced could be a possible cause for the acceleration of the instantaneous reaction rate with time as depicted in Fig 3.35.

There is no literature reported on the mechanism of the degradation of Sevoflurane in the presence of hydroxyl radicals. However, literature reports HF and CO_2 as the final two oxidation products of Sevoflurane in a closed loop reactor, with TiO_2 as a photocatalyst coated on a glass tubular support in the presence of 36 W UV lamp emitting 9W in the range of 315-405 nm, when measured using specialized sensors.[76.]

4.Conclusions and Future Work

4.1.Summary of Results

In this project, a treatment system was successfully designed and tested to completely oxidize three common anesthetic gases (Halothane, Isoflurane and Sevoflurane) that are vented untreated into the environment from the medical facilities. Gas chromatography with an FID and an IC instrument were used for the quantification and identification of these gases and their oxidation by-products. A set of process and environmental parameters were tested for their influence on the anesthetic gas degradation rate.

UV-photocatalysis with a 254 nm light source and TiO_2 photocatalyst was found to be the most efficient advanced oxidation process in degrading 99.9 % of the 1296 ng/ml of Halothane among the ones tested. This process demonstrated similar degradation efficiency with 847 ng/ml of Sevoflurane and 911 ng/ml of Isoflurane. UV-photolysis and UV-ozonation both gave 36% degradation with 1296 ng/ml of Halothane. TiO_2 was found to be more efficient than ZnO as a photocatalyst since it degraded 100% of injected 1111.4 ng/ml of Halothane in comparison to the 29% by ZnO due to its speculated greater absorption coefficient in the incident light wavelength region of 254 nm. TiO_2in the presence of 1511 ng/ml of Halothane gave 87% degradation with a 9 W 254 nm light source when compared to 5.4% degradation with the 365 nm light source due to its greater absorption coefficient in the 254 nm region.

Of the three support surfaces tested, the plain, flat aluminum support was found to be more effective due to its larger illuminated area, uniform surface and lack of absorption of the TiO_2 molecules into the bulk of the support surface. The photocatalytic degradation rate increased with increase in the incident light intensity due to the greater number of the incident photons which generated more hydroxyl

radicals. For a fixed amount of catalyst, the rate of degradation decreased with increase in the reactant inlet concentration due to greater competition for adsorption on to the available catalytic sites. For a fixed reactant inlet concentration, the rate of degradation increased up to a limit with increase in catalyst loading due to increased generation of hydroxyl radicals, after which for any further increase the rate of degradation decreased due to catalyst overloading.

The instantaneous rate constants for Halothane decreased with time due to depletion of the reactant or reduced catalyst activity, however, the instantaneous reaction rate constants, when plotted against time for Isoflurane and Sevoflurane was found to increase, reach a maximum and then decrease with time. It was determined that both Sevoflurane and Isoflurane underwent a chain reaction mechanism whereby initially the hydroxyl radicals acted as a primary oxidizing agent which then generated halogenated free radicals (F^{o} and Cl^{o} respectively) which accelerated the chain degradation. This conclusion was supported by the IC analysis that demonstrated the production of chloride and fluoride radicals from the UV-photocatalysis of Isoflurane and Sevoflurane. The results presented here suggest that UV-photocatalysis is a promising technique to treat out any leftover anesthetic gas before being released out into the environment.

4.2.Recommendations

To ensure that no further anesthetic gases are released untreated into the environment this treatment system should be installed in the healthcare facilities as a final degradation technique after the initial anesthetic recovery has been done.

In a worst case scenario, if the anesthetic recovery setup present before the photocatalytic oxidation system fails to capture the emitted anesthetic gas, assuming that the anesthetic gas had a flow rate of 0.5 ml/min then in 24 hrs, 770.4 g of HF is expected to be formed if the degradation pathway

mentioned in Equation 12 is followed. This amount corresponds to 127 ppm HF inside the photoreactor which over time has the potential to damage the equipment used in the setup. The below recommendations are being suggested as the probable next steps:

1. Test the degradation efficiency of UV-photocatalysis in a flow through system
2. Test the setup in a small-scale onsite system to determine the actual inlet anesthetic gas conditions (temperature, pressure, humidity, pH and oxygen concentration) and their effect on the degradation efficiency
3. Use BET (Brunauer-Emmett-Teller) theory and testing to obtain an estimate of the actual catalyst surface area available for the absorption of the anesthetic gas
4. Test for catalyst deactivation in a flow through system and install a sensor at the exit end to determine and identify when the anesthetic gas concentrations are higher than expected
5. Confirm the oxidation by-products of Sevoflurane and Isoflurane and ensure sufficient safety measures are in place to handle any harmful emissions like HF or HCl
6. Determine ways to handle and accurately quantify the highly volatile Desflurane and test its degradation rate using UV-photocatalysis.

References

1.Clar D, Richards J. Anesthetic Gases [Internet]. Ncbi.nlm.nih.gov.2020.Availablefrom:https://www.ncbi.nlm.nih.gov/books/NBK537013/2

2.Bowdle T, Knutsen L, Williams M. Local and Adjunct Anesthesia. Comprehensive Medicinal Chemistry II. 2007;351-367.

3.Inhalation Anesthesia Market Size & Share | Industry Report, 2019-2025 [Internet]. Grandviewresearch.com.Available from: https://www.grandviewresearch.com/industry-analysis/inhalation-anesthesia-market

4.[Internet]. Accessdata.fda.gov. 2020. Available from:https://www.accessdata.fda.gov/drugsatfda_docs/label/2010/017624s036lbl.pdf

5.Aronson J, Meyler L. Meyler's side effects of drugs. 16th ed. 225 Wyman Street, Waltham, MA 02451, USA: Lisa Tickner; 2016.

6.Abts D. Volatile Anesthetics and Climate Change: How You Can Make a Difference. Presentation presented at; 2019.

7.Vollmer M, Rhee T, Rigby M, Hofstetter D, Hill M, Schoenenberger F et al. Modern inhalation anesthetics: Potent greenhouse gases in the global atmosphere. Geophysical Research Letters [Internet]. 2015;42(5):1606-1611. Available from: https://sci-hub.tw/10.1002/2014gl062785

8.Sulbaek Andersen M, Sander S, Nielsen O, Wagner D, Sanford T, Wallington T. Inhalation anaesthetics and climate change † †This article is accompanied by the Editorial. British Journal of Anaesthesia [Internet]. 2010; 105(6):760-766. Available from: https://doi.org/10.1093/bja/aeq259

9.Krishnan S, Rawindran H, Sinnathambi C, Lim J. Comparison of various advanced oxidation processes used in remediation of industrial wastewater laden with recalcitrant pollutants. IOP

Conference Series: Materials Science and Engineering. 2017;206:012089.

10. Braslavsky S. Glossary of terms used in photochemistry, 3rd edition (IUPAC Recommendations 2006). Pure and Applied Chemistry. 2007;79(3):293-465.

11. Wekhof A. Treatment of contaminated water, air and soil with UV flashlamps. Environmental Progress. 1991;10(4):241-247.

12. Bhowmick M, Semmens M. Ultraviolet photooxidation for the destruction of vocs in air. Water Research. 1994;28(11):2407-2415.

13. Deng Y, Zhao R. Advanced Oxidation Processes (AOPs) in Wastewater Treatment. Current Pollution Reports. 2015;1(3):167-176.

14. Zazouli M, Ghanbari F, Yousefi M, Madihi-Bidgoli S. Photocatalytic degradation of food dye by Fe3O4–TiO2 nanoparticles in presence of peroxymonosulfate: The effect of UV sources. Journal of Environmental Chemical Engineering. 2017;5(3):2459-2468.

15. Dascalaki E, Gaglia A, Balaras C, Lagoudi A. Indoor environmental quality in Hellenic hospital operating rooms. Energy and Buildings. 2009;41(5):551-560

16. Balaras C, Dascalaki E, Gaglia A. HVAC and indoor thermal conditions in hospital operating rooms. Energy and Buildings. 2007;39(4):454-470.

17. Barrett W, Garber S. Surgical smoke: a review of the literature. Surgical Endoscopy. 2003;17(6):979-987.

18. Farré M, Franch M, Ayllón J, Peral J, Domènech X. Biodegradability of treated aqueous solutions of biorecalcitrant pesticides by means of photocatalytic ozonation. Desalination. 2007;211(1-3):22-33.

19. Mare M, Waldner G, Bauer R, Jacobs H, Broekaert J. Degradation of nitrogen containing organic compounds by combined photocatalysis and ozonation. Chemosphere. 1999;38(9):2013-2027.

20. Piera E, Calpe J, Brillas E, Domènech X, Peral J. 2,4-Dichlorophenoxyacetic acid degradation by catalyzed ozonation: TiO2/UVA/O3 and Fe(II)/UVA/O3 systems. Applied Catalysis B: Environmental.

2000;27(3):169-177.

21. Kopf P, Gilbert E, Eberle S. TiO2 photocatalytic oxidation of monochloroacetic acid and pyridine: influence of ozone. Journal of Photochemistry and Photobiology A: Chemistry. 2000;136(3):163-168.

22. Gomes de Moraes S, Sanches Freire R, Durán N. Degradation and toxicity reduction of textile effluent by combined photocatalytic and ozonation processes. Chemosphere. 2000;40(4):369-373.

23. Balcioglu I, Getoff N, Bekbölet M. A comparative study for the synergistic effect of ozone on the γ-irradiated and photocatalytic reaction of 4-chlorobenzaldehyde. Journal of Photochemistry and Photobiology A: Chemistry. 2000;135(2-3):229-233.

24. Malato S, Blanco J, Richter C, Braun B, Maldonado M. Enhancement of the rate of solar photocatalytic mineralization of organic pollutants by inorganic oxidizing species. Applied Catalysis B: Environmental. 1998;17(4):347-356.

25. Wang Y, Hong C. Effect of hydrogen peroxide, periodate and persulfate on photocatalysis of 2-chlorobiphenyl in aqueous TiO2 suspensions. Water Research. 1999;33(9):2031-2036.

26. Cornish B, Lawton L, Robertson P. Hydrogen peroxide enhanced photocatalytic oxidation of microcystin-LR using titanium dioxide. Applied Catalysis B: Environmental. 2000;25(1):59-67.

27. Shen Y, Ku Y. Decomposition of gas-phase trichloroethene by the UV/TiO2 process in the presence of ozone. Chemosphere. 2002;46(1):101-107.

28. Pengyi Z, Fuyan L, Gang Y, Qing C, Wanpeng Z. A comparative study on decomposition of gaseous toluene by O3/UV, TiO2/UV and O3/TiO2/UV. Journal of Photochemistry and Photobiology A: Chemistry. 2003;156(1-3):189-194.

29. Dibble L, Raupp G. Kinetics of the gas-solid heterogeneous photocatalytic oxidation of trichloroethylene by near UV illuminated titanium dioxide. Catalysis Letters. 1990;4(4-6):345-354.

30.PERAL J, OLLIS D. Heterogeneous photocatalytic oxidation of gas-phase organics for air purification: Acetone, 1-butanol, butyraldehyde, formaldehyde, and m-xylene oxidation. Journal of

Catalysis. 1992;136(2):554-565.

31. Hodnett B. Photocatalytic purification and treatment of water and air. Applied Catalysis B: Environmental. 1994;3(2-3):N22-N23.

32. Obee T, Brown R. TiO2 Photocatalysis for Indoor Air Applications: Effects of Humidity and Trace Contaminant Levels on the Oxidation Rates of Formaldehyde, Toluene, and 1,3-Butadiene. Environmental Science & Technology. 1995;29(5):1223-1231.

33. Jacoby W, Blake D, Penned J, Boulter J, Vargo L, George M et al. Heterogeneous Photocatalysis for Control of Volatile Organic Compounds in Indoor Air. Journal of the Air & Waste Management Association. 1996;46(9):891-898.

34. Alberici R, Jardim W. Photocatalytic destruction of VOCs in the gas-phase using titanium dioxide. Applied Catalysis B: Environmental. 1997;14(1-2):55-68.

35. Peral J, Domènech X, Ollis D. Heterogeneous Photocatalysis for Purification, Decontamination and Deodorization of Air. Journal of Chemical Technology & Biotechnology. 1997;70(2):117-140.

36. Canela M, Alberici R, Sofia R, Eberlin M, Jardim W. Destruction of Malodorous Compounds Using Heterogeneous Photocatalysis. Environmental Science & Technology. 1999;33(16):2788-2792.

37. Noguchi T, Fujishima A, Sawunyama P, Hashimoto K. Photocatalytic Degradation of Gaseous Formaldehyde Using TiO2Film. Environmental Science & Technology. 1998;32(23):3831-3833.

38. Vorontsov A, Stoyanova I, Kozlov D, Simagina V, Savinov E. Kinetics of the Photocatalytic Oxidation of Gaseous Acetone over Platinized Titanium Dioxide. Journal of Catalysis. 2000;189(2):360-369.

39. Maira A, Yeung K, Soria J, Coronado J, Belver C, Lee C et al. Gas-phase photo-oxidation of toluene using nanometer-size TiO2 catalysts. Applied Catalysis B: Environmental. 2001;29(4):327-336.

40. Shang J, Du Y, Xu Z. Photocatalytic oxidation of heptane in the gas-phase over TiO2.

Chemosphere. 2002;46(1):93-99.

41. Ollis D, Al-Ekabi H. Photocatalytic purification and treatment of water and air. Amsterdam, Netherlands: Elsevier; 1993.

42. Peral J, Ollis D. TiO2 photocatalyst deactivation by gas-phase oxidation of heteroatom organics. Journal of Molecular Catalysis A: Chemical. 1997;115(2):347-354.

43. Larson S, Falconer J. Characterization of TiO2 photocatalysts used in trichloroethene oxidation. Applied Catalysis B: Environmental. 1994;4(4):325-342.

44. Alberici R, Mendes M, Jardim W, Eberlin M. Mass spectrometry on-line monitoring and MS2 product characterization of TiO2/UV photocatalytic degradation of chlorinated volatile organic compounds. Journal of the American Society for Mass Spectrometry. 1998;9(12):1321-1327.

45.Méndez-Román R, Cardona-Martínez N. Relationship between the formation of surface species and catalyst deactivation during the gas-phase photocatalytic oxidation of toluene. Catalysis Today. 1998;40(4):353-365.

46. Luo Y, Ollis D. Heterogeneous Photocatalytic Oxidation of Trichloroethylene and Toluene Mixtures in Air: Kinetic Promotion and Inhibition, Time-Dependent Catalyst Activity. Journal of Catalysis. 1996;163(1):1-11.

47. Cao L, Gao Z, Suib S, Obee T, Hay S, Freihaut J. Photocatalytic Oxidation of Toluene on Nanoscale TiO2 Catalysts: Studies of Deactivation and Regeneration. Journal of Catalysis. 2000;196(2):253-261.

48. Larson S, Falconer J. Catalysis Letters. 1997;44(1/2):57-65.

49. Ameen M, Raupp G. Reversible Catalyst Deactivation in the Photocatalytic Oxidation of Diluteo-Xylene in Air. Journal of Catalysis. 1999;184(1):112-122.

50. Mo J, Zhang Y, Xu Q, Lamson J, Zhao R. Photocatalytic purification of volatile organic compounds in indoor air: A literature review. Atmospheric Environment. 2009;43(14):2229-2246.

51. Tian F, Wu Z, Yan Y, Ge X, Tong Y. Photodegradation of formaldehyde by activated carbon

loading TiO2 synthesized via microwave irradiation. Korean Journal of Chemical Engineering. 2015;32(7):1333-1339.

52. Schneider J, Matsuoka M, Takeuchi M, Zhang J, Horiuchi Y, Anpo M et al. Understanding TiO2Photocatalysis: Mechanisms and Materials. Chemical Reviews. 2014;114(19):9919-9986.

53. Khan F, Kr. Ghoshal A. Removal of Volatile Organic Compounds from polluted air. Journal of Loss Prevention in the Process Industries. 2000;13(6):527-545.

54. Ai Z, Huang Y, Lee S, Zhang L. Monoclinic α-Bi2O3 photocatalyst for efficient removal of gaseous NO and HCHO under visible light irradiation. Journal of Alloys and Compounds. 2011;509(5):2044-2049.

55. Arai T, Horiguchi M, Yanagida M, Gunji T, Sugihara H, Sayama K. Complete oxidation of acetaldehyde and toluene over a Pd/WO3 photocatalyst under fluorescent- or visible-light irradiation. Chemical Communications. 2008;(43):5565.

56. Dong F, Wang Z, Li Y, Ho W, Lee S. Immobilization of Polymeric g-C3N4on Structured Ceramic Foam for Efficient Visible Light Photocatalytic Air Purification with Real Indoor Illumination. Environmental Science & Technology. 2014;48(17):10345-10353.

57. Soreanu G, Dixon M, Darlington A. Botanical biofiltration of indoor gaseous pollutants – A mini-review. Chemical Engineering Journal. 2013;229:585-594.

58. Meng Z, Juan Z., "Wastewater treatment by Photocatalytic oxidation of nano-ZnO", Global Environmental Policy in Japan, vol. 12, pp. 1-9, 2008.

59. Adams L, Lyon D, Alvarez P. Comparative eco-toxicity of nanoscale TiO2, SiO2, and ZnO water suspensions. Water Research. 2006;40(19):3527-3532.

60. Khezrianjoo S and Revanasiddappa H 2012 Chemical Sciences Journal CSJ 1-7, pp.1-7.

61.C. Hariharan, "Photocatalytic degradation of organic contaminants in water by ZnO nanoparticles: Revisited," Applied Catalysis A: General, 304, 2006, pp. 55-61.

62. Jin Y, Wang J, Sun B, Blakesley J, Greenham N. Solution-Processed Ultraviolet Photodetectors Based on Colloidal ZnO Nanoparticles. Nano Letters. 2008;8(6):1649-1653.

63. Yang J, An S, Park W, Yi G, Choi W. Photocatalysis Using ZnO Thin Films and Nanoneedles Grown by Metal-Organic Chemical Vapor Deposition. Advanced Materials. 2004;16(18):1661-1664.

64. Liu Z, Fang P, Wang S, Gao Y, Chen F, Zheng F et al. Photocatalytic degradation of gaseous benzene with CdS-sensitized TiO2 film coated on fiberglass cloth. Journal of Molecular Catalysis A: Chemical. 2012;363-364:159-165.

65.D. Robert, A. Piscopo, O. Heintz, and J. V. Weber, Photocatalytic detoxification with TiO 2 supported on glass-fibre by using artificial and natural light, Catal. Today, vol.54, pp.291-296, 1999

66. Raillard C, Héquet V, Le Cloirec P, Legrand J. Kinetic study of ketones photocatalytic oxidation in gas phase using TiO2-containing paper: effect of water vapor. Journal of Photochemistry and Photobiology A: Chemistry. 2004;163(3):425-431.

67. Sleiman M, Conchon P, Ferronato C, Chovelon J. Photocatalytic oxidation of toluene at indoor air levels (ppbv): Towards a better assessment of conversion, reaction intermediates and mineralization. Applied Catalysis B: Environmental. 2009;86(3-4):159-165.

68. Ao C, Lee S, Yu J, Xu J. Photodegradation of formaldehyde by photocatalyst TiO2: effects on the presences of NO, SO2 and VOCs. Applied Catalysis B: Environmental. 2004;54(1):41-50.

69. Ye X, Chen D, Gossage J, Li K. Photocatalytic oxidation of aldehydes: Byproduct identification and reaction pathway. Journal of Photochemistry and Photobiology A: Chemistry. 2006;183(1-2):35-40.

70. Chen W, Zhang J. Photocatalytic Oxidation of Multi-Component Systems – An Investigation Using Toluene/Ethylbenzene, Octane/Decane/Dodecane and Formaldehyde/Acetaldehyde. Journal of Advanced Oxidation Technologies. 2008;11(1).

71. Yu Q, Brouwers H. Indoor air purification using heterogeneous photocatalytic oxidation. Part I: Experimental study. Applied Catalysis B: Environmental. 2009;92(3-4):454-461.

72. Zhao J, Yang X. Photocatalytic oxidation for indoor air purification: a literature review. Building and Environment. 2003;38(5):645-654.

73. Hay S, Obee T, Luo Z, Jiang T, Meng Y, He J et al. The Viability of Photocatalysis for Air Purification. Molecules. 2015;20(1):1319-1356.

74. George C, Beeldens A, Barmpas F, Doussin J, Manganelli G, Herrmann H et al. Impact of photocatalytic remediation of pollutants on urban air quality. Frontiers of Environmental Science & Engineering. 2016;10(5).

75. Whyte H, Raillard C, Subrenat A, Héquet V. Influence of environmental parameters on the photocatalytic oxidation efficiency of acrylonitrile and isoflurane; two operating room pollutants. Building and Environment. 2019;154:97-106.

76. Balikhin I, Kabachkov E, Kurkin E, Martynenko V, Troitskii V, Domashnev I et al. Prospects for Using Photocatalytic Air Cleaning Technology to Provide Safety of Sevoflurane Application to Parturition Anesthesia in Obstetric Hospitals. High Energy Chemistry. 2018;52(4):360-363.

77.Mönig J, Krischer K, Asmus K. One-electron reduction of halothane and formation of halide ions in aqueous solutions. Chemico-Biological Interactions. 1983;45(1):43-52.

78.[Internet].2020[cited5July2020].Availablefrom:https://www.sigmaaldrich.com/catalog/product/aldrich/718467

79. Mo J, Zhang Y, Xu Q, Lamson J, Zhao R. Photocatalytic purification of volatile organic compounds in indoor air: A literature review. Atmospheric Environment. 2009;43(14):2229-2246.

80. Choi E. The Role of Germicidal Ultraviolet Light in the Formation of Secondary Organic Aerosols [Masters]. University Of Waterloo; 2017.

81. Bajraktarova-Valjakova E, Korunoska-Stevkovska V, Georgieva S, Ivanovski K, Bajraktarova-Misevska C, Mijoska A et al. Hydrofluoric Acid: Burns and Systemic Toxicity, Protective Measures, Immediate and Hospital Medical Treatment. Open Access Macedonian Journal of Medical Sciences.

2018;6(11):2257-2269.

82. Barrett A, Nunn J. absorption spectra of the common anaesthetic agents in the far ultra-violet. British Journal of Anaesthesia. 1972;44(4):306-312.

83. Langbein T, Sonntag H, Trapp D, Hoffmann A, Malms W, Röth E et al. Volatile anaesthetics and the atmosphere: atmospheric lifetimes and atmospheric effects of halothane, enflurane, isoflurane, desflurane and sevoflurane. British Journal of Anaesthesia. 1999;82(1):66-73.

84. Keller-Rudek H, Moortgat G, Sander R, Sörensen R. The MPI-Mainz UV/VIS Spectral Atlas of Gaseous Molecules of Atmospheric Interest. Earth System Science Data. 2013;5(2):365-373.

85. Molina L, Molina M. Absolute absorption cross sections of ozone in the 185- to 350-nm wavelength range. Journal of Geophysical Research. 1986;91(D13):14501.

86. Batakliev T, Georgiev V, Anachkov M, Rakovsky S. Ozone decomposition. Interdisciplinary Toxicology. 2014;7(2):47-59.

87. Zhao L, Xia M, Liu Y, Zheng B, Jiang Q, Lian J. Structure and Photocatalysis of TiO₂/ZnO Double-Layer Film Prepared by Pulsed Laser Deposition. MATERIALS TRANSACTIONS. 2012;53(3):463-468.

88. Lin C, Hsu L. Removal of polyvinyl alcohol from aqueous solutions using P-25 TiO2 and ZnO photocataysts: A comparative study. Powder Technology. 2013;246:351-355.

89. Chantes P, Jarusutthirak C, Danwittayakul S. A Comparison Study of Photocatalytic Activity of TiO_2 and ZnO on the Degradation of Real Batik Wastewater. International Conference on Biological, Environment and Food Engineering (BEFE-2015) May 15-16, 2015 Singapore. 2015.

90. Han J, Liu Y, Singhal N, Wang L, Gao W. Comparative photocatalytic degradation of estrone in water by ZnO and TiO_2 under artificial UVA and solar irradiation. Chemical Engineering Journal. 2012;213:150-162.

91. Gonçalves P, Bertholdo R, Dias J, Maestrelli S, Giraldi T. Evaluation of the Photocatalytic Potential of TiO2 and ZnO Obtained by Different Wet Chemical Methods. Materials Research. 2017;20(suppl 2):181-189.

92. Chakrabarti S, Dutta B. Photocatalytic degradation of model textile dyes in wastewater using ZnO as semiconductor catalyst. Journal of Hazardous Materials. 2004;112(3):269-278.

93. Ibrahim H. Photo-catalytic conversion of air borne pollutants Effect of catalyst type and catalyst loading in a novel photo-CREC-air unit. Applied Catalysis B: Environmental. 2002;38(3):201-213.

94. Saquib M, Abu Tariq M, Faisal M, Muneer M. Photocatalytic degradation of two selected dye derivatives in aqueous suspensions of titanium dioxide. Desalination. 2008;219(1-3):301-311.

95. Chen L, Huang C, Tsai F. Characterization and photocatalytic activity of K+-doped TiO2 photocatalysts. Journal of Molecular Catalysis A: Chemical. 2007;265(1-2):133-140.

96. Huang M, Xu C, Wu Z, Huang Y, Lin J, Wu J. Photocatalytic discolorization of methyl orange solution by Pt modified TiO2 loaded on natural zeolite. Dyes and Pigments. 2008;77(2):327-334.

97. Sun J, Qiao L, Sun S, Wang G. Photocatalytic degradation of Orange G on nitrogen-doped TiO2 catalysts under visible light and sunlight irradiation. Journal of Hazardous Materials. 2008;155(1-2):312-319.

98. Zhiyong Y, Keppner H, Laub D, Mielczarski E, Mielczarski J, Kiwi-Minsker L et al. Photocatalytic discoloration of Methyl Orange on innovative parylene–TiO2 flexible thin films under simulated sunlight. Applied Catalysis B: Environmental. 2008;79(1):63-71.

99.M. Jafarikojour, M. Sohrabi, S.J. Royaee, A. Hassanvand, Evaluation and Optimization of a Novel Immobilized Photoreactor for the Degradation of Gaseous Toluene, CLEAN - Soil, Air, Water. 43 (2015) 662–670. doi:10.1002/clen.201300985.

100. Boulamanti A, Philippopoulos C. Photocatalytic degradation of methyl tert-butyl ether in the gas-phase: A kinetic study. Journal of Hazardous Materials. 2008;160(1):83-87.

101. Hager S, Bauer R, Kudielka G. Photocatalytic oxidation of gaseous chlorinated organics over titanium dioxide. Chemosphere. 2000;41(8):1219-1225.

102. Wang K, Hsieh Y, Lin C, Chung C. The study of the photocatalytic degradation kinetics for dichloroethylene in vapor phase. Chemosphere. 1999;39(9):1371-1384.

103. Mo J, Zhang Y, Xu Q. Effect of water vapor on the by-products and decomposition rate of ppb-level toluene by photocatalytic oxidation. Applied Catalysis B: Environmental. 2013;132-133:212-218.

104. Zhong L, Haghighat F, Lee C, Lakdawala N. Performance of ultraviolet photocatalytic oxidation for indoor air applications: Systematic experimental evaluation. Journal of Hazardous Materials. 2013;261:130-138.

105. Kim S, Hong S. Kinetic study for photocatalytic degradation of volatile organic compounds in air using thin film TiO2 photocatalyst. Applied Catalysis B: Environmental. 2002;35(4):305-315.

106. Hegedüs M, Dombi A. Comparative study of heterogeneous photocatalytic decomposition of tetrachloroethene and trichloroethene in the gas phase. Applied Catalysis A: General. 2004;271(1-2):177-184.

107. Joung S, Amemiya T, Murabayashi M, Itoh K. Mechanistic Studies of the Photocatalytic Oxidation of Trichloroethylene with Visible-Light-Driven N-Doped TiO2 Photocatalysts. Chemistry - A European Journal. 2006;12(21):5526-5534.

108. Bito H, Suzuki A, Sanjo Y, Katoh T, Sato S. Comparison of compound A concentrations with sevoflurane anaesthesia using a closed system with a PhysioFlexanaesthesia machine vs a low-flow system with a conventional anaesthesia machine. British Journal of Anaesthesia. 2000;84(3):350-353.

109. Mehrata M. Hospital Air Emission Capture and Recovery [Masters]. University of Waterloo; 2014.

Appendices

TESTING FOR BYPRODUCTS OF UV-PHOTOCATALYSIS

By product Estimation with Sevoflurane

a) $2C_4H_3F_7O + 5O_2 + 4H_2O \rightarrow 8\ CO_2 + 14\ HF$

5 ul of sevo = 3.81×10^{-5} moles

1 mol of Sevo → 7 mol of HF

Therefore,

3.81×10^{-5} moles → 5.34 mg of HF

b) $C_4H_3F_7O \rightarrow HF + C_4H_2F_6O$

1 mol of Sevo → 1 mol of HF

Therefore,

3.81×10^{-5} moles → 0.762 mg of HF

By product Estimation with Isoflurane

a) $C_3H_2ClF_5O + H_2O \rightarrow C_3F_5OH + HCl + H_2O$

5 ul of iso = 4.05×10^{-5} moles

1 mol of Iso → 1 mol of HCl

Therefore,

4.05×10^{-5} moles → 1.48 mg of HCl

3.2.1UV-Photolysis

Calculate the absorbance of Halothane using the absorption cross section

A=Abs. cross section (cm^2/molecule) * absorption path length(cm) * density of absorber (molecule/cm^3)

At 254 nm with 1400 ng/ml of Halothane

$A = 4.5 \times 10^{-20} * 10.2 * 1.62 \times 10^{19} / 3787$

$=0.00196$

$T = 10^{-A}$

$= 10^{-0.00196} = 1 - \text{abs fraction}$

Abs fraction = 0.0045

3.1.2UV-Ozonation

Calculate the concentration of ozone produced in the reactor

$T = 10^{-A}$ where A is the absorbance obtained using the spectrometer

$T = 10^{-1.808533}$

$=0.016$

Concentration (molecule/cm^3) = Ln(T)/ (Abs cross section at 254 nm * path length of the cell)

= Ln (0.016)/ ($-1.159 \times 10^{-17} \times 10$)

$=2.8 \times 10^{16}$ molecules/cm^3

$= 1.1 \times 10^{20}$ molecules

$=8.77 \times 10^{6}$ ng Ozone = 2315.87 ng Ozone/ml

Calculate the absorbance of ozone using the absorption cross section

A=Abs. cross section (cm^2/molecule) * absorption path length(cm) * density of absorber (molecule/cm^3)

At 254 nm with 1.1 $x10^{20}$of ozone

A= $1.5x10^{-17}$* 10.2*$1.1x10^{20}$/3787

=4.44

Abs fraction= 0.9999

3.4 **Influence of the incident light source wavelength on the anesthetic gas degradation rate**

Number of photons emitted by 9W lamp at 254 nm:

E= (($6.626x10^{-34}$) X ($3x10^{8}$))/ ($254x10^{-9}$)

=$7.83x10^{-19}$ J

Number of photons in the 9W lamp (assuming 33.3% conversion) = 3/$7.83x10^{-19}$ J

= $3.83x10^{18}$ photons/sec

Similarly,

Number of photons emitted by 9W lamp at 365 nm = $5.50x10^{18}$ photons/sec

Therefore, with an absorption fraction of 0.00441 @ 254 nm and $1.17x10^{-16}$ @ 365 nm

In 30 min at 254 nm, Halothane will absorb $3.04x10^{19}$ photons and at 365 nm Halothane will absorb $1.17x10^{16}$ photons